INSTITUTO
UNIVERSITÁRIO
DE LISBOA

Impact of physical layer impairments on multi-band metro networks

Filipa Ferreira Gomes

Master degree in Telecommunications and Computer Engineering,

Supervisor:
PhD, Luís Gonçalo Lecoq Vences e Costa Cancela, Assistant Professor
Iscte-Instituto Universitário de Lisboa

Co-Supervisor:
PhD, João Lopes Rebola, Associate Professor
Iscte-Instituto Universitário de Lisboa

November, 2021

TECNOLOGIAS
E ARQUITETURA

Department of Information Science and Technology

Impact of physical layer impairments on multi-band metro networks

Filipa Ferreira Gomes

Master degree in Telecommunications and Computer Engineering,

Supervisor:
PhD, Luís Gonçalo Lecoq Vences e Costa Cancela, Assistant Professor
Iscte-Instituto Universitário de Lisboa

Co-Supervisor:
PhD, João Lopes Rebola, Associate Professor
Iscte-Instituto Universitário de Lisboa

November, 2021

Família

Acknowledgments

The end of this work also marks the end of five enriching and incredible years at Iscte-IUL. I would like to thank to Iscte-IUL, for always having been a second home and for giving me the opportunity to enjoy the best years I could have had been. I want to thank all those who have crossed paths with me, teachers, staff and colleagues, and who were present in classes, events and organizations and contributed to everything I have experienced at this university, helped me get this far and inevitably had an impact on me. Thanks to the Instituto de Telecomunicações, for the access provided to its facilities and material conditions. To my supervisors, Prof. Luís Cancela and Prof. João Rebola, a special thanks for the monitoring and support throughout this year of work, which made me learn so much and challenged me so many times.

Thanks to all my course mates, Iscte colleagues and friends in Lisbon, who helped me to adapt to a new environment and were always available to listen to me and advise me throughout this process. A special thanks to Adriana Silva, João Antão, André Glória, Rita Peixoto, Eduardo Ferreira and Henrique Vitória, for their friendship, patience and support in any time and any place. To my friends from Leiria, Mariana Vieira, Beatriz Francisco and Eugénia, thank you for understanding me for so many moments of absence when my life in Lisbon was tighter and demanded a lot from me.

The biggest thank you goes to my family, who were always the first to celebrate all the good moments and to accept and support me throughout all the challenging ones over the last years. To my parents, Mário and Carmen, for being the most present and attentive and for all the effort put into my education. To my brother, Alexandre, for his tireless presence, even from the Netherlands, and for accepting and understanding my doubts and fears better than anyone. To my twin sister, Inês, who lived with me 24 hours a day and shared these 5 happy years with me, and because without her, nothing would have been the same. Thanks to my uncles and cousins, for encouraging me during all this time. To my grandfather who is always present and, I hope, very proud of my path, for all the support and escapes that he has provided me over these years. Finally, thank you, grandmas. I hope that, in some way, you are seeing what I have managed to achieved.

Resumo

O aumento de tráfego nas redes metropolitanas irá saturar a capacidade das redes num futuro próximo, principalmente devido aos novos serviços em nuvem e 5G, bem como ao aumento do número de utilizadores. O uso de novas bandas na fibra ótica, além da banda C, é visto como uma possível solução para responder a esse aumento de capacidade.

Neste trabalho, é apresentada a topologia de rede "horseshoe", que contém nós com capacidade para comutar sinais nas bandas C e L. Na banda C, consideram-se as arquiteturas com multiplexadores de inserção/extração reconfiguráveis e arquiteturas sem filtragem, e na banda L, consideram-se apenas soluções sem filtragem, com e sem amplificação. São estudadas, analiticamente, as limitações físicas da transmissão na fibra e comutação dos sinais nos nós da rede "horseshoe". Além disso, é realizado um estudo do custo, consumo e capacidade dos nós nas bandas C e L.

Num cenário de fim de vida da rede, o custo dos nós na banda L é 3.5 vezes superior aos da banda C. O custo dos transponders constitui 99% do custo final. Na banda L, o sinal pode atravessar várias secções de 10 ou 60 km na solução amplificada. Na solução não amplificada, onde existe reuso de frequência, só há uma secção de 10 km devido ao orçamento máximo de potência na ligação. Para um nível de diafonia de -20 dB, o orçamento de potência diminui 1.5 dB.

Palavras-Chave: Crosstalk homódino, Interferência não-linear, Redes metropolitanas, ROADM, Ruído ASE, Soluções sem filtragem, Transmissão em multibanda.

Abstract

The traffic increase in optical metro networks will saturate the network capacity in a near future, mainly due to new cloud and 5G services, as well as to an increasing number of network users. The use of other fiber bands, than the usual C-band, is seen as a possible near term solution, for this probable capacity crunch.

In this work, a metro network horseshoe topology with nodes capable of switching both C and L-band signals is studied. In particular, we have considered for switching C-band signals, reconfigurable optical add/drop multiplexer and Filterless Drop and Waste (FD&W) node architectures, whereas for switching L-band signals, we have considered only FD&W solutions, both amplified and unamplified. An analytical formalism was developed to assess the impact of the physical layer impairments due to fiber transmission and switching node in a horseshoe network performance. Moreover, the cost and power consumption of the C-band and L-band nodes are analyzed.

We concluded that in a network end of life scenario, the L-band nodes cost is 3.5 times higher than the C-band nodes, being 99% of this cost attributed to the transponders. In L-band transmission, a lightpath can cross several spans with 10 or 60 km in the amplified solution. In the unamplified solution, where frequency reuse is allowed, a lightpath consists only on a single 10 km span due to the maximum optical link budget. Considering a -20 dB crosstalk level, a 1.5 dB degradation on the optical power budget is observed.

Keywords: ASE noise, Filterless solutions, In-band crosstalk, Metro networks, Multi-band transmission, Non-linear interference noise, ROADM.

Contents

List of Figures

List of Tables

List of Acronyms

A/D: Add/Drop.

ASE: Amplified Spontaneous Emission.

AWG: Arrayed Waveguide Grating.

B&S: Broadcast and Select.

BER: Bit Error Rate.

BVT: Bandwith Variable Transponder.

C: Colorless.

CD: Colorless and Directionless.

CDC: Colorless, Directionless and Contentionless.

ChD: Coherent Detection.

Cl: Contentionless.

CW: Continuous Wave.

D: Directionless.

DD: Direct Detection.

DEMUX: Demultiplexer.

DR: Dual Region.

DSP: Digital Signal Processing.

EDFA: Erbium-Doped Fiber Amplifier.

FD&W: Filterless Drop and Waste.

FEC: Forward Error Correction.

FF: Fixed-Filter.

FOADM: Fixed Optical Add/Drop Multiplexer.

GN: Gaussian-Noise.

HD: Hard-Decision.

ILs: Insertion losses.

ITU: International Telecommunication Union.

LCoS: Liquid Crystal on Silicon.

LO: Local Oscillator.

MAN: Metro Area Network.

MBT: Multi-Band Transmission.

MCS: MultiCast Switch.

MEMS: Micro-Electro-Mechanical Systems.

MUX: Multiplexer.

NLI: Non-Linear Interference.

OA: Optical Amplifier.

OS: Optical Switch.

OSNR: Optical Signal-to-Noise Ratio.

PLI: Physical Layer Impairment.

PSD: Power Spectral Density.

QAM: Quadrature Amplitude Modulation.

QPSK: Quadrature Phase-Shift Keying.

R&S: Route and Select.

RIN: Relative Intensity Noise.

ROADM: Reconfigurable Optical Add/Drop Multiplexer.

RRC: Root Raised Cosine.

Rx: Receiver.

S/C: Splitter/Combiner.

SD: Soft-Decision.

SMF: Single-Mode Fiber.

SNR: Signal-to-Noise Ratio.

SPM: Self-Phase Modulation.

SR: Single Region.

SRS: Stimulated Raman Scattering.

TIA: Transimpedance Amplifier.

Tx: Transmitter.

vCPU: Virtual Centralized Processing Unit.

VOA: Variable Optical Attenuator.

WDM: Wavelength-Division Multiplexing.

WSS: Wavelength Selective Switch.

XPM: Cross-Phase Modulation.

List of Symbols

β_2	Group velocity dispersion
β_3	Higher order dispersion
Δ_{fm}	WDM channel bandwidth
ϵ	Coherence factor
η_{NLI}	NLI parameter in the C-band
η_n	NLI parameter in the L-band
η_{SPM}	Self-phase modulation contribution to the NLI parameter
η_{XPM}	Cross-phase modulation contribution to the NLI parameter
γ	Fiber non-linearity coefficient
λ_0	Central channel wavelength
ρ_{FEC}	FEC overhead
σ^2_{nLO}	Variance of the local oscillator transmitter relative intensity noise
σ^2_{shot}	Variance of the shot noise
σ^2_{th}	Variance of the transimpedance amplifiers
υ_o	Carrier frequency of the optical signal central channel
A/D_{ratio}	Add/Drop ratio
a	Blocking amplitude
A_{exc}	Excess losses
B_0	Reference optical bandwidth
B^{RX}_{eq}	Equivalent noise bandwidth of the receiver
B_i	Bandwidth of the i-th WDM channel
c	Light velocity in a vacuum
C_r	Slope of the linear regression of the normalized Raman gain spectrum
$CMRR$	Common mode rejection ratio
D_λ	Fiber dispersion parameter
$E_{LO}(t)$	Local oscillator eletrical field
$E_r(t)$	Received signal eletrical field
$E_{X_c}(t)$	In-band crosstalk eletrical field

f_m	Central channel frequency
$f_{n,pos,i}$	Post-amplifier noise figure
$f_{n,pre,i}$	Pre-amplifier noise figure
f_n	Optical amplifier noise figure
g	Optical amplifier gain
$G_{add-FD\&W}$	Add structure optical amplifier gain after a FD&W ChD node
$G_{add-ROADM}$	Add structure optical amplifier gain after a ROADM node
G_m	Signal power spectral density
$g_{NLI}(\nu_0)$	Power spectral density of NLI noise
$g_{pos,i}$	Post-amplifier gain
$g_{pre,i}$	Pre-amplifier gain
$g_{SCI}(\nu_0)$	Self-channel interference noise power spectral density
$g_{XCI}(\nu_0)$	Cross-channel interference noise power spectral density
h	Planck constant
$H_b(f)$	Transfer function of optical stopband filter
$H_p(f)$	Transfer function of optical passband filter
i_{TIA}	Input-referred noise current density
$IL_{S/C}$	Splitter/Coupler insertion losses
M	Number of WSS outputs
$M_{symbols}$	Number of symbols
n	Super-Gaussian filter order
N_{ch}	Number of wavelengths per direction
N_{sec}	Number of sections
n_{spans}	Number of fiber spans
N_{X_c}	Total number of interfering terms
$Number(Tx/Rx)$	Number of transmitters/receivers
$OSNR_{R,ref}$	OSNR for the reference bandwidth
$p_{ASE,pos,i}$	ASE noise power at each i-th pos-amplifier
$p_{ASE,pre,i}$	ASE noise power at each i-th pre-amplifier
p_{ASE}	ASE noise power
$P_{ch,opt}$	Optimum channel power
$P_{i,j}$	Power of i-th channel at frequency f_i at the j-th span
p_{in}	Input primary signal power

P_L^{CW}	Local oscillator continuous wave optical power
p_{NLI}	Non-linear interference power
P_{out}	Signal power at the optical amplifier output
p_{R_x}	Signal power at the receiver input
P_s	Channel power per polarisation
P_{tot}	WDM signal launch power
$p_{X_{c,i}}$	Interfering term power
p_{X_c}	Crosstalk power
q	Electron charge
R	Number of directions per node
R_λ	Responsivity
$R_{b,i}$	Information bit rate
$R_{b,l}$	Line bit rate
$R_{s,l}$	Symbol rate
S	Dispersion slope
S_{ASE}	Power spectral density of the ASE noise
SNR_Q	Signal-to-noise ratio implementation penalty in unamplified system
$X_{c,i}$	Crosstalk level of the i-th interfering term
X_c	Crosstalk level

CHAPTER 1

Introduction

1.1. Motivation and context

Nowadays, the Internet traffic continuous to grow at an unprecedented scale because new cloud and 5G services are becoming increasingly important and also because the number of users, which include person-to-person communications and machine-to-machine communications, is growing faster. This scenario will probably contribute to saturate the actual metro networks capacity in a near future [**1**].

Recent studies, such as [**2**]-[**3**], have shown that Multi-Band Transmission (MBT) aims at enabling transmissions beyond the C-band by opening the second and third low-loss windows of Single-Mode Fiber (SMF) ITU-T G-652.A/D [**4**], being the most straightforward solution upgrading the optical transmission to the L-band [**5**]. In Tab. 1.1, the wavelength ranges of the transmission bands, in nm, supported by the SMF as defined by the International Telecommunication Union (ITU) are listed [**6**].

TABLE 1.1. ITU-T band definition for SMF.

Band	**O**	**E**	**S**	**C**	**L**
Wavelength [nm]	1260-1360	1360-1460	1460-1530	1530-1565	1565-1625
C-Band				35 nm	
C+L-Band				95 nm	
All Bands	325 nm				

Several solutions based on MBT are being investigated to overcome the possible metro network capacity crunch [**4**]. The introduction of the L-band, by adding more Wavelength-Division Multiplexing (WDM) channels to the already in use C-band channels opens the opportunity for cheaper solutions than placing several fibres in parallel working in the C-band [**7**]. Also, filterless node solutions, both amplified and unamplified for the L-band, are being proposed to reduce even more the cost of upgrading the optical metro networks to the L-band [**6**], [**8**] and [**9**]. The filterless solution is usually proposed for metro networks using the horseshoe topology [**8**]. In [**9**], the L-band filterless unamplified solution is proposed, but due to frequency reuse, in-band crosstalk becomes a relevant impairment that degrades the network performance. As this solution is only suitable for short-reach spans, noise from the amplifiers and fiber non-linearities can be neglected. Due to the

impossibility of reusing frequencies in the amplified solution, amplified spontaneous emission (ASE) noise and fiber non-linear interference (NLI) become the main impairments that degrade the network performance.

In this work, we will develop a simple analytical formalism to assess the impact of the referred Physical Layer Impairment (PLI) in L-band network solutions, both amplified and unamplified. Note that in [**8**]-[**10**], the impact of these PLIs is assessed experimentally and by Monte-Carlo simulation. Moreover, in this work, we will also perform a performance study of the PLIs in C-band metro network solutions considering different node architectures. Finally, a detailed cost and power consumption analyses of L-band network solutions and also C-band network solutions is performed.

1.2. Goals

The main goal of this dissertation is to understand the impact of PLIs on multi-band metro networks. First, we study the C-band node architectures, as well as their components, cost, power consumption and node capacity. Then, we will study the PLIs originating in the C-band fibre and also due to node architectures (e.g. Broadcast and Select (B&S) Reconfigurable Optical Add/Drop Multiplexer (ROADM), Fixed Optical Add/Drop Multiplexer (FOADM), Filterless Drop and Waste (FD&W)) [**8**]. Also, in the L-band, considering FD&W amplified and unamplified solutions, the same study (cost, power consumption, nodes capacity and PLIs) is done. Finally, a comparison between these node architectures concerning the network performance is also made.

1.3. Dissertation organization

This dissertation is organized as follows. Chapter 2 is focused on the study of C-band node architectures for the horseshoe topology and its components. The architectures studied are the ROADM, FOADM and FD&W. A comparative hardware analysis, a study of the total cost and power consumption of an entire horseshoe network and a study of PLIs such as Insertion losses (ILs), ASE noise power, NLI noise power, optical filtering penalty and crosstalk is performed.

Chapter 3 is dedicated to study the horseshoe topology considering transmission in the C+L-band and the L-band node architectures are presented, such as amplified and unamplified solutions considering filterless architectures. The PLIs are also studied: the ILs for both solutions, the accumulated ASE noise and the NLI noise for the amplified solution and the in-band crosstalk for the unamplified solution.

Finally, all conclusions of this work, as well as some future work are summarized in Chapter 4.

1.4. Main contributions

This work has the following main contributions:

- Node cost and power consumption study and comparison considering different architectures for horseshoe network nodes, namely the ROADM and FD&W node architectures for the C-band and the FD&W amplified and unamplified for the L-band. We show that, in the L-band, the cost and power consumption of each one of the solutions is very similar, since the same number of transponders is used and the transponder cost contributes the most to the total cost.
- We show that the PLIs studied for the C-band metro networks such as ILs, ASE noise power, NLI power, optical filtering and crosstalk gives higher OSNRs when the nodes are ROADMs, in comparison to FD&W nodes.
- We study the PLIs for L-band metro network solutions, such as ILs, ASE noise power and NLI power for the amplified solutions and ILs and in-band crosstalk for the unamplified solutions. We show that the unamplified solution can only support 1 span of 10 km in horseshoe networks.

CHAPTER 2

General concepts of optical metropolitan networks

2.1. Introduction

This chapter is focused on understanding the main role of metro networks (section 2.2) and explain the different physical topologies for this type of networks, in particular the horseshoe topology (section 2.3). In section 2.4, three different types of node architectures for the horseshoe topology are described and a comparative analysis of hardware cost is performed in section 2.5. In section 2.6, the PLI are analyzed as well as their influence on the OSNR. Finally, the main conclusions are drawn.

2.2. The role of metro networks

The MANs are having a decisive role in increasing the telecommunications infrastructure efficiency, in order to support the bandwidth and flexibility requirements for 5G services and cloud services [**11**]. These services impose a wide array of requirements on the networks such as capacity/flexibility or cost/complexity, because the need for more capacity in optical transport networks, as there are no signs of a slowdown [**12**]. This way, transport metro networks must provide flexibility in manage diverse service requirements [**11**]. In Fig. 2.1, it is possible to see an example of a metro network and how this network connects with the access and core networks.

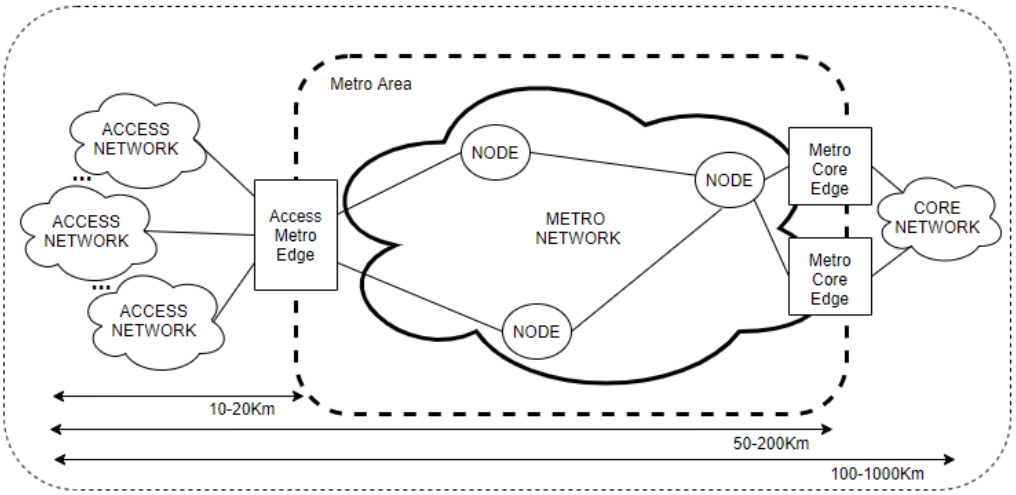

FIGURE 2.1. Example of a MAN network and its connections to the access and core networks.

The metro network main function is to transport data between the core and access networks. These network comprises up to 100 nodes, a cost-effective flexibility and it can reach distances between 20, 50 and 100 km. As can be seen in Fig. 2.1, the distance between access metro edges and access networks is among 10 and 20 km, the distance to the core edge metro goes up to 200 km and the distance between access metro network and core network is among 100 and 1000 km. It usually carries any data between 10 and 25 Gbps [**13**].

The access metro edge node includes several functionalities, such as remote storage and switching. It performs switching in the order of terabytes to access network, which work with Gbps. It is characterised by a throughput of 32 Gbps and storage of 22.5 Tbps for video streaming on UHD/4K/8K and by a throughput of 40 Gbps on video traffic inspection, analysis and cache reconfiguration and 4 Virtual Centralized Processing Unit (vCPU) for computing capacity [**13**].

The metro core edge includes larger cloud capabilities, such as data center functions. It consists of a ROADM structure with a sliceable spectrum, i.e., flows can be flexibly associated to the incoming traffic requests, and, besides composing a super-channel, they can be directed toward different destinations [**13**]. This node has got throughput values of 24 Gbps and storage of 22.5 Tbps for video streaming on UHD/4K/8K and by a throughput of 48 Gbps on video traffic inspection, analysis and cache reconfiguration and 5 vCPU for computing capacity [**14**].

In metro networks, main requirement are low cost because signals are WDM between 10G and 25G with a limited range of 50 km, as tipical values [**13**].

2.3. Physical topologies for the metro network

The physical topology of a network is defined by the way the nodes are physically connected to each other. There are many types of architectures considered for metro networks, such as meshed, chains and horseshoes.

In Fig. 2.2, two usual topologies used in metro networks, the ring and horseshoe topologies are represented. The metro network infrastructure usually comprises ring physical topologies interconnecting the nodes, with one or two nodes attached to the core.

Another topology, known as the horseshoe topology is also being used for MAN networks [**11**], [**15**]. This topology, represented with more detail in Fig. 2.3, is also referred as an open ring topology, since there are two nodes connected to the core network [**10**],

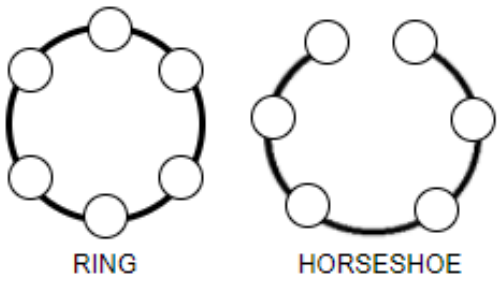

FIGURE 2.2. Physical topologies examples.

includes several intermediate metro-access node points, known also as tributary nodes and represented by N1, in Fig. 2.3. Each node N1 usually includes a connection leading to an array of local Transmitter (Tx) and Receiver (Rx) and corresponds to the interface between the access network (client) and the metro network [**11**]. The wavelengths added and dropped, which are necessary for the communication between the network and clients, take place at these nodes. In addition, these nodes are connected to central nodes of the metro network, known as hub nodes that are represented by N2 in Fig. 2.3, which are colocated with a transport network optical node.

The function of nodes N2 is to interface and provide connections between the nodes N1 and the metro-core nodes and ensure the downlink and uplink directions in the horseshoe network. The downlink represents the transmission from N2 to N1 and the uplink direction represents the data transmission from N1 to N2. To implement these downlink and uplink communications, two unidirectional fibres are typically used [**9**]. So, the network represented in Fig. 2.3, comprises two metro-core edge nodes having a node degree of five and four access-metro edge nodes having a node degree of two, allowing a ring-meshed metro network topology [**3**]. In section 2.4, the operation of the nodes N1 and N2 is described with more detail, considering different types of node architectures.

The main difference between the horseshoe and ring network is in the communication of the nodes N2 and its communication with the link to the core network. The horseshoe network, as it is open, is similar to a chain network. In a ring network, only one node in the core is connected to the metro network, whereas in a horseshoe network, two nodes N2 are connected. In the horseshoe network, the two nodes N2 communicate with the mesh network, i.e., with the network interface. The connection between N2-N2 does not follow the optical path of the entire network so that communication can take place on another network. These characteristics make it possible to introduce redundancy in the network and, therefore, in failure situations, it is possible to maintain communication. In

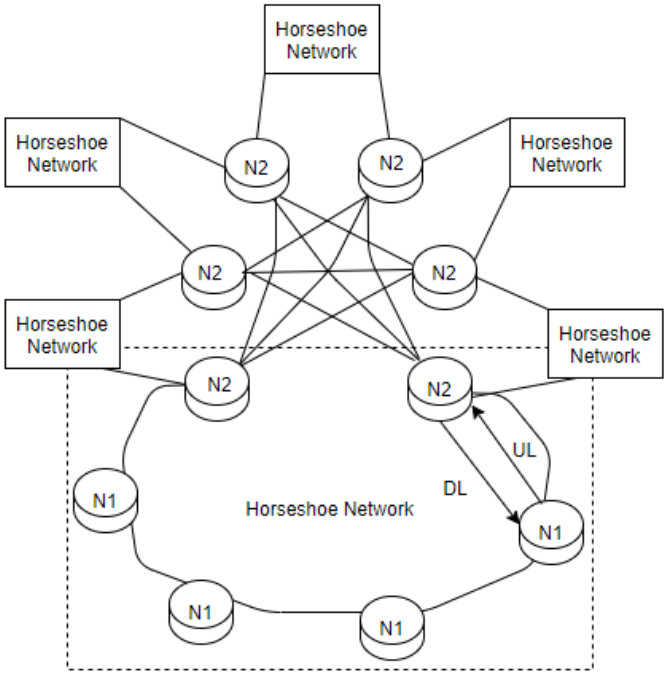

FIGURE 2.3. Example of a metro network composed by 6 horseshoe networks interconnected by a mesh network, where DL stands for downlink and UL stands for uplink [**3**].

ring networks, as only one node communicates with the other networks, in case of failure, the network is isolated and unavailable. In this work, we will consider only networks with horseshoe topologies.

2.4. C-band node architectures for the horseshoe topology

There are several node architectures typically used in horseshoe metro transports networks operating in the C-band: ROADMs, FOADM and FD&W [**11**], [**15**]. Fig. 2.4 shows a schematic of the networks with nodes using these different architectures. All the tributary nodes identified by N1 have the same configuration than the node N1 at the bottom of the horseshoe, where SC represents Splitter/Combiner (S/C), WSS represents Wavelength Selective Switch (WSS) and FF represents Fixed-Filter (FF). The wavelength channels from 1 to N represented in Fig. 2.4, are the channels to be added/dropped at each tributary node. In the following subsections, these different node architectures are described with detail.

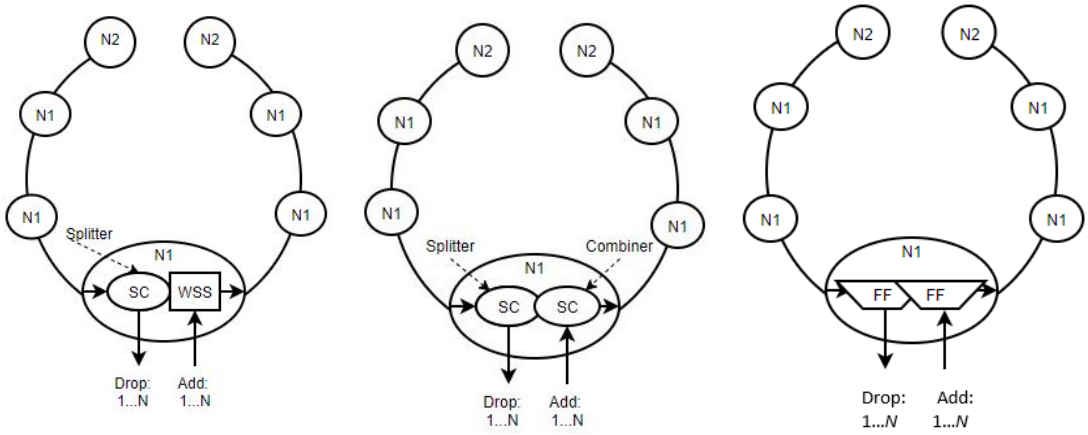

FIGURE 2.4. Examples of a horseshoe network with five tributary nodes N1 and two hub nodes N2, with different nodes architectures: (a) B&S ROADM; (b) FD&W and (c) FOADM.

2.4.1. ROADM-based node architectures

The ROADMs nodes are able to increase network flexibility as required by the growth of traffic in optical networks. In ROADM-based node architectures, each tributary node express structure is typically based on the B&S architecture, composed by an input stage of S/C, represented as SC, followed by a WSS, as shown in Fig. 2.5 (a). This allows the system to freely use the wavelengths to be added/dropped or expressed by the nodes N1 (represented by *A*, *B*, *C*, *D* and *E* in Fig. 2.5 (b)). In ROADM-based networks, it is possible to reuse wavelengths in different links, as depicted in Fig. 2.5 (b), where the same wavelength (for example λ_1) is used for several paths inside the horseshoe topology, such as between nodes *F* and *B*, *B* and *C* and *C* and *D*. Hence, this node architecture allows an "any-to-any" connection between nodes with full frequency reuse [**15**], which means that any wavelength can pass through any node, even after being used on another connection. So, in Fig. 2.5 (b), each hub node of the network can communicate with the remaining five tributary nodes of the network and each tributary nodes communicate with the remaining 6 nodes of the network, making up to fourty possible communication paths for a network with 2 hub nodes and 5 tributary nodes. The B&S ROADM architecture is the node architecture of the three architectures depicted in Fig. 2.4 that provides greater flexibility and capacity to several traffic patterns, supporting a full mesh logical topology.

The ROADM nodes are typically organized in two structures, Add/Drop (A/D) structure and express structure. The A/D structure, as shown in Fig. 2.6, is typically based on WSSs or Multicast Switches (MCSs). The express structure routes the wavelengths

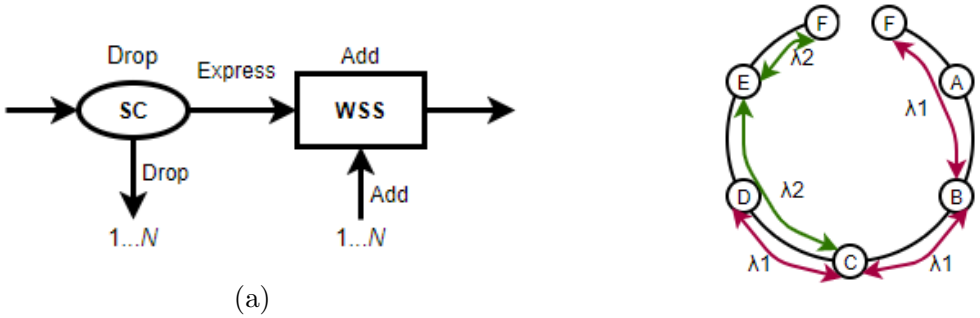

FIGURE 2.5. B&S ROADM-based horseshoe network with 7 nodes: (a) Express structure of a node N1 and (b) Example of wavelength assignment showing the frequency reuse possibility in these networks.

from the inputs to the outputs ports. The express structure can have mainly two types of architectures, the B&S and Route and Select (R&S) [**16**]. In a B&S architecture, all ROADM degrees (which are the ROADM inputs/outputs or directions) have an input stage composed by an S/C (component A) and an output stage (component B) composed by a WSS, as in the case of Fig. 2.5 (a). In a R&S architecture, the main difference in is that component A is a WSS, instead of a S/C.

In a B&S architecture, the signal passing through the node suffers less filtering than in a R&S, being the B&S more suitable for networks where the optical signal passes through a higher number of nodes, compared to networks with the same number of nodes, but where R&S architecture was implemented.

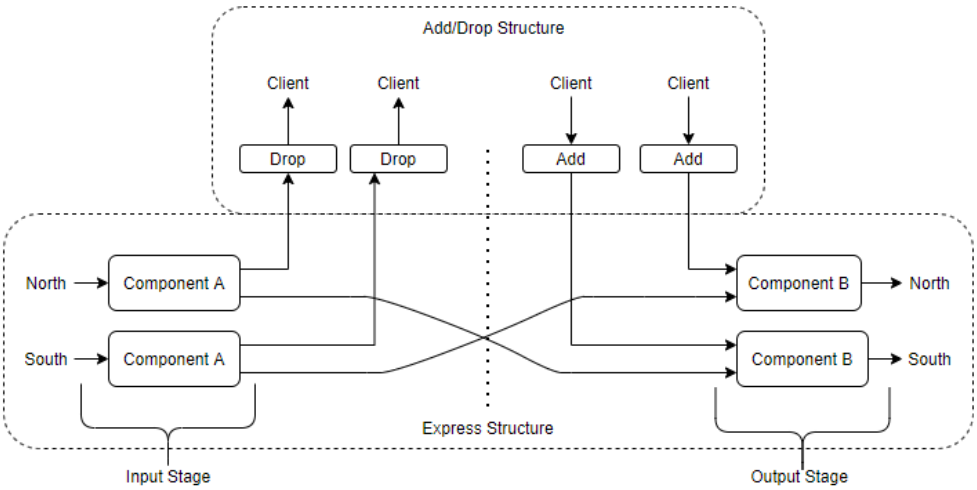

FIGURE 2.6. Generic 2-degree ROADM structure.

The ROADM components for the B&S and R&S architectures are described with more detail in the following [**17**]:

- Optical S/C: this element works in two different ways, depending on the direction of transmission. If it works as a splitter, it receives an optical signal at its input and splits its power equally into a specific number of outputs. In the other direction, it works as a combiner, which receives multiple optical signals and merges them into the same output.
- WSSs: Being the most important component of the ROADMs, this component is the combination of Optical Switch (OS) and multiplexers/demultiplexers MUXs/DEMUXs. Nowadays, Liquid Crystal on Silicon (LCoS) it is one of the most used technologies used to implement WSSs [**12**],[**18**]. Three different types of WSSs can be implemented [**18**]:
  - $1 \times M$ WSS: it receives a signal at its inputs and each WDM signal wavelength can be selected to a certain output M. An example of a 1×4 WSS structure is shown in Fig. 2.7.
  - $N \times 1$ WSS: N WDM signals are received at their inputs and the desired wavelengths are selected to its output. It corresponds to Fig. 2.7, but working in the reverse direction.
  - $N \times M$ WSS: Works like the previous WSS, but in this case, the N WDM signals are selected to the desired M outputs.

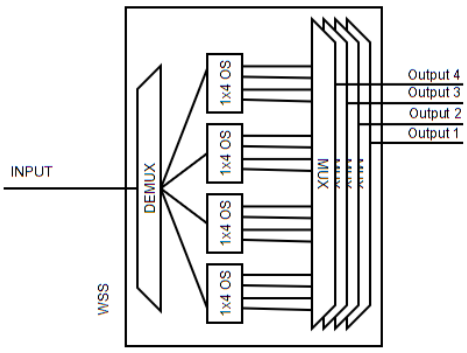

FIGURE 2.7. WSS 1×4 diagram.

The ROADM nodes have the important function of adding or dropping wavelengths to the client networks, besides routing optical signals [**19**] and, thus, it is important to describe and understand the several solutions that exist for these nodes in a horseshoe network. The characteristics of the A/D structure have evolved along time, according to the flexibility desired in a network. In the first generation of A/D structures, each port was set to operate in a certain fixed wavelength, being these structures called colored [**20**].

Eventually, with the network evolution to a more dynamic environment, this colored property became a huge limitation. By substituting the Arrayed Waveguide Grating (AWG)s by WSSs in the A/D structure, the previous limitation was overcome, providing a Colorless (C) solution, because it became possible to add or drop any wavelength in any port of the ROADM A/D structure.

Another property of the ROADM A/D structure, called Directionless (D), is related to the need to redirect any input signal from one direction to any ROADM output direction. It is possible to have a ROADM with A/D structures in all directions, but this is only required if there is the need to add or drop two or more optical signals with the same wavelength in the same A/D section [**21**]. In order to avoid wavelength contention inside the ROADMs, the A/D structures must be Contentionless (Cl), which defines another property of a ROADM-based node architecture. Nowadays, the most used structure to build Colorless, Directionless and Contentionless (CDC) ROADMs are the $N \times M$ MCS [**22**], but WSS are also being considered for building these A/D structures [**23**], [**24**].

In this work, we have considered 40 wavelengths per fiber and an add/drop ratio of 20% in each node N1 [**3**]. This means that, per direction, must be an A/D structure that is capable of adding or dropping 8 wavelengths.

$$Number_(Tx/Rx) = A/D_{ratio} \times N_{Ch} \times R \tag{2.1}$$

In Equation (2.1), $\mathrm{A/D}_{ratio}$ represents the A/D ratio, N_{Ch} represents the number of wavelengths per direction reaching the node and R represents the number of directions to consider for each node. In a horseshoe network, each node N1 is connected to 2 directions, being R=2, which means that the A/D structures should be connected to a total of 16 Tx and 16 Rx, respectively.

In Figs. 2.8 and 2.9, the structure of N1 B&S nodes is represented, respectively, for a ROADM C solution and a ROADM Colorless and Directionless (CD) solution. In this way, for the C solution, there are no fixed wavelengths assignments in the A/D structure [**20**], which means any wavelength can be added or dropped at any port. The main difference between the C and CD solutions lies in the fact that the WSSs before the Rx and the S/C after the Tx allow to redirect any particular wavelength to any of the ROADM directions.

Two more solutions for node N1 are studied in this work for ROADM-based networks. Although, in horseshoe networks these solutions are not usually implemented, they have been considered in this work. This ROADM node architecture is presented in Fig. 2.10,

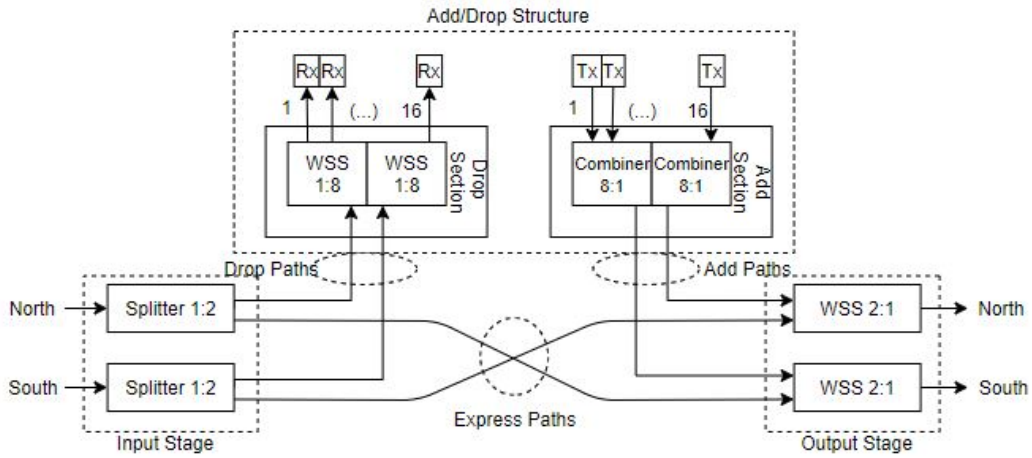

FIGURE 2.8. 2-Degree C ROADM B&S structure.

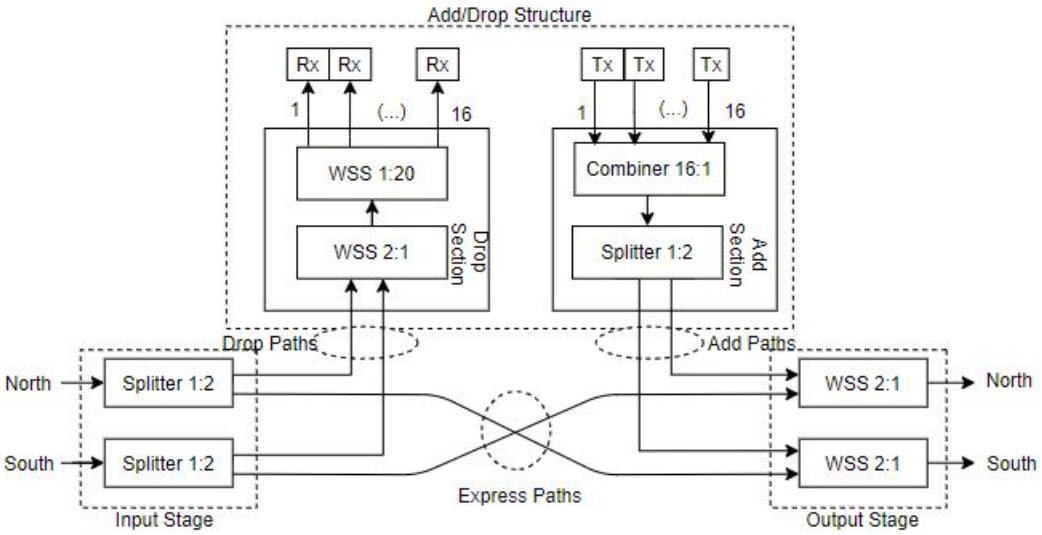

FIGURE 2.9. 2-Degree CD ROADM B&S structure.

which shows a single A/D structure with CD functionality and the ability to add and drop multiple instances of the same wavelength, or color inside the same A/D structure adding the contentionless functionality. In this case, it is possible to use a component known as "$N \times M$ WSS", which is composed by one array of OS, and an array of WSSs. Therefore, in this solution, N corresponds to the number of Tx/Rx and, then, to the number of OS and M to the number of ROADM directions, which also corresponds to the number of WSS in the A/D structure [**12**].

In Fig. 2.11, it is shown the "Mixed" solution, which allows to consider a fixed assignment of wavelengths (colored) or a variable assignment (colorless) inside the A/D

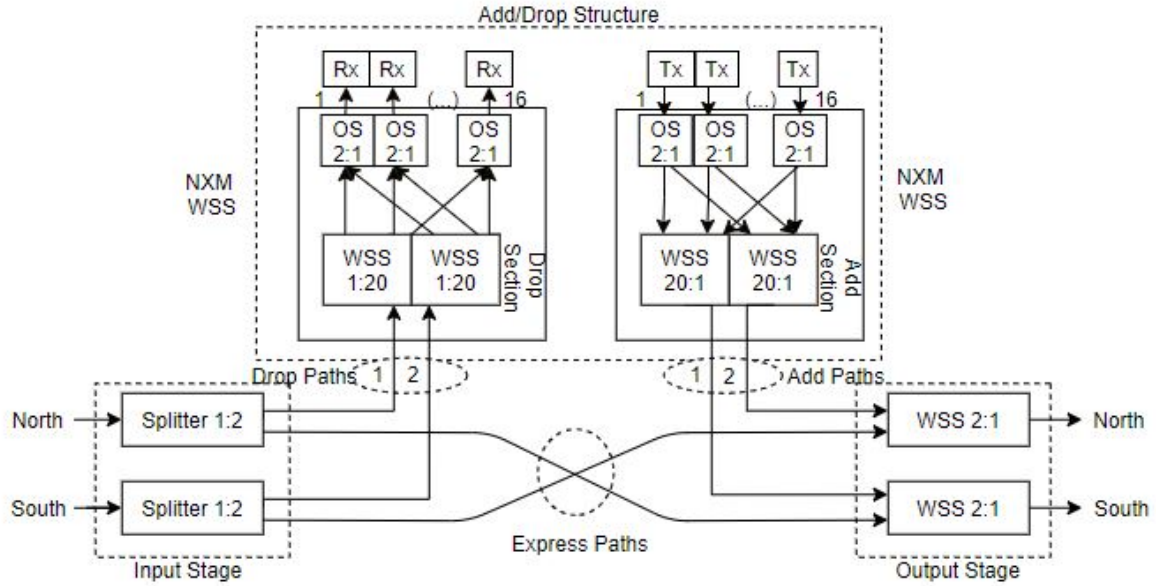

FIGURE 2.10. 2-Degree CDC ROADM B&S structure.

structure [**3**]. It gives the possibility to choose the signal connectivity at the optical layer between MUX/DEMUX or WSS depending on the network planning.

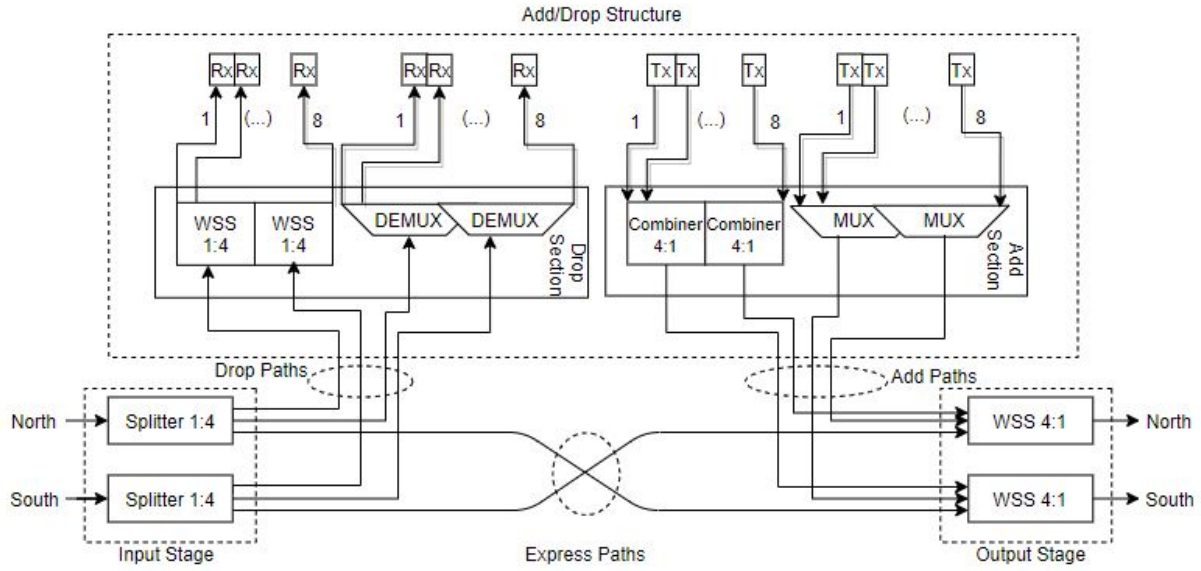

FIGURE 2.11. 2-Degree Colored and Colorless ROADM B&S structure.

All four options for N1 ROADM B&S nodes: C, CD, CDC and mixed solution can be also implemented using a R&S architecture. The only difference in Figs. 2.8-2.11 is in the input stage, where instead of broadcasting the input optical signal with S/Cs 1:4, there is a selection of the signal using a route WSS 1:4 at the ROADM input.

2.4.2. FOADM-based node architectures

In FOADM-based node architectures, which is the legacy solution, the wavelength plan is fixed, as exemplified in Fig. 2.12 (b). In this figure, each color corresponds to a different wavelength [**11**], i.e., if green line corresponds to λ_{36}, the purple line must be λ_{37}, and so on.

The available C-band spectrum is distributed to connections between each tributary node N1 (represented by *A*, *B*, *C*, *D* and *E* in Fig. 2.12) and the hub nodes N2 (represented by *F*), so that the nodes closer to the hub require less spectrum to transmit the same capacity than nodes further away, because of the distance, by using higher order modulation formats [**11**]. Moreover, considering 40 wavelengths per fibre and a A/D ratio of 20%, a common portion of the spectrum, represented by the wavelength range between λ_1 and λ_{35}, is saved for the connections between adjacent neighbours, as depicted in Fig. 2.12 (b). This wavelength assignment allows logical connectivity between tributary nodes to occur in two different ways: i) between two arbitrary non-adjacent nodes, that is routed through the central hub N2 and ii) between adjacent nodes, using the common portion of spectrum [**10**]. The wavelengths used between *F* nodes and nodes of N1 type are different from the wavelengths used between nodes of type N1. In this case, just 5 of total wavelengths are reserved for connections between nodes *F* and nodes of N1 type.

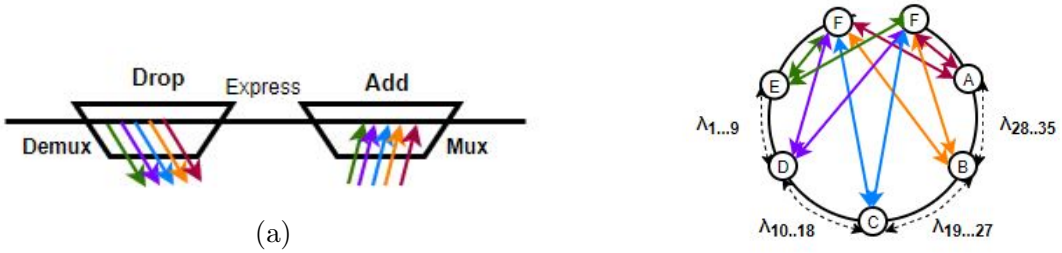

(a) (b)

FIGURE 2.12. FOADM: (a) Example of a node N1 function and (b) Example of wavelength assignment in FOADM-based metro networks.

Since transmissions between neighboring nodes are considered, the logical topology becomes a mesh logical topology, so it should be the one considered, because these transmissions are possible as long as there is spectrum allocated for this purpose.

The A/D structure of this component consists of a MUX/DEMUX, which has the function of multiplexing/demultiplexing WDM signals, with fixed assignment of wavelengths. Each wavelength is sent to a specific output port, for a MUX/DEMUX with 4

wavelengths selection capability. The AWG is the most used technology to implement this device, which are capable of multiplexing many wavelengths into a single optical fibre.

In Fig. 2.13, the schematic of a node N1 with a FOADM architecture considering the same parameters as the ROADM B&S node described in section 2.4.1, is shown. This structure has two DEMUX/MUX in each express structure, enabling a colored solution by the transmission of fixed wavelengths to each A/D port. For each DEMUX/MUX, 30 wavelengths can be expressed, because an AWG with 40 inputs/outputs is being considered [**3**]. Only 8 fixed wavelengths can be added/dropped by node direction.

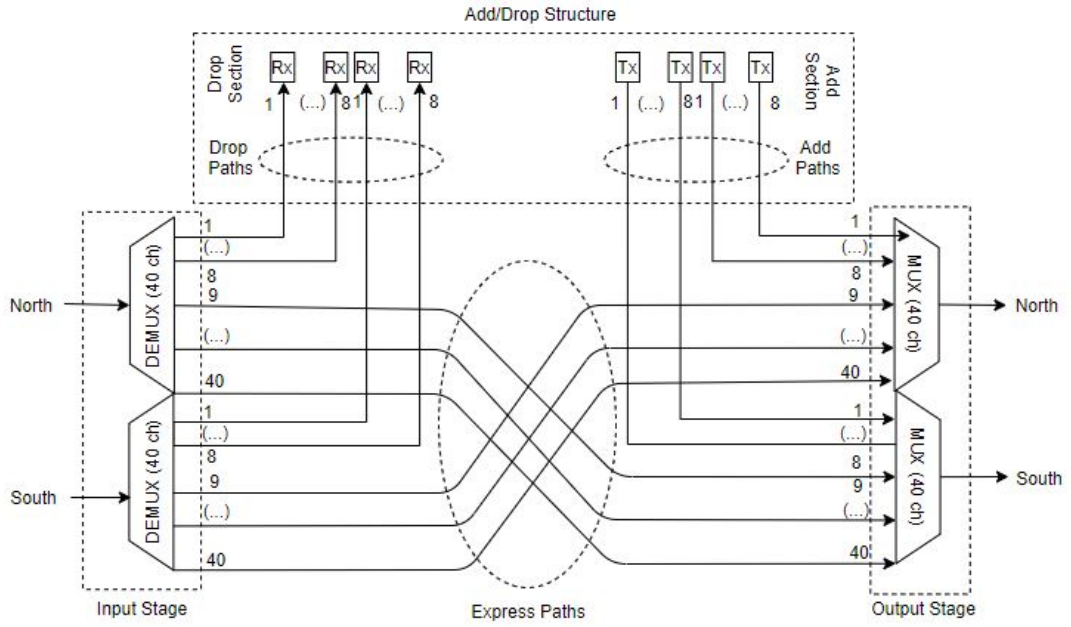

FIGURE 2.13. 2-Degree FOADM structure.

2.4.3. Filterless drop and waste-based node architectures

The FD&W node is shown in Fig. 2.14 (a). In this case, the network nodes are composed solely by S/C. So, each node receives the assigned wavelengths and then, they are split to both the express and A/D ports. Each wavelength is used only once in the whole ring, allowing an "any-to-any" connection without frequency reuse [**15**], i.e., since a wavelength used in a particular link, it will not be reused in any other link of the network, until it is extracted from the network by nodes N2 (represented by F in Fig. 2.14 (b)). For example, the purple wavelength allocated to the link between F and B in Fig. 2.14 (b), is not reused in the link between B and C, although it remains in the network until it is extracted.

In this solution, it is assumed that the hub nodes are the only nodes with wavelength selection capability, implemented through WSSs. So, each wavelength is used only once in the network and then it is filtered and eliminated from the horseshoe network by the hub node. Therefore, this solution has been proposed to reduce the nodes N1 cost in comparison with the solutions with ROADM or FOADM nodes [**10**].

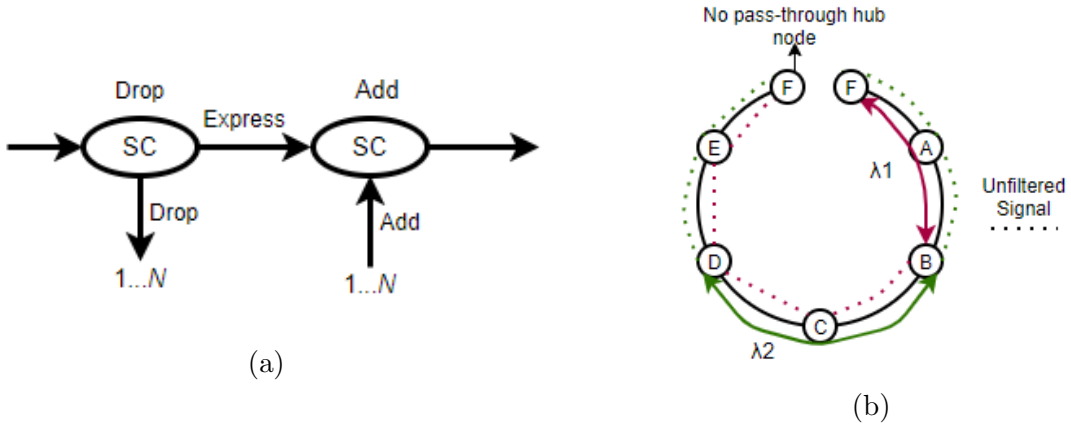

FIGURE 2.14. Filterless D&W: (a) Example of a node N1 and (b) Example of wavelength assignment in FD&W-based metro networks. The unfiltered signals (dotted lines) represent the wavelengths that cannot be reused between that specific pair of nodes.

For the characterization of the node N1 with the filterless architecture, the possibility of Coherent Detection (ChD) or Direct Detection (DD) in the Rxs must be considered. The ROADM and FOADM node solutions discussed in the previous section can work with both detection solutions. The ChD solution for the filterless node, shown in Fig. 2.15, uses a Local Oscillator (LO) at the Rx and the optical Rx can perform the selection of a wavelength channel from the whole WDM signal. The DD filterless solution, shown in Fig. 2.16, has a photodetector in the optical Rx which has no filtering capability.

2.4.4. ROADM-based node architectures for the hub node

The node N2 is a ROADM node, with a 5-Degree R&S architecture [**3**], and is represented in Figs. 2.17, 2.18 and 2.19, for, respectively, a C, CD and CDC solutions. For these nodes, it is considered a number of 80 wavelengths added and dropped per fibre and a 20 % A/D ratio [**3**]. The C solution presented in Fig. 2.17 is similar to the C ROADM B&S shown for the node N1 in Fig. 2.8, generalized for 5 directions.

The CD solution, shown in Fig. 2.18, shows a similar structure to the node N1 with a ROADM R&S CD. Nevertheless, it differs from the previous one in having 16 Rx/Tx per direction. As WSSs with maximum dimension of 1:20 are considered [**3**], it is necessary, in

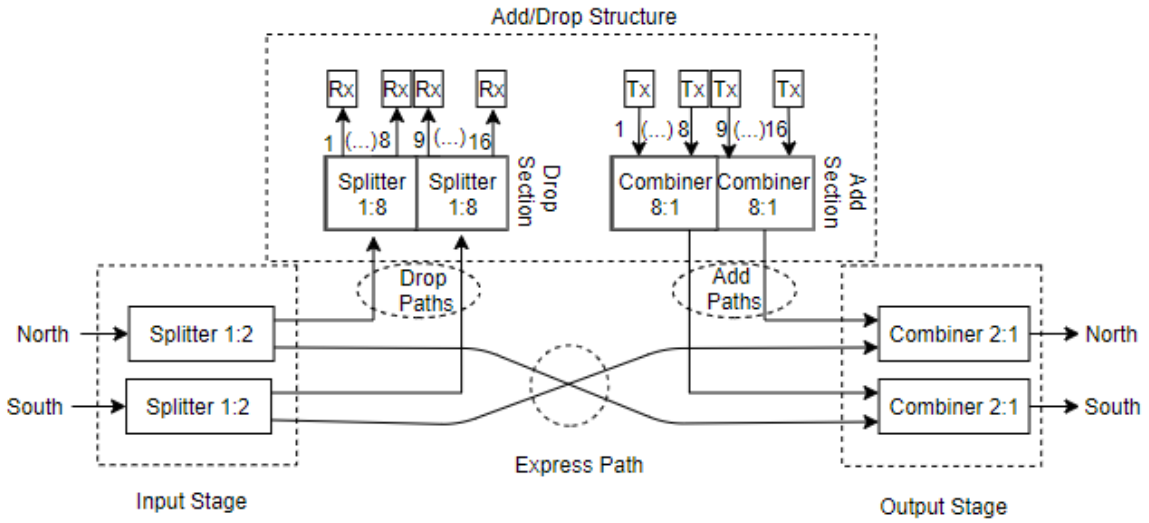

FIGURE 2.15. 2-Degree FD&W ChD structure.

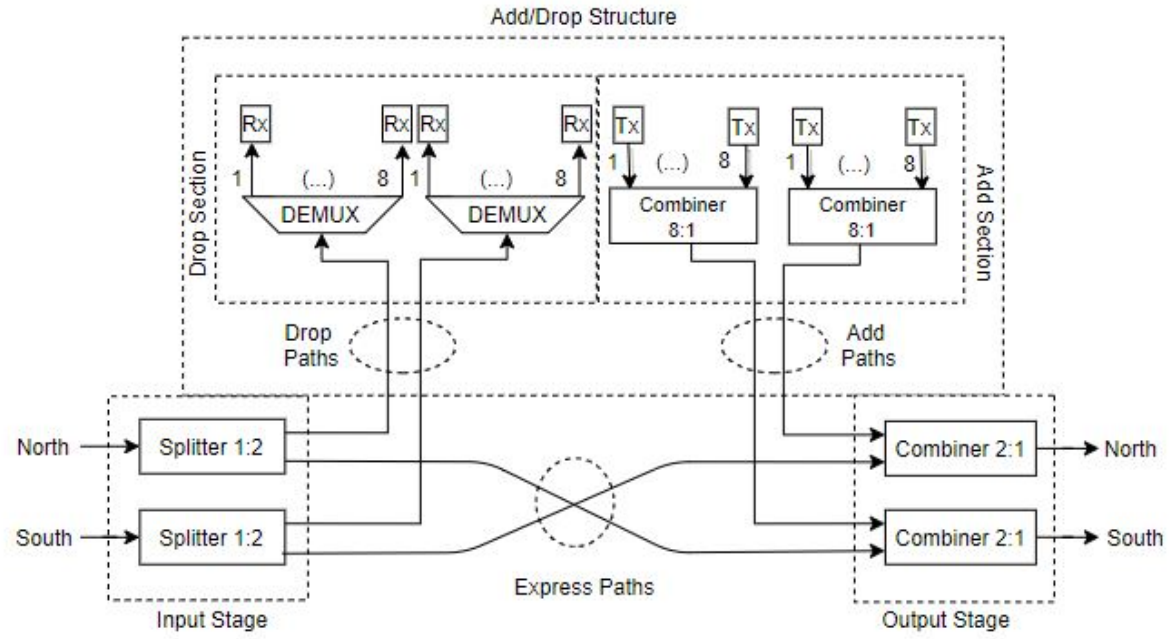

FIGURE 2.16. 2-Degree FD&W DD structure.

the A/D structure to use 4 A/D cards to achieve a total of 80 added/dropped wavelengths, using a 20% A/D ratio. Both A/D structures contains a WSS and a S/C connected by a single path causing contention between the two structures because only one WDM signal can be sent at a time. All inputs and outputs of the input/output stage structures are occupied, 4 for the express structure and the remaining 4 are occupied for the add/drop structure for each car, making a total of 8 filled channels by each WSSs.

The CDC solution must be implemented using 8×24 WSSs, as the maximum size of these elements is 8×24 [**12**]. So, 4 A/D cards in the A/D structure are required once

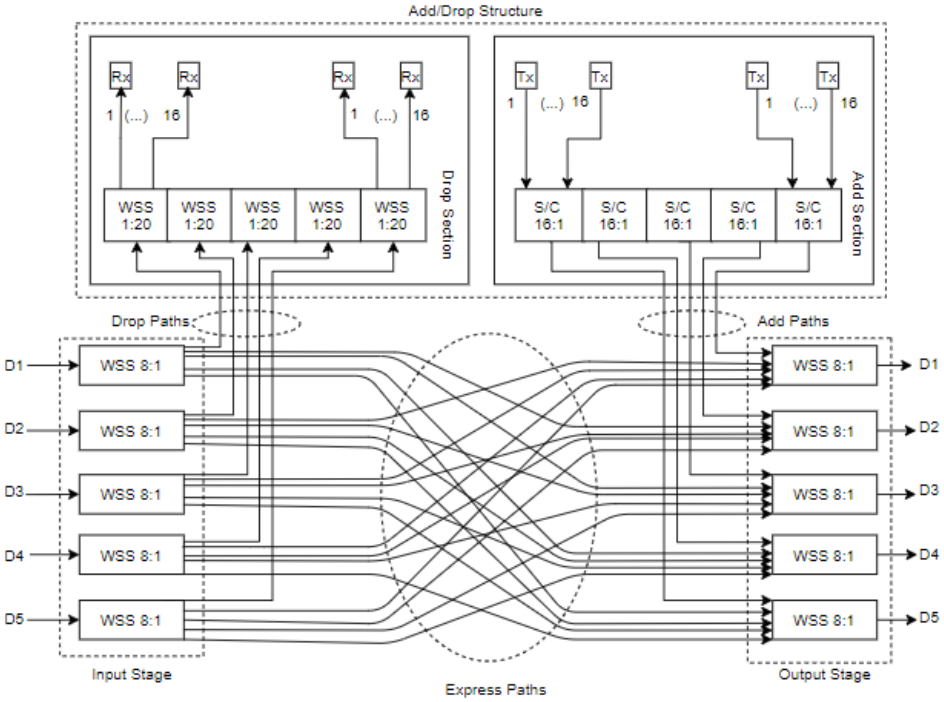

FIGURE 2.17. 5-Degree C ROADM R&S structure.

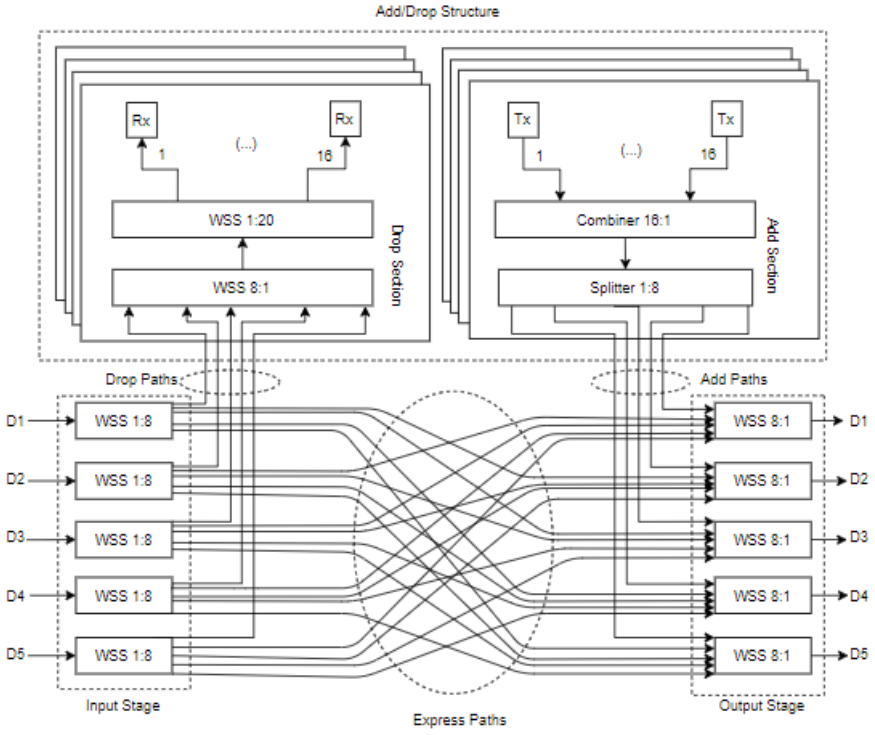

FIGURE 2.18. 5-Degree CD ROADM R&S structure.

again, because there are 16 signal being added or dropped on each card per fibre. Thus, each A/D stage, there are 3 inputs/outputs of the WSSs 1:8 and 6 OS inside each A/D card that are not connected. For hardware counting purposes, a 8×24 WSS is constructed with 8 WSSs interconnected with 24 OSs, as shown the example of drop structure in Fig.

2.20 [**12**]. So, A/D structures based on WSSs have wavelength selection capability, The schematic model for the add structures is the same as the one shown in 2.20, just to be noted the direction of the data flow, when a signal is added to the network.

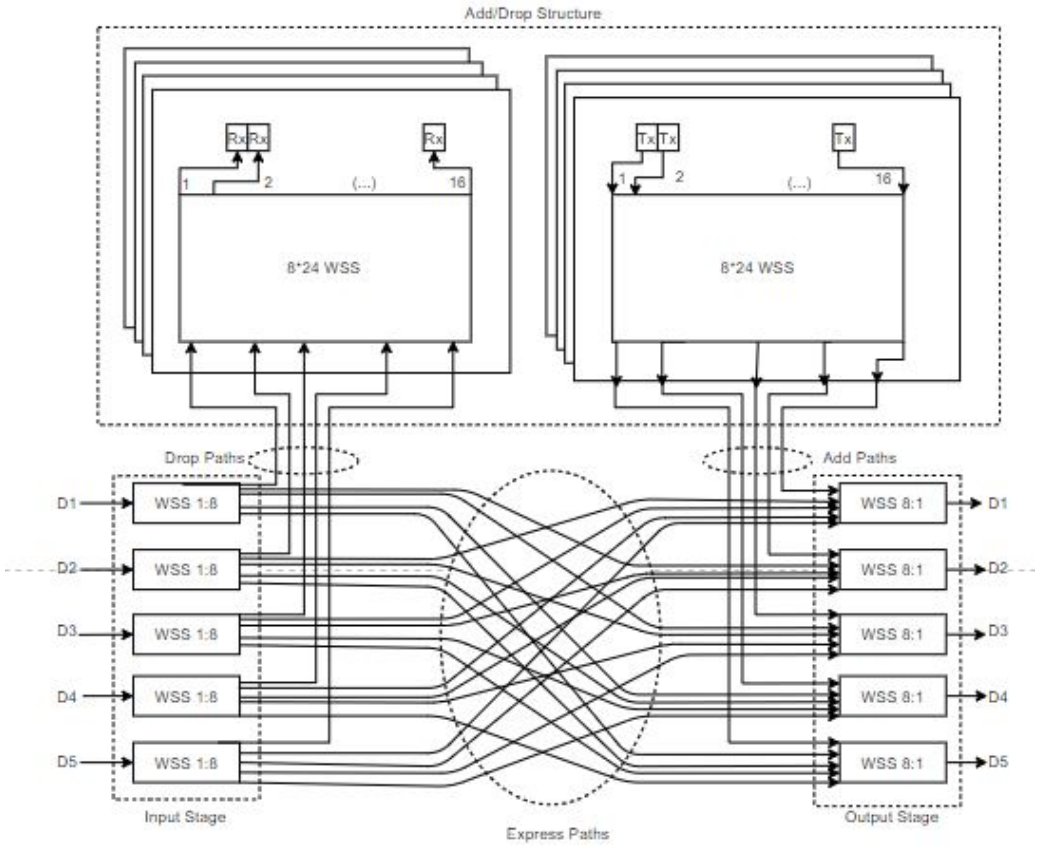

FIGURE 2.19. 5-Degree CDC ROADM R&S structure.

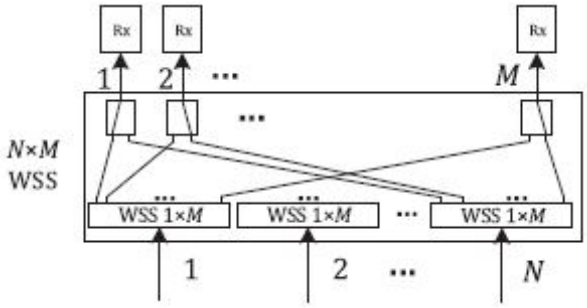

FIGURE 2.20. Drop structures of a CDC ROADM R&S based on $N \times M$ WSSs.

2.5. Comparative analysis of hardware cost and power consumption

An analysis regarding the number of components involved in each of the metro network solutions described in section 2.4 is performed in this section. he associated cost, assuming

an end of life scenario, and power consumption of each solution are also estimated, as well as the capacity of each node of the network.

The number of optical components to be considered in a network with eleven nodes per each horseshoe network, as considered in [**3**], similar to the one shown in Figure 2.4, where two of the nodes are the hub nodes which make the interface with the core network and the other nine nodes are tributary, is presented in Table 2.1, considering all the node architectures presented in sections 2.4.1, 2.4.2 and 2.4.3. For each architecture, the associated power consumption and cost are shown being the cost normalized to the cost of a 10 Gbps transponder, whose price is around 330 € [**3, 25**].

The cost of the S/C 1:2, S/C 1:4, S/C 1:8, WSS 1:4, WSS 1:20, MUX/DEMUX 80-Channels and the three transponders: flexible 200 Gbps Bandwith Variable Transponder (BVT), 10 Gbps transponder and 100 Gbps coherent are taken from Tab. 2 in [**3**]. For the components WSS 1:2, S/C 1:16, 40-channel MUX/DEMUX, the values presented in Tab. 2.1 are set to half the cost and consumption of the WSS 1:4, S/C 1:8 and 80-channel MUX/ DEMUX, respectively. In the case of WSS 1:8, as the cost and power consumption for WSS 1:9 are known, the same values are considered. In the case of the 8-channel MUX/DEMUX, its cost is determined proportionally the cost of the 80-channel AWG. The optical switches considered are 1×2 Micro-Electro-Mechanical Systems (MEMS) [**26**] and their normalized cost is assumed equal to the WSS 1:2 cost. Their power consumption is calculated from the multiplication between the electrical voltage (15 VDC) and the eletrical power (300 mA), given in [**26**], giving a maximum power consumption of 4.5 W, for the worst case. In the case of Optical Amplifier (OA)s, we consider the Erbium-Doped Fiber Amplifier (EDFA) dual-stage presented in [**3**], with a power consumption of 33 W and a normalized cost of 0.3 because it is divided by a booster and a pre-amplifier, which is not considered. Notice that optical switches are only used in CDC ROADM architectures.

The type of transponders should be suitably chosen for each node architecture. They can be fixed, if they only have the capacity to receive and transmit on a fixed wavelength, or tunable, when their receiving/transmitting wavelength can be adjusted. For the cases of FD&W ChD and FOADM, 100 Gbps coherent transponder, shown in table 2 of [**3**] are chosen, because they are fixgrid transponders more suitable for FOADM nodes that work with fixed wavelengths and FD&W ChD. For the ROADMs, the flexible 200 Gbps BVT has been chosen because this transponder is typically used in networks with small dimensions [**3**] and allows the use of 100 Gbps QPSK, 150 Gbps 8QAM and 200 Gbps

16QAM, while keeping the bit rate, respectively. For FD&W DD, the 10G transponders have been chosen.

Considering all possible nodes architectures for the construction of the horseshoe metro network and the respective number of components required, it is possible to estimate the cost and power consumption per node, as shown in the bottom of Tab. 2.1, and the total cost of the horseshoe network with 2 hub nodes and 9 tributary nodes as shown in Tab. 2.2. Notice that Tabs. 2.1 and 2.2 show also results for networks with nodes N1 having a R&S architecture, which were only briefly described in section 2.4.1.

The total capacity per fiber, in Tbps, is determined from the number of WDM channels passing through the node and the transponder capacity chosen for each architecture. For the nodes N1 and N2, 40 and 80 WDM channels are considered, respectively. FD&W DD nodes deliver a capacity per fiber of only 0.4 Tbps, FOADM nodes and FD&W ChD reach capacities of 4 Tbps, while ROADM nodes reach a higher capacity of 8 Tbps. The node N2 leads to a total fiber capacity of 16 Tbps. The total capacity per node, considering the A/D ratio of 20%, is of 0.16, 3.2 and 1.6 Tbps for, respectively, FD&W DD, ROADM and FD&W ChD and FOADM. For the case of N2 nodes, the average capacity per node is achieved by considering 64 transponders $\times$ capacity of the transponder $\times$ 2/5 (considering the two N1 nodes connections) plus 64 transponders $\times$ capacity of the transponder $\times$ 3/5 (considering the three connections to other three N2 nodes), and is equal to 12.8 Tbps. This values are calculated from the multiplication between the number of transponders and the transponders symbol rate (for N2 node we consider 100 Gbps).

Most of the networks presented in Tab. 2.2 have a similar cost, because the hardware component that most contributes to the cost and power consumption is the transponder. As can be seen in the Tab. 2.1, for networks whose nodes have ROADM-based architectures, the transponders represent 98% of the total node cost, in a total node cost of approximately of 133. Only for the CDC ROADM B&S/R&S architectures, the cost is also slightly influenced by the use of optical switches, with a cost of 13% of the total node cost, approximately. For nodes N2 C and CD, the transponders contribute for 63% of the total node cost.

For a network with a number of 9 nodes N1 and 2 nodes N2, the configuration with the best combination of cost and consumption (the lowest cost and lowest power consumption) is the FD&W DD combined with a C ROADM R&S nodes N2, with a normalized cost of 1.77 k and a total power consumption of 32.9 kW, as can be seen in Tab. 2.2.

For all networks architectures using the same number and type of transponders, the network topology is more expensive and consumes more power when there are more WSS in its configuration. Therefore, it is possible to see that the ROADM B&S-based network with nodes N1 either, C, CD or CDC, is cheaper and less power consuming than the corresponding ROADM R&S-based network, although the difference is minimal, due to the cost burden of the transponders. The ROADM-based networks have very similar costs (between 3.4 k and 3.6 k) and power consumption values. The most expensive network is the one that consumes the most power, with a normalized cost of 3.6 k, is the network consisting of 9 N1 CDC ROADM R&S nodes and 2 N2 CDC ROADM R&S, with a power consumption of 110.6 kW and the network consisting of 9 N1 CDC ROADM B&S nodes and 2 N2 CDC ROADM R&S, with a cost normalized of 5.8 k and 48.9 kW. It can also be concluded that the FOADM and FD&W ChD architectures have approximately the same cost and the FD&W DD architecture is the cheapest. However, it is cheaper at the cost of much less capacity. For any of the networks, there are always 2 nodes N2, which are quite costly because they have a CD ROADM R&S architecture and therefore have a lot of components inside, as depicted in 2.18. Note that the cost of fibre was not considered in the total cost of the network.

Fig. 2.21 shows the total normalized cost of a horseshoe network as a function of the number of nodes N1 considering three different horseshoe networks, one based on FD&W DD nodes N1, other on CD ROADM B&S nodes N1 and the third based on FD&W ChD, all three considering CD ROADM R&S nodes N2. In Fig. 2.21, the maximum and minimum cost values for each architecture, for 9 and 63 nodes, respectively, are also represented. The higher the number of nodes N1, the greater is the difference between the total network cost of the different architectures.

The CD ROADM R&S architecture for the nodes N2 is chosen because CD solutions are more typically in metro networks than CDC. Most of the cost difference is related to the type of transponders used in each architecture. It can be seen from Fig. 2.21, that the network cost growth with the increasing number of nodes for the case CD ROADM B&S is more significant. For the FD&W DD architecture, the total cost of the network does not increase significantly as the number of nodes N1 increases, being less than twice the cost of the same network with 10 nodes for 60 nodes N1. Hence, the cost of scalability of this network is very low. The FD&W ChD architecture is considered because it maintains a capacity similar to the ROADM architecture, decreasing the total network cost. In CD

TABLE 2.1. Hardware count, cost and power consumption of each optical component existing in the nodes N1 and N2 for the several node solutions. The total cost of the nodes N1 and N2 is shown at the bottom of the table.

Optical Components			**Number of components for each node architecture**															
			ROADM								Filterless D&W		N2 ROADM					
Name	Normalized cost	Power consumption [W]	ROADM B&S C	ROADM B&S CD	ROADM B&S CDC	ROADM B&S Mixed	ROADM R&S C	ROADM R&S CD	ROADM R&S CDC	ROADM R&S Mixed	FOADM	FD&W DD	FD&W ChD	C	CD	CDC
Optical Switch 1×2	0.55	4.5			32				32							192
S/C 1×2	0.004	0	2	3	2			1				4	4					
S/C 1×4	0.01	0				4				2								
S/C 1×8	0.02	0	2				2					2	4		4			
S/C 1×16	0.04	0		1				1						5	4			
WSS 1×2	0.55	25	2	3	2		4	5	4									
WSS 1×4	1.1	50				4				6								
WSS 1×8	2.2	75	2				2							10	14	10		
WSS 1×20	3	100		1	4			1	4					5	4	64		
MUX/DEMUX 8 Ch	0.08	0				4				4		2						
MUX/DEMUX 40 Ch	0.4	0									4							
MUX/DEMUX 80 Ch	0.8	0																
Optical amplifier	0.3	33	2	2	2	2	2	2	2	2	2	2	2	2	2	2		
Flexible 200 Gbps BVT	8	145	16	16	16	16	16	16	16	16				64	64	64		
10 Gbps transponder	1	77										16						
100 Gbps coherent transponder	5	120									16		16					
Normalized cost per node			134.15	133.3	159.3	133.4	135.24	134.39	160.4	135.5	82.2	16.82	80.7	805.8	811.64	1088		
Power Consumption per node [kW]			2.59	2.56	2.98	2.59	2.64	2.61	3.03	2.69	1.99	1.3	1.99	10.6	10.8	17.36		

TABLE 2.2. Network total cost and power consumption considering several node N1/N2 architectures for a horseshoe network with 9 nodes N1 and 2 nodes N2.

node N1	**Total Cost [k]**			**Total Pow.Cons. [kW]**		
	C N2	CD N2	CDC N2	C N2	CD N2	CDC N2
C ROADM B&S	2.8	2.8	3.4	44.5	44.9	58
CD ROADM B&S	2.8	2.8	3.4	44.2	44.6	57.8
CDC ROADM B&S	3.1	3.1	3.6	48	48.4	61.5
Mixed ROADM B&S	2.8	2.8	3.4	44.5	44.9	58
C ROADM R&S	2.8	2.8	3.4	44.96	45.4	58.5
CD ROADM R&S	2.8	2.8	3.4	44.7	45.1	58.2
CDC ROADM R&S	3.1	3.1	3.6	48.5	48.9	62
Mixed ROADM R&S	2.8	2.8	3.4	45.4	45.8	58.9
FOADM	2.4	2.4	2.9	39.1	39.5	52.6
FD&W DD	1.77	1.77	2.33	33.3	32.9	46.4
FD&W ChD	2.4	2.4	2.9	39.1	39.5	52.6

ROADM B&S, the node N1 cost represents between 35% and 43% of the total network whereas in the case of the FD&W ChD architecture, it represents only 25% and 30% with N2 C/CD nodes or N2 CDC nodes, respectively. This means that, for the FD&W ChD architecture, the N2 nodes represents the largest percentage of the network cost, which does not vary regardless of the number of nodes N1.

As previously mentioned, the network costs presented are obtained in relation to the cost of a 10 Gbps transponder, which is around 330 € [**3**], [**25**]. Hence, it is possible to predict the real cost of the horseshoe networks. With FD&W DD nodes N1 and CD ROADM R&S nodes N2, the total estimated cost of the network (for 9 N1 nodes) is around 584 k€. The total cost of the network with CD B&S ROADM nodes N1 and CD ROADM R&S nodes N2 is about 924 k€ and the total cost of the network with FD&W ChD nodes N1 and CD ROADM R&S nodes N2 is 792 k€. If the goal is to have an accessible metropolitan network with a high data capacity, the FD&W ChD architecture provides a good solution. If a higher flexibility metropolitan network is desired, then, the CD ROADM B&S solution for the nodes N1 is a preferable option.

2.6. Physical layer impairments impact in C-band metro networks

In this section, the analysis of some PLIs of the hardware components belonging to the nodes and of the overall network, such as ILs, ASE noise, filtering effects, crosstalk level and NLI noise is performed.

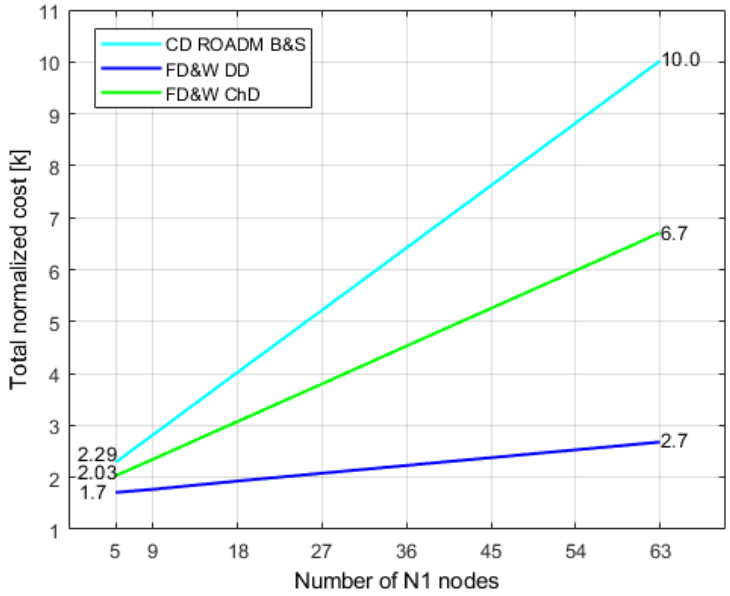

FIGURE 2.21. Total cost of a horseshoe network with two nodes N2 as a function of the number of nodes N1, for three architectures, CD ROADM B&S, FD&W DD and FD&W ChD.

The analysis will focus on the most feasible and cheaper horseshoe network solutions, CD ROADM B&S and FD&W ChD nodes N1, both combined with CD ROADM R&S nodes N2. The CD ROADM B&S solution is the most common solution for metropolitan networks and the FD&W ChD solution is the less expensive, while maintaining a capacity similar or very close to the first solution (as analyzed in Tab. 2.1). The FD&W DD solution will not be analyzed in this section because, despite having a very low cost, it is very limited in capacity as also presented in Tab. 2.1.

2.6.1. Insertion losses

The ILs of the components are physical impairments that must be carefully characterized because they have a strong influence on the amplifiers used in the network. Focusing on the two chosen architectures, the hardware components of the nodes N1, whose ILs are characterized, are S/Cs 1:2, 1:4 and 1:16 and WSSs 1:2 and 1:20. The nodes N2 are composed by S/C 1:8 and 1:16 and WSSs 1:8 and 1:20. The ILs introduced by the optical S/C 1:N are given by [**27**]:

$$IL_{S/C} = 10\log_{10}N + A_{exc} \tag{2.2}$$

where N is the number of inputs/outputs of the optical S/C and A_{exc} represents the excess losses. In the case of WSSs, the ILs considered are around 7 dB, independently of the number of WSS outputs, which is a typical value [**12**].

In Tab. 2.3, the ILs of each hardware component of the CD ROADM B&S nodes N1, FD&W ChD nodes N1 and CD ROADM R&S nodes N2 are presented.

TABLE 2.3. ILs of each component and the corresponding components quantity per node for nodes N1 with CD ROADM B&S, FD&W FD&W ChD architectures and N2 CD ROADM R&S node architecture.

Component		**N1 CD ROADM B&S**	**N1 FD&W ChD**	**N2 CD ROADM R&S**
Designation	ILs [dB]	#	#	#
S/C 1×2	4	3	4	-
S/C 1×8	11	-	4	4
S/C 1×16	15	1	-	4
WSS 1×2	7	3	-	-
WSS 1×8	7	-	-	14
WSS 1×20	7	1	-	4

Considering the node architectures presented in sections 2.4.1 and 2.4.3 and the ILs associated to each component presented in Tab. 2.3, it is possible to determine the total paths losses along the node. In this calculation, the losses of the connectors and splices are neglected. For each architecture, the ILs are assessed for the express, add and drop paths along the node and presented in Tab. 2.4. For simplicity, we assume that all fibre spans have the same length. We have considered two scenarios, 10 km and 60 km spans. For example, the 10 km scenario is predominant in the Italian metro-regional network [**13**], while the 60 km scenario, is considered as a worst case scenario. The fibre losses are presented in the last row of Tab. 2.4, for spans of 10km and 60km, calculated using the attenuation coefficient $\alpha = 0.22$ dB/km [**28**], [**29**].

After assessing the node and fibre span losses, we are going to assess the ILs along the worst case path in the horseshoe topology. We will consider that at the node input and output, there are EDFAs. The input amplifier (pre-amplifier, represented by the orange color in Fig. 2.22 (a)) compensates the fibre losses and the output amplifier (post-amplifier, represented by blue color in Fig. 2.22 (a)) compensates the node losses. Fig. 2.22 (a) shows the worst-case path along the horseshoe topology considering the pre-amplifiers and post-amplifiers. Note that for both node architectures considered, CD ROADM B&S and FD&W ChD, the worst-case signal path is from node A (where the signal is added) to node N2 (where the signal is dropped), passing through all the

TABLE 2.4. ILs of the node N1, for the CD ROADM B&S and FD&W ChD architectures and for the CD ROADM R&S for the node N2.

Node	**N1 CD ROADM B&S**	**N1 FD&W ChD**	**N2 CD ROADM R&S**
Add_{path} [dB]	S/C 1:16+S/C 1:2+WSS 1:2 15+4+7 = 26	S/C 1:8+S/C 1:2 11+4=15	S/C 1:16+S/C 1:8+WSS 1:8 15+11+7=33
$Drop_{path}$ [dB]	S/C 1:2 +WSS 1:2+WSS 1:20 4+7+7 = 18	S/C 1:2+S/C 1:8 4+11=15	WSS 1:8+WSS 1:8+WSS 1:8 7+7+7=21
$Express_{path}$ [dB]	S/C 1:2+WSS 1:2 4+7=11	S/C 1:2+S/C 1:2 4+4=8	WSS 1:8+WSS 1:8 7+7=14
10 km fiber [dB]	2.2		
60 km fiber [dB]	13.2		

remaining nodes N1. The total losses along each path are determined for this path, which has the longest distance in the network, as shown in Fig. 2.22 (a). The amplifiers gain is set to exactly compensate the losses, leading to a 0 dB gain at the EDFAs output. The post-amplifier gain is set to compensate the node higher losses, which occur in the add path (see Tab. 2.4), being 26 dB for the ROADM node N1 case and 11 dB for the FD&W ChD node N1. Variable Optical Attenuator (VOA) are inserted in the express paths, to ensure the same signal power level for all wavelengths at the node output, and ensure a 0 dB gain at the amplifiers output. So, for the worst path, the total network losses correspond to the add losses of one node N1, express losses of 8 nodes N1 and the drop losses of the nodes N2 taken from Tab. 2.4.

There is another possible worst path that corresponds to the signal insertion at node N2 and the signal extraction at node N1 represented by the letter *I*, as shown in Fig. 2.22 (b). In this case, the signal is added at the nodes N2, is transmitted along 8 nodes N1 and then removed at node *I*. The distance is the same, because spans with equal lengths have been considered. For this signal path, the total losses increase because the node N2 in Fig. 2.22 (a) exhibits higher losses than each node N1.

Based on Fig. 2.22 (a) and (b) and on Tab. 2.4, the gains of the pre and post-amplifiers along the network can be assessed in order to compensate the referred ILs. Higher overall network losses will demand amplifiers with higher gain to ensure exact loss compensation, leading to a higher ASE noise accumulation in N1 CD ROADM B&S-based networks. In cases of networks where only pre-amplification is used, the gains of the amplifiers of the N1 nodes must increase because they compensate the losses of the span and the node. The node N2 needs an amplifier with more gain due to the higher losses of the CD ROADM

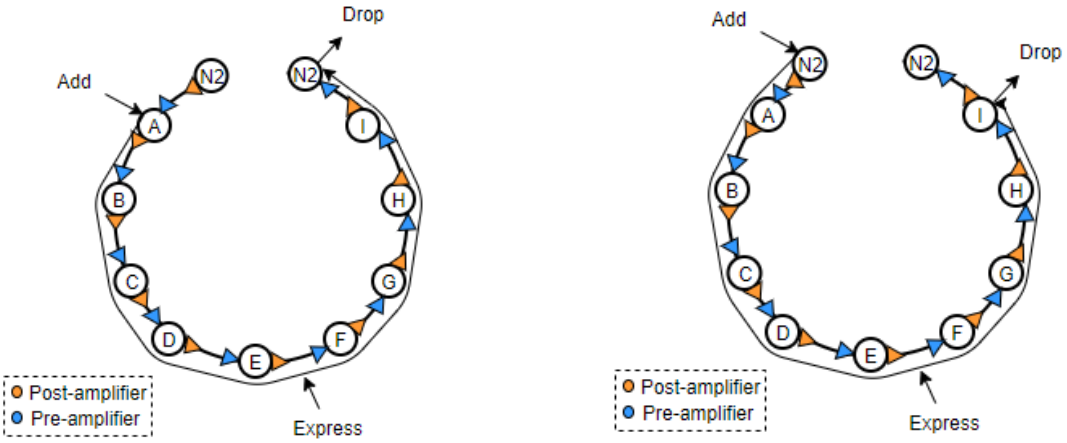

FIGURE 2.22. Signal route for the worst path (longest path) within a horseshoe network with 9 nodes N1 and 2 nodes N2 with pre and post-amplification. (a) With signal insertion at the first node N1 (denoted as A), and signal drop at the node N2. (b) With signal insertion at node N2 and signal drop at the last node N1 (denoted as I).

R&S architecture.

TABLE 2.5. Pre and post EDFA gains for cases with 10 km and 60 km spans, for the N1 CD ROADM B&S and FD&W ChD node architectures and N2 CD ROADM R&S node architecture.

Architecture Type	**N1 CD ROADM B&S**		**N1 FD&W ChD**		**N2 CD ROADM R&S**	
	10 km	60 km	10 km	60 km	10 km	60 km
$G_{pre,i}$ [dB]	28.2	13.2	17.2	13.2	2.2	13.2
$G_{pos,i}$ [dB]	-	26	-	15	33	33

2.6.2. Accumulation of ASE noise

The OA considered in this work is the EDFA, which can achieve around 30 dB of gain [**30**]. OAs are commonly used to compensate the path losses (pre-amplifiers) and power losses inside the nodes (post-amplifiers). However they lead to a system performance degradation by originating ASE noise [**31**].

The degradation induced by the ASE noise power is typically quantified by the Optical Signal-to-Noise Ratio (OSNR) given by [**31**]

$$osnr = \frac{p_{Rx}}{p_{n,ASE}} \tag{2.3}$$

where p_{Rx} is the average signal power at the optical Rx input and $p_{n,ASE}$ is the accumulated ASE noise power at the Rx input considering a horseshoe topology and considering the two polarizations, given by:

$$p_{n,ASE} = 2 \times \sum_{i=1}^{n_{spans}} [p_{ASE,pre,i} + p_{ASE,pos,i}] \tag{2.4}$$

where n_{spans} represents the number of spans, $p_{ASE,pre,i}$ represent the ASE noise power per polarization generated at each i-th pre-amplifier output defined by (2.5) and $p_{ASE,pos,i}$ represent the ASE noise power per polarization generated at each i-th post-amplifier output, defined by (2.6):

$$p_{ASE,pre,i} = \frac{f_{n,pre,i}}{2} \times (g_{pre,i} - 1) \times h \times \nu_0 \times B_o \tag{2.5}$$

$$p_{ASE,pos,i} = \frac{f_{n,pos,i}}{2} \times (g_{pos,i} - 1) \times h \times \nu_0 \times B_o \tag{2.6}$$

where $g_{pre,i}$ and $g_{pos,i}$, represent, respectively, the pre-amplifier and post-amplifier gains, $f_{n,pre,i}$ and $f_{n,pos,i}$, the corresponding EDFA noise figures, whose typical value is between 5 and 7 dB [**32**], h is the Planck constant = 6.6261×10^{-34} J·s, ν_o is the WDM central channel frequency and B_o is the reference optical bandwidth, which in coherent detection systems is typically equal to the symbol rate, $R_{s,l}$, calculated from

$$R_{s,l} = \frac{R_{b,l}}{2 \times \log_2 M_{symbols}} = \frac{R_{b,i} \times (1 + \rho_{FEC})}{2 \times \log_2 M_{symbols}} \tag{2.7}$$

where $R_{b,l}$ is the line bit rate, $R_{b,i}$ is the information bit rate, ρ_{FEC} is the FEC overhead and $M_{symbols}$ is the number of symbols used in the Quadrature Amplitude Modulation (QAM). Considering the transponders presented in Tab. 2.1, with QPSK modulation, 100 Gbit/s information bit rate [**3**] and a typical FEC overhead of 7% [**33**], the symbol rate is 26.75 Gbaud.

For the case study with 10 km spans, as it is possible to do exact loss compensation with pre-amplification only, we set $g_{pos,i}$=1 in (2.6).

From Eq. (2.4)-(2.6), the ASE noise power along the network is calculated for all EDFAs, with CD ROADM B&S and FD&W ChD architectures, 10 km and 60 km spans and signal insertion at node N1 and extraction at node N2, as shown in Fig. 2.23 (a), and signal insertion at node N2 and extraction at node N1, as shown in Fig. 2.23 (b). With the amplifier gains shown in Tab. 2.5, the ASE noise power generated at each amplifier in the network are shown in Tab. 2.6, for $f_{pre,i}$ = 6 dB, $f_{pos,i}$ = 6 dB and for

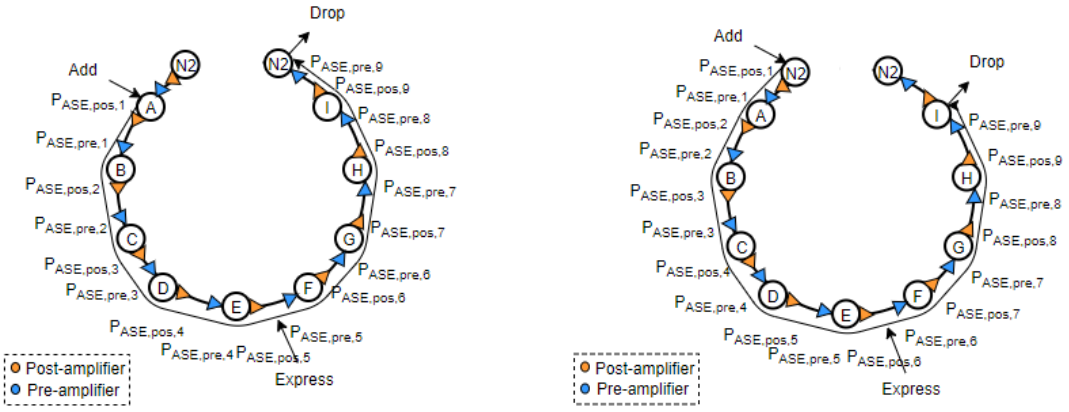

(a) (b)

FIGURE 2.23. Worst paths along the horseshoe topology with pre- and post-amplification: (a) Signal worst path with insertion at node N1 and (b) Signal worst path with insertion at node N2.

$\nu_0 = 194.1$ THz, as the nominal frequency of the WDM central channel, per polarization. The higher the amplifier gain, the higher the ASE noise power generated at the amplifier output. Therefore, pre-amplifiers in architectures without post-amplification lead to a higher ASE noise power than pre- and post-amplifiers in networks that compensate only, respectively, spans and nodes losses.

As shown in Tab. 2.6, in the case of architectures with pre- and post-amplification, the node N2 is the one that most contributes for the ASE noise power accumulation along the whole networks with 10 km and 60 km spans. For the N1 node architecture, the post-amplifier originates an about 12 dBm ASE noise power higher for N1 node CD ROADM B&S architectures than for FD&W ChD architectures. The corresponding OSNRs are calculated with Eq. (2.3), for P_{Rx} =0 dBm (in two polarizations), assuming exact loss compensation along the network, and the results are presented in Tab. 2.7.

TABLE 2.6. ASE noise power originated at each pre- and post- amplifier for 10 km and 60 km spans, for the N1 CD ROADM B&S and FD&W ChD node architectures and N2 CD ROADM R&S node architecture.

Node architecture	**N1 CD ROADM B&S**		**N1 FD&W ChD**		**N2 CD ROADM R&S**	
	10 km	60 km	10 km	60 km	10 km	60 km
$P_{ase,pre,i}$ [dBm]	-23.4	-34.5	-38.7	-38.7	-53.5	-38.7
$P_{ase,pos,i}$ [dBm]	-	-25.7	-	-36.8	-18.6	-18.6

Fig. 2.24 represents the evolution of the OSNR along the network nodes for (a) 10 km and (b) 60 km spans, and signal worst paths after insertion at node N1 or at node

N2. Figs. 2.24 (a) and 2.24 (b) shows that the OSNR is less harmful in networks with N1 FD&W ChD nodes due to lower gain amplifiers, because it reaches high OSNRs. When the node N1 has FD&W ChD architecture and the signal is inserted in the horseshoe at node N2 (pink line), the post-amplifier at the output of this node, due to its very high gain (33 dB), introduces so much ASE noise power, that along the network propagation, the ASE noise contributions originated at the nodes N1 practically do not contribute to the overall accumulated ASE noise. As shown in Fig. 2.24, for this case, the OSNR decreases only 0.5 dB from the first to the last node. Therefore, as the post-amplifiers N2 nodes must have a higher gain, these amplifiers should have a lower noise figure to increase the OSNR. Considering the signal insertion at the node N1, the OSNR decreases between 9.2 dB and 11.1 dB from the first to the last node, for both N1 node architectures and span lengths. When considering the signal insertion at the node N2 and N1 CD ROADM B&S nodes, the OSNR decrease is higher, 5.6 dB, for 10 km spans, than for 60 km, where the OSNR reduction is 4.2 dB. The difference between the OSNR obtained for networks with FD&W ChD nodes with spans of 60 km and spans of 10 km is due to the fact that in the case of Fig. 2.23 (b), there is no post-amplifier after signal extraction at node N2 to contribute to the overall accumulated ASE noise power.

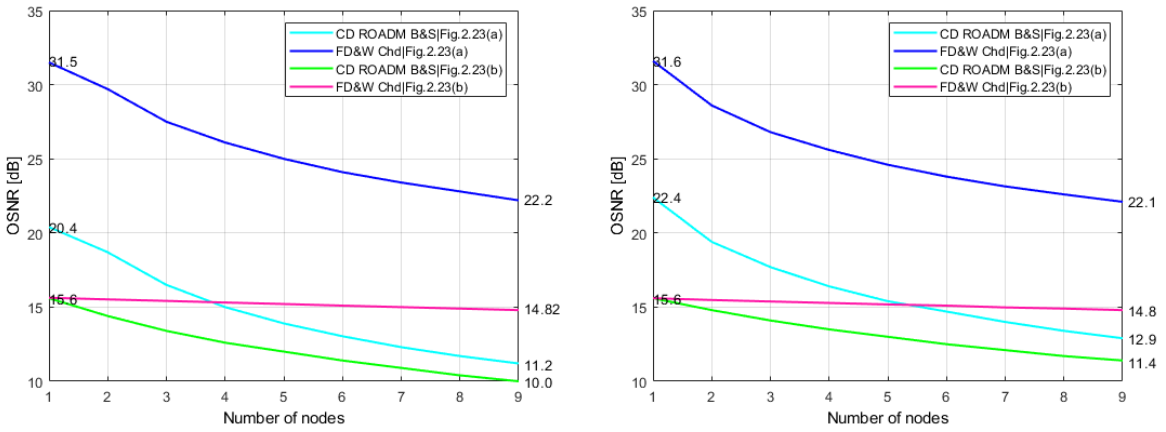

(a) (b)

FIGURE 2.24. OSNR in the horseshoe topology, for the signal worst path with insertion at node N1 and the signal worst path with insertion at node N2, for N1 CD ROADM B&S and N1 FD&W ChD nodes (a) 10 km spans (b) 60 km spans, for P_{Rx} equal to 0 dBm (assuming exact loss compensation).

For the 100G coherent transponders presented in Tab. 2.1 and that are used in the horseshoe network shown in Fig. 2.23, since we are using QPSK modulation, we assume a line bit error probability of 4×10^{-3} [**34**], corresponding to Hard-Decision (HD)-Forward

Error Correction (FEC). For square $M_{symbols}$-QAM constellations, the line Bit Error Rate (BER) can be related with the electrical Signal-to-Noise Ratio (SNR) by [**35**]

$$BER \approx \frac{2}{\log_2(M_{symbols})}\left(1-\frac{1}{\sqrt{M_{symbols}}}\right)\operatorname{erfc}\left(\sqrt{\frac{3snr}{2(M_{symbols}-1)}}\right) \tag{2.8}$$

For the Quadrature Phase-Shift Keying (QPSK) modulation ($M_{symbols}$=4), the theoretical required SNR must be 8.5 dB to achieve the required target line BER. When $B_o = Rs$, considering polarization-dividion multiplexing and dual polarization, the electrical SNR is equivalent to the OSNR. Therefore, the minimum reference OSNR of the horseshoe network in study is also 8.5 dB.

In Tab. 2.7, the OSNRs that reach the optical Rx input for the case of Figs. 2.23 (a) and 2.23 (b) with 10 km and 60 km spans, for the N1 CD ROADM B&S and FD&W ChD, considering only the ASE noise, are presented. For all the cases studied, the minimum OSNR required for the QPSK modulation is achieved. Analysing the results, we can conclude that for networks with either N1 FD&W ChD nodes or N1 CD ROADM B&S nodes and for any of the two worst paths, the OSNR is lower for 10 km spans than for 60 km spans, due to the higher accumulated ASE noise power at the end of the optical path. When signal insertion occurs at nodes N2 and extraction at node N1 (Fig. 2.22 (b)), for both node architectures, the achieved OSNR is lower than when signal insertion occurs at node N1 and extraction at node N2, being at least 7 dB lower for N1 nodes with a FD&W ChD architecture and 1 dB lower for N1 nodes with a CD ROADM B&S architecture. The best OSNR achieved corresponds to the case of N1 FD&W ChD nodes in networks with 10 km spans and insertion in node N1, with the value of 22.2 dB. This highest OSNR correspond to networks whose amplifiers have lower gains and have pre- and post-amplification. This means that, in these networks, when the amplifiers have a higher gain, such as the post-amplifier in the N2 node, or with 10 km spans where there is only pre-amplification, these amplifiers should present a lower noise figure than the other amplifiers in the network to reduce the performance degradation due to the ASE noise accumulation. Another solution is to use also post-amplification in these networks, to reduce the gain of the pre-amplifiers, at the expense of increasing the network cost due to the higher number of amplifiers.

2.6.3. Non-linear interference noise

In this section, the study of the impact of the NLI on the performance of systems with coherent detection is performed. The influence of this impairment is quantified using the

TABLE 2.7. OSNR for the case of Fig. 2.23 (a) and 2.23 (b) with 10 km and 60 km spans, for the N1 CD ROADM B&S and FD&W ChD node architectures, at the end of the network after signal extraction.

Node architecture	**N1 CD ROADM B&S**		**N1 FD&W ChD**	
	10 km	60 km	10 km	60 km
$OSNR_{R,min}$ [dB]	8.5			
$OSNR_{Fig.2.23(a)}$ [dB]	11.2	12.9	22.2	22.1
$OSNR_{Fig.2.23(b)}$ [dB]	10.0	11.4	14.82	14.8

Gaussian-Noise (GN) model for NLI assessment [**36**]. The system performance can be evaluated just by correcting the OSNR, i.e., by adding the NLI noise power, p_{NLI} to the accumulated ASE noise power at the optical Rx input by [**36**]

$$osnr = \frac{p_{Rx}}{p_{n,ASE} + p_{NLI}} \tag{2.9}$$

NLI noise can be modelled as Gaussian additive noise, independent of ASE noise. Thus, the NLI power can be computed using [**36**]

$$p_{NLI} = B_o \times g_{NLI}(\nu_o) \tag{2.10}$$

where g_{NLI} represents the NLI Power Spectral Density (PSD) that reaches the optical Rx input at the WDM center channel frequency ν_0, which is given by

$$g_{NLI}(\nu_o) = n_{spans} \times [g_{XCI}(\nu_o) + g_{SCI}(\nu_o)] \tag{2.11}$$

where $g_{XCI}(\nu_o)$ is the cross-channel interference noise PSD at the nominal frequency ν_0, and $g_{SCI}(\nu_o)$ is the self-channel interference noise PSD calculated by [**37**]

$$g_{SCI}(f_m) = G_m^3 \left(\frac{3\gamma^2}{2\pi\alpha|\beta_2|}\right) \text{arcsinh}\left(\frac{\pi^2|\beta_2|}{2\alpha} \times \Delta f_m^2\right) \tag{2.12}$$

where f_m is the frequency of the central channel in lowpass equivalent corresponding to ν_0, G_m is the signal PSD of the central channel, γ is the fibre non-linearity coefficient, with the value of 1.3 W/km, $|\beta_2|$ represents the group velocity dispersion parameter and Δf_m represents the bandwidth of each WDM channel, which is equal to $R_{s,l} = 26.75$ Gbaud. The signal PSD of the central channel and the group velocity dispersion parameter are calculated, respectively, by [**37**]

$$G_m = \frac{p_{Rx}}{\Delta f_m} \tag{2.13}$$

$$|\beta_2| = \frac{D_\lambda \lambda_0^2}{2\pi c} \tag{2.14}$$

where p_{Rx} represents the channel power, D_λ is the fiber dispersion parameter, with the value of 18 ps/(nm×km), λ_0 is the wavelength of the central channel and c is the light velocity, c=2.9979 $\times 10^8$ m/s.

The cross-channel interference noise PSD is calculated by [**37**]

$$g_{XCI}(f_m) = G_m^3 \times \frac{3\gamma^2}{2\pi\alpha|\beta_2|} \sum_{m'=1;m\neq m'}^{n_{spans}} \left[G_{m'}^2 \times \ln\left(\frac{|f_{m'} - f_m| + \frac{\Delta f_{m'}}{2}}{|f_{m'} - f_m| - \frac{\Delta f_{m'}}{2}} \right) \right] \tag{2.15}$$

where $f_{m'}$ is the frequency of the channel m', $\Delta f_{m'}$ is the bandwidth of channel m' and $G_{m'}$ is the signal PSD of the channel m'.

The optimum channel power that should be lauched in an optical link impaired by NLI and ASE noise, that leads to the maximum OSNR at the Rx input, is given by [**36**]

$$p_{ch,opt} = \sqrt[3]{\frac{p_{n,ASE}}{\eta_{NLI}}} \tag{2.16}$$

where η_{NLI} is the parameter that characterizes the NLI impact in an optical link and is given by [**36**]

$$\eta_{NLI} = \frac{p_{NLI}}{p_{Rx}^3} \tag{2.17}$$

where p_{NLI} is calculated from (2.10). Note that the computation of η_{NLI} gives the same for all horseshoe networks in study, since the NLI PSD model proposed in [**37**] does not depend on the span length.

Hence, it is possible to calculate the OSNR penalty due to NLI by the difference between the OSNR without NLI given by (2.3) and the OSNR in presence of NLI given by (2.9). For the optimum channel power, the OSNR penalty is 1.76 dB [**38**].

The OSNRs at the optical Rx input considering the NLI are shown in Tab. 2.8, obtained using Eqs. (2.10)-(2.17), for the optimal channel power, also present in Tab. 2.8. We have verified that, for the optimal channel powers calculated, there is always a degradation of 1.76 dB of OSNR compared to the situation where only ASE noise power is considered, as expected. Note that, the OSNRs present in Tab. 2.7 are calculated for a $p_{Rx} = 0$ dBm, while the values presented in Tab. 2.8 are calculated for the optimal power per channel, which is different for all architectures. Therefore, the OSNRs calculated considering only ASE noise power or considering both ASE noise powers and NLI power

cannot be directly compared. Note that, for the optimal channel power, the NLI power is half of the ASE noise power [**39**].

TABLE 2.8. OSNR for the cases of Fig. 2.23 with 10 km and 60 km spans, for the N1 CD ROADM B&S and FD&W ChD node architectures, at the end of the network after signal extraction, considering NLI power and for the optimal power per channel, $P_{ch,opt}$.

Node architecture	**N1 CD ROADM B&S**		**N1 FD&W ChD**	
	10 km	60 km	10 km	60 km
$OSNR_{R,min}$ [dB]	8.5			
$p_{ch,opt,Fig.2.23(a)}$ [mW]	1.09	0.96	0.47	0.47
$OSNR_{Fig.2.23(a)}$ [dB]	9.8	10.9	17.2	17.0
$p_{ch,opt,Fig.2.23(b)}$ [mW]	1.19	1.08	0.82	0.83
$OSNR_{Fig.2.23(b)}$ [dB]	9.0	9.9	12.2	12.2

As shown in Tab. 2.8, the node architecture where the OSNR decreases the most is the FD&W ChD, in comparison with the OSNRs obtained in Tab. 2.7. These values of OSNR are justified because in networks with N1 FD&W ChD nodes the optimal power, calculated by (2.16), is around -3.5 dBm, which is lower than 0 dBm, as considered in Tab. 2.7. For the case of Fig. 2.23 (b), the OSNR is between 4.8 dB and 5.1 dB lower than for the case of Fig. 2.23 (a) because the NLI power is higher, which depends of the optimal power per channel, twice higher in the second case for FD&W ChD-based networks and at least 0.1 dB higher in the case of ROADM-based networks, which contributes to an higher OSNR degradation on FD&W ChD-based networks. The OSNRs obtained for CD ROADM B&S-based networks are the lowest for all network types. When the signal insertion occurs at N1 node, the OSNR is higher between 0.8 dB and 1 dB than the case of the signal insertion occurs at N2 node, for 10 km and 60 km spans, respectively. This occurs because when the signal is inserted at the N2 node, at the optimal power per channel, the accumulated ASE noise and NLI powers are higher.

2.6.4. Optical filtering

In the network topologies analyzed in this work, the filtering effects come mainly from the WSSs inside the nodes. These components can be characterized by their corresponding transfer functions, for both operation scenarios: selection and channel blocking. For selecting a signal, the WSS transfer function can be modelled by a Super-Gaussian passband filter defined by [**40**]

$$H_p(f) = \exp\left[-\left(\frac{f^2}{2 \times \sigma_{sg}^2}\right)^n\right] \tag{2.18}$$

where n represents the super-Gaussian filter order and σ_{sg} is related to the m-dB bandwidth of the Gaussian filter, BW_{mdB}, given by [**40**]

$$\sigma_{sg} = \frac{BW_{mdB}}{2 \times [2(\ln \sqrt{10^{\frac{m}{10}}})^{\frac{1}{n}}]^{\frac{1}{2}}} \tag{2.19}$$

For blocking a signal, the WSS transfer function can be modelled by [**12**]

$$H_b(f) = 1 - (1 - a) \times \exp\left[-\left(\frac{f^2}{2 \times \sigma_{sg}^2}\right)^n\right] \tag{2.20}$$

where a is the blocking amplitude given by $a = 10^{\frac{A(dB)}{20}}$ in linear units.

When the signal goes through a cascade of several nodes before being extracted, it is filtered by several passband filters and can experience a severe distortion, known as the passband narrowing effect, which becomes a relevant physical impairment in the system performance [**41**], [**42**]. On networks based on CD ROADM B&S nodes, this effect should have a great impact on the network performance because there is one filtering stage per node [**12**], [**43**]. On networks based on FD&W ChD nodes architectures, the passband narrowing effect due to cascading optical filters should be minimal, because the nodes contain only S/Cs, and the only filtering performed is the Digital Signal Processing (DSP) at the Rx by the Nyquist filter [**44**].

In Fig. 2.25, the transfer function of the stopband filter obtained using (2.20), for the WSS blocking amplitudes of (i) $A = -30$ dB and (ii) $A = -35$ dB, is represented. These values are typical WSS isolations for the LCoS technology [**42**], [**45**]. The BW_{-3dB} is used to calculate the parameter σ_{sg} (2.19), and it has the value of 100 GHz.

The main objective of the stopband filter is to block the signal power of a desired channel around its center frequency, which, the study performed in this section has a 26.75 GHz of bandwidth. As can be seen in Fig. 2.25, the isolation level has a width much closer to the signal bandwidth, which means that is suitable for channel blocking in the studied system.

In Fig. 2.26, the passband narrowing effect is depicted for 1 (reference case), 10 and 20 cascaded filters for different -3 dB bandwidths (a) 44 GHz and (b) 94 GHz for a super-Gaussian optical filter with third order, n=3, with transfer function given by (2.18) [**3**].

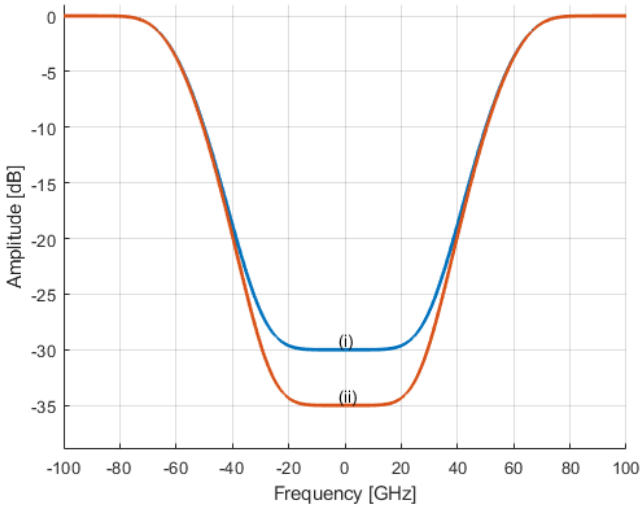

FIGURE 2.25. Transfer functions of the super-Gaussian stopband filter $H_b(f)$ with different blocking amplitudes (i) -30 dB and (ii) -35 dB.

In Fig. 2.26 (a), the -3 dB signal bandwidth when the signal goes through the filter cascade narrows from 44 GHz to around 26 GHz from 1 to 20 cascaded filters, respectively, leading to a passband narrowing of 18 GHz. As the signal bandwidth considered in this work is 26.75 GHz, which is similar to the bandwidth after the 20 filters cascading, the passband narrowing should lead to some performance degradation in this case [**46**].

In Fig. 2.26 (b), the signal will be filtered by bandwidths between 94 GHz and 57 GHz, after passing 1 filter and 20 filters, respectively. As this optical filter bandwidth is much larger than the signal bandwidth, the performance degradation for this channel spacing after 20 filters cascading should be negligible.

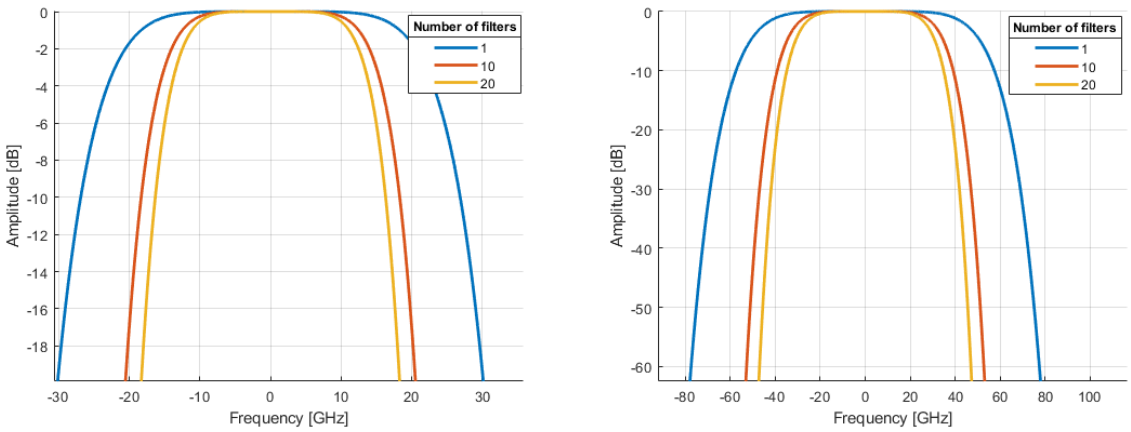

(a) (b)

FIGURE 2.26. Transfer function of the super-Gaussian passband filter, after cascading several filters, with n=3 and (a) BW_{-3dB}=44 GHz and (b) BW_{-3dB}=94 GHz.

In this work, when the CD ROADM B&S architecture is used for node N1, the signal must pass through 11 optical filters, regardless of the nodes where insertion and extraction occur. In [**41**], a study of the OSNR penalty as a function of the number of cascaded WSSs using the QPSK modulation format has been performed. From [**41**], for 11 cascaded filters, the OSNR penalty can be neglected for a channel spacing of 100 GHz. Therefore, it is expected that the penalty due to optical filtering induced by passband narrowing is insignificant in the horseshoe network studied, for both N1 nodes architectures and for 10 cascaded filters, where the -3 dB signal bandwidth after passband narrowing is 30 GHz and 57 GHz, respectively, in Fig. 2.26 (a) and 2.26 (b) (yellow line).

2.6.5. Crosstalk

The signal performance in optical networks can be degraded by optical linear crosstalk, which is a physical layer impairment. The existence of crosstalk is mainly due to imperfect isolation of the components within the nodes, such as WSSs [**42**]. The imperfect isolation causes signal power leakages along the entire network, that impair and degrade a selected signal along its network path [**47**]. The selected signal is a signal centered at a specific wavelength, which is chosen to assess the impact of crosstalk along its entire optical path, from its insertion in the network to its network drop.

There are two types of linear crosstalk: out-of-band crosstalk and in-band crosstalk [**47**]. When the interfering signals have a different nominal wavelength from the selected signal, it corresponds to out-of-band crosstalk, which is not much problematic, as it can be removed by filtering at the Rx. In-band crosstalk occurs when different optical sources produce interfering signals with the same nominal wavelength than the selected signal, which can not be removed after interfering [**12**]. To evaluate the impact of crosstalk in a network, it is necessary to characterize the number of interfering terms and the crosstalk level of each interfering term. There are first and second order interfering terms. The crosstalk is considered 1^{st} order, when an optical signal overcomes the isolation of one optical component. When it overcomes the isolation of two optical components, the crosstalk is considered 2^{nd} order, and its contribution to the performance degradation is lower. Typically, second order interfering terms are neglected in a crosstalk analysis [**47**].

The number of interfering terms depends on the ROADM or FD&W node degree. In this work, as the horseshoe topology is considered, the nodes N1 are 2-degree, the nodes N2 are 5-degree and the worst-case scenario of in-band crosstalk is considered, when the

wavelength corresponding to the primary/selected signal appears in all possible inputs and add ports of the network nodes.

In Fig. 2.27, the way the selected signal travels within the 2-degree CD ROADM B&S node is represented, as well as the interfering signals. In the input stage, there are 2 signals, represented by 2 distinct colors, where each one represents a distinct wavelength. In the worst case of crosstalk, the orange wavelength of the North direction, that corresponds to the primary signal, is reused in all fibre links, which means that the signal is added and dropped at every node N1.

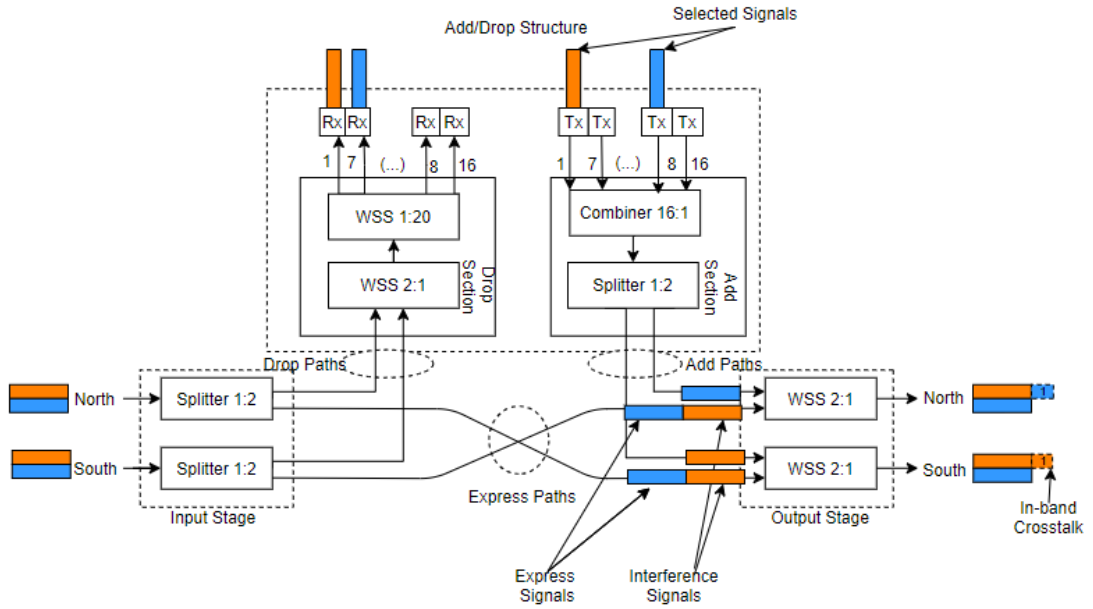

FIGURE 2.27. In-band crosstalk inside CD ROADM B&S nodes. Each color corresponds to a signal at a different wavelength.

In this case, the routing occurs as follows: the orange signal and the blue signal are extracted from the North and South directions, respectively and the orange signal and the blue signal in the South and North directions, respectively, are expressed. The orange signal is inserted and sent to the South direction, while the blue signal is inserted and sent to the North direction. This routing, in a CD ROADM B&S node architecture generates one in-band crosstalk interfering term of 1^{st} order per direction, each associated with the orange and blue expressed signals.

In Fig. 2.28, the signal path that will originate the worst possible crosstalk in the horseshoe topology is presented, where the same primary signal is added and dropped successively in all nodes, after: 2.28 (a) a first insertion in node N1 A, and until extraction from the horseshoe topology by the last node N2 or 2.28 (b) a first insertion in node N2

and until extraction by node N1 *I*. Therefore, it is considered that all the nodes N1 communicate with the next node N1 using the same wavelength, occuring a total reuse of this wavelength. In each of the inputs of the nodes N1 following node A, the primary signal inserted in a node is impaired by the accumulation of 1^{st} order in-band crosstalk terms arising in the previous nodes. In the case of Fig. 2.28 (b), the signal inserted in a node not only is impaired by the accumulation of 1^{st} order in-band crosstalk terms but also of four 2^{nd} intefering terms which came from node N2. Note that, although in any of the cases of Fig.2.28 (a) or Fig. 2.28 (b), the number of 1^{st} and 2^{nd} order interfering terms is the same, and therefore the crosstalk level is the same, the OSNR calculation will also depend on the ASE noise power and the NLI, studied in sections 2.6.2 and 2.6.3, respectively, which are different for each type of network.

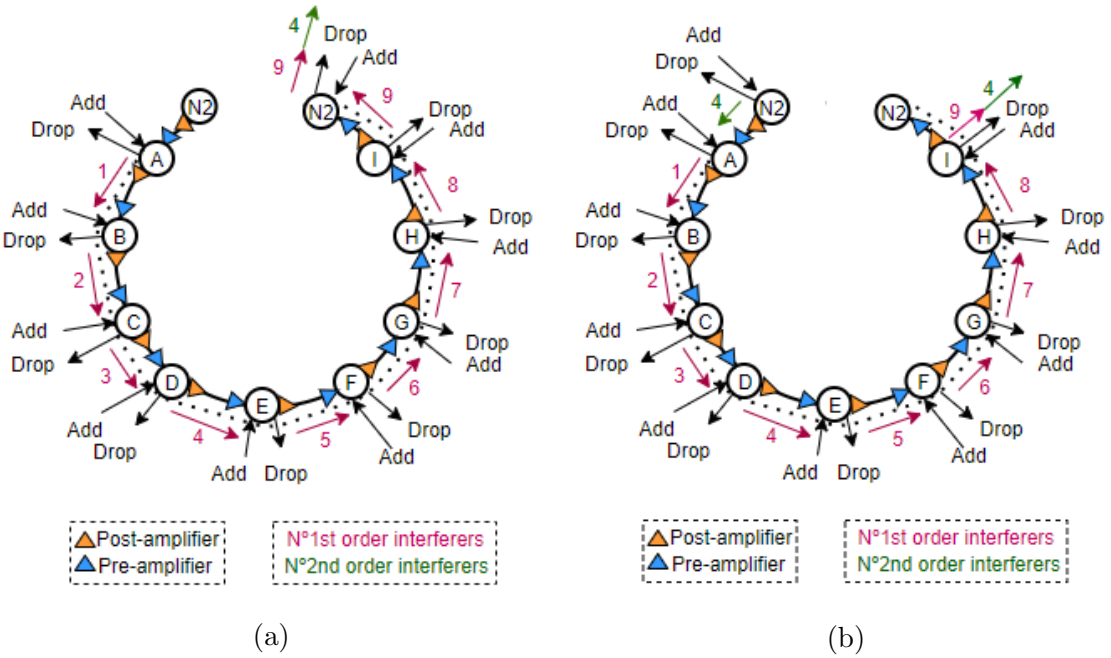

FIGURE 2.28. Worst case in-band crosstalk in a network with horseshoe topology and the number of interfering terms along the network for (a) Insertion signal at node N1 and extraction at node N2 and (b) Insertion signal at node N2 and extraction at node N1.

It is also necessary to take into account that the nodes N2 are 5-degree CD ROADM R&S nodes, and therefore the number of interferers will be different from those arising in the nodes N1. As the nodes N2 are integrated in a metro-core network whose physical topology is meshed, as mentioned in Section 2.3, and have a R&S architecture, they lead to four 2^{nd} order interfering terms at the output of the node N2 [**43**].

Concerning the N1 FD&W ChD node architecture, as mentioned in section 2.4.3, each wavelenght is only used once in an optical path of the horseshoe topology, and, therefore,

there is no frequency reuse. Hence, the wavelength being added in a network node is always different from the wavelength dropped in that same node. As shown is Fig. 2.29, when a signal (represented with yellow color) is added, which has a different wavelength from the signals represented by the orange and blue colors, there is no in-band crosstalk at the node N1 for this architecture. Only wavelengths that are expressed reach the output stage, as well as the added signals that have a different wavelength from the expressed signals. Thus, in networks with horseshoe physical topology with N1 FD&W ChD nodes architectures, the selected signal is only impaired by in-band crosstalk introduced by the last node N2.

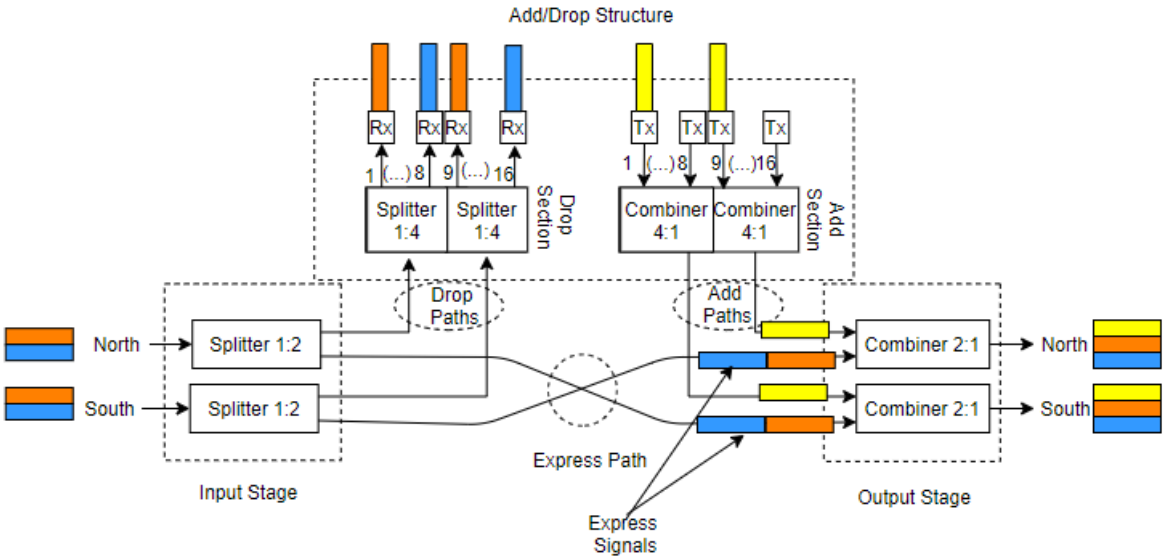

FIGURE 2.29. In-band crosstalk inside FD&W ChD nodes. Each color corresponds to a signal with a different wavelength.

In Tab. 2.9, the number of interfering terms is presented, considering the two node N1 architectures (CD ROADM B&S and FD&W ChD), per node and for the total network, which has 9 nodes N1. There are considerably more interfering terms in the CD ROADM B&S case than in the FD&W ChD case, because in the last architecture, only the node N2 contributes to the total number of interfering terms in the network. The 13 interfering terms associated to networks with N1 CD ROADM B&S nodes result from the accumulation of in-band crosstalk along nine nodes N1 and the last node N2. In Tab. 2.9, it is also presented the total crosstalk level at the network output, defined by [**48**]

$$X_c = \frac{\sum_{i=1}^{N_{X_c}} P_{X_c,i}}{p_{R_x}} = \sum_{i=1}^{N_{X_c}} X_{c,i} \tag{2.21}$$

where $P_{X_{c,i}}$ is the power of the interfering term, p_{R_x} is the power of the input primary signal, N_{X_c} is the total number of interfering terms and $X_{c,i}$ is the crosstalk level of the i-th interfering term.

Regarding the crosstalk level and taking into account that in the FD&W ChD architecture there is no in-band crosstalk introduced in the N1 nodes, only the N1 CD ROADM B&S nodes generate interfering terms. The nodes N2 also contribute with four 2^{nd} order interfering terms. The crosstalk level in Tab. 2.9 is calculated using (2.21), considering that each WSS inside the node has a typical isolation of -30 dB and -35 dB, which leads to a crosstalk level of -30 or -35 dB per 1^{st} order interferer, respectively, and -60 or -70 dB per 2^{nd} order interferer. As such, in Tab. 2.9, the architectures with CD ROADM B&S nodes lead to a higher crosstalk level at the output of the horseshoe topology, which is of 38.5 dB and 35.5 dB above the crosstalk level obtained with the FD&W ChD architecture for, respectively, $A = -35$ dB and $A = -30$ dB. The difference of 5 dB in the WSS isolation produces a 5 dB higher total crosstalk level, when 1^{st} order interference is dominant and 10 dB, when there exists only 2^{nd} order interference.

TABLE 2.9. Total number of interfering terms of in-band crosstalk and crosstalk level for the worst-case crosstalk in a horseshoe network.

Interfering terms	**ROADM B&S**		**FD&W ChD**	
Per node	N1 1 1^{st} order term	N2 4 2^{nd} order terms	N1 0	N2 4 2^{nd} order terms
Total number of interferers	13 (9+4)		4 (0+4)	
Total X_c level [dB] for A=-35 dB	-25.46		-63.98	
Total X_c level [dB] for A=-30 dB	-20.46		-53.98	

In Tab. 2.10, the values of the OSNR with in-band crosstalk, calculated using

$$osnr = \frac{p_{R_x}}{p_{n,ASE} + p_{X_c} + p_{NLI}} \tag{2.22}$$

are shown for WSS isolations of -30 dB and -35 dB and where $p_{X_c} = X_c \times p_{R_x}$. These OSNR values are calculated for networks with 10 km spans and with 60 km spans, with signal insertion at node N1 and extraction at node N2 and with signal insertion at node N2 and extraction at node N1, as shown in Figs. 2.23 (a) and 2.23 (b), respectively. At the top of the Tab. 2.10, the common parameters between both cases of Figs. 2.23 (a) and 2.23 (b), such as the $OSNR_{R,min}$, the power of interfering terms for isolations of -30 and -35 dB and the parameter η_{NLI} are presented. Then, the parameters associated to each

Figs. 2.23 (a) and 2.23 (b) are shown, such as the ASE noise power, studied in section 2.6.2, the optimum channel power and the power of NLI studied in section 2.6.3. At last, the OSNR is determined using (2.22) for all combinations of node architectures, spans lenghts, WSS isolations and signal insertion at node N1 or at node N2. Note that, all OSNRs values presented in Tab. 2.10 are calculated for the optimal power per channel.

From Tab. 2.10, the crosstalk power does not modify the OSNRs for networks with N1 FD&W ChD nodes because its value is more than 3 orders of magnitude lower than the ASE noise power, for both WSS isolations. For this node architecture, the associated OSNRs are at least 6 dB and 2.7 dB higher, respectively, with signal insertion at node N1 (Fig. 2.23 (a)) and with signal insertion at node N2 (Fig. 2.23 (b)), than all architectures with CD ROADM B&S nodes. This happens because the ASE noise and NLI powers that reach the optical Rx input are lower than in the case of ROADM nodes.

In case of networks with N1 CD ROADM B&S nodes, due to in-band crosstalk, the OSNR decreases less than 0.14 dB for WSSs with $A = -35$ dB for all cases studied. For WSSs with $A = -30$ dB, due to in-band crosstalk, the OSNR decreases less than about 0.4 dB for all cases studied. So, for CD ROADM B&S-based networks, the highest OSNRs are achieved in networks with 60 km spans, with a difference between 0.8 dB and 1.1 dB above the corresponding cases with 10 km spans, as a consequence of the lower impact of ASE noise, NLI, and in-band crosstalk.

Although the OSNR that reaches the optical Rx input decreases in all cases, it is still higher than the minimum OSNR of 8.5 dB required to reach the target line BER.

Analysing the final OSNRs considering the accumulation of the ASE noise, NLI and crosstalk effects, the ASE noise power is the one that most impacts, the NLI power contributes to the OSNR always with half the ASE noise power at the optimum power per channel, and the crosstalk is the one that contributes less to the OSNR degradation, mainly in the FD&W ChD node architecture, where it is negligible. On networks with N1 CD ROADM B&S nodes, the crosstalk contributes around 10% to the total noise power used to calculate the OSNR compared to total noise power used to calculate the OSNR without considering crosstalk.

It is noticeable that in all cases, the OSNRs in networks with FD&W ChD nodes are higher than in networks with CD ROADM B&S nodes, as expected. As all networks comply with the minimum OSNR required, our results indicate that any of the networks studied can be implemented. However, if we add a safety margin to the OSNR, networks

with N1 CD ROADM B&S nodes will hardly accomplish the minimum OSNR. In these networks, the solution to increase the OSNR margin is to increase the line BER by considering a stronger FEC, or by decreasing the reach of the network below 10 cascaded nodes.

TABLE 2.10. OSNR for the cases of Figs. 2.23 (a) and 2.23 (b), with 10 km and 60 km spans, for the N1 CD ROADM B&S and FD&W ChD node architectures, considering the crosstalk power, $P_{x_{c,i}}$ for the WSS isolations of -30 dB and -35 dB, and considering the optimal power per channel.

OSNR	**CD ROADM B&S**		**FD&W ChD**	
km/span	**10 km**	**60 km**	**10 km**	**60 km**
$OSNR_{R,min}$ [dB]	8.5			
$p_{X_{c,i}}$ [W] for A=-30 dB	9×10^{-6}		4×10^{-9}	
$p_{X_{c,i}}$ [W] for A=-35 dB	2.85×10^{-6}		4×10^{-10}	
η_{NLI}	2.36×10^{5}			
Parameters associated to the case of Fig 2.28 (a)				
$p_{n,ASE,Fig.2.28(a)}$ [W]	8×10^{-5}	5×10^{-5}	6×10^{-6}	6.2×10^{-6}
$p_{ch,opt,Fig.2.28(a)}$ [mW]	1.09	0.96	0.47	0.47
$p_{NLI,Fig.2.28(a)}$ [W]	3.8×10^{-5}	2.6×10^{-5}	3.0×10^{-6}	3.11×10^{-6}
OSNR [dB] for A=-30 dB, Fig: 2.28 (a)	9.4	10.5	17.15	17.04
OSNR [dB] for A=-35 dB, Fig: 2.28 (a)	9.66	10.8	17.15	17.04
Parameters associated to the case of Fig 2.28 (b)				
$p_{n,ASE,Fig.2.28(b)}$ [W]	10×10^{-5}	7.3×10^{-5}	3.3×10^{-5}	3.3×10^{-5}
$p_{ch,opt,Fig.2.28(b)}$ [mW]	1.19	1.08	0.81	0.82
$p_{NLI,Fig.2.28(b)}$ [W]	5×10^{-5}	3.7×10^{-5}	1.7×10^{-5}	1.7×10^{-5}
OSNR [dB] for A=-30 dB, Fig: 2.28 (b)	8.76	9.6	12.2	12.2
OSNR [dB] for A=-35 dB, Fig: 2.28 (b)	8.94	9.8	12.2	12.2

2.7. Conclusions

In this chapter, the C-band node architectures such as ROADM R&S or B&S, FD&W and FOADM have been presented, as well as their cost assuming an end of life scenario, their main features, characteristics, main hardware components and its main PLIs.

A study on all the necessary hardware as well as the capacity of horseshoe networks with the different node architectures has been performed and their estimated costs and power consumption have been estimated. From this analysis, we have concluded that the networks with the best cost/power consumption ratio, are those composed of 2 hub N2 nodes based on CD ROADM R&S and tributary N1 nodes based on CD ROADM B&S and 2 hub nodes based on CD ROADM R&S and tributary nodes based on FD&W ChD. The ROADM-based networks have a normalized cost of 2.8 and a power consumption

of 44.6 kW. The FD&W-based networks have a normalized cost of 2.4 and a value of power consumption of 39.5 kW. The hardware component that contributes most to power consumption is the transponder.

Then, several PLIs such as ILs, ASE noise, non-linear interference, optical filtering and crosstalk have been studied for the horseshoe network (with 2 hub nodes and 9 tributary nodes) with these two chosen architectures, with 10 km and 60 km spans, for the worst path when the signal is inserted at node N1 and extracted at nodes N2 or when the signal is inserted at node N2 and extracted at node N1. The highest ILs imposed by the tributary nodes are 22 dB higher, concerning N1 node , which values are present in Tab. 2.4) in CD ROADM B&S nodes than in FD&W ChD nodes, which leads to a higher ASE noise accumulation in the ROADM-based networks. In these networks, the OSNR is at least 9 dB lower than in FD&W based networks, when signal insertion occurs at node N1, and at least 3.4 dB lower, when signal insertion occurs at node N2. In this latter case, it has been observed that the hub node N2 introduces the main contribution to the total ASE noise power, due to a very high post-amplifier gain. At the optimal channel power, the NLI contribution has a stronger impact on the OSNR degradation, leading to a minimum 2.6 dB degradation for FD&W-based networks, while in ROADM-based networks the degradation is between 1 and 2 dB. We have also shown that the passband narrowing due to optical filtering is negligible and that the in-band crosstalk only influence the performance on CD ROADM B&S-based node architectures by decreasing the OSNR about 1 dB. The addition of the NLI effect contributes to a dfference of 7.4 dB in the OSNR higher in FD&W-based nodes architecture than in networks with CD ROADM B&S nodes, in the worst case.

Among the two architectures, the architecture using ROADM nodes provides more capacity to the network (8 Tbps/node against 4 Tbps/node considering FD&W nodes) , but at the expense of higher cost and power consumption and requiring higher system margins to work has considering all PLIs compared to the FD&W ChD architecture.

CHAPTER 3

C+L-bands node architectures for the horseshoe topology

3.1. Introduction

This chapter is focused on analysing some of the node architectures for the C+L-bands, considering metro networks based on the horseshoe topology. These nodes are typically based on two main blocks, one for the C-band and another one for the L-band.

The main goal in introducing L-band solutions is to increase the network capacity without increasing too much the actual C-band network cost. Other solutions for increasing capacity, but involving more investments, are the ones that rely on placing more fiber [**1**]. These L-band solutions typically rely on the simple and low cost FD&W architectures. In the last few years, some companies such as Nokia and Infinera already started offering C+L-band solutions for open line systems in order to increase the network capacity over existing fiber routes already implemented [**5**].

In section 3.2 we review some of node architectures solutions used for the C+L-band scenario. In section 3.3, the L-band node architectures are presented, in particular the L-band amplified and unamplified solutions. In section 3.4, we perform an analysis regarding the hardware cost and power consumption concerning the L-band solutions. In section 3.5, the main PLIs such as the ILs, the accumulated ASE noise power and the NLI, in the L-band, in a horseshoe topology are discussed, assuming an amplified solution. Likewise, in section 3.5.4, the most relevant PLIs in the unamplified solution, such as the in-band crosstalk, are analyzed and discussed. Finally, in section 3.6, the conclusions are drawn.

3.2. Node architecture for C+L-band

Metro networks with C+L band transmission are usually based on the horseshoe topology with two hub nodes (node N2) and several tributary nodes (node N1), as described in the section 2.3. As shown in Fig. 3.1, a C+L node architecture has two independent structures, one for C-band signals and another one for the L-band signals, as proposed in [**10**]. These two bands are separated by a C/L band filter at the input of the node [**10**]. These filters typically provide high channel isolation contributing to low ILs typically ∼0.6 dB [**49**], but introduce a band gap between the C and L bands, typically between 300

and 500 GHz [**50**], which reduce the capacity of the fiber. The L-band solution, being an independent part of the node completely dedicated to the routing in the L-band, causes a minimum disruption with the pre-existing metro network working only in the C-band [**10**].

The node configuration used for the C-band, which is shown at the top of Fig. 3.1 by the blue color, can be implemented with various nodes architectures explained in section 2.4, and based on FD&W, FOADM and ROADM solutions. However, in this work, it is considered only FD&W and ROADM solutions, for the reasons explained in sections 2.5 and 2.6. The node configuration for the L-band is shown at the bottom of Fig. 3.1 by the orange color, and is based only the FD&W solution, which can be either amplified or unamplified. These solutions have no filtering in the tributary nodes, which means that when a wavelength is added to the network, it remains in the network until the hub node removes it (amplified solution) or until it is used once again in the network (unamplified solution). The unamplified solution is intended to reduce even further the node cost.

In the next sections we are going to discuss the L-band node functionality, cost and PLIs.

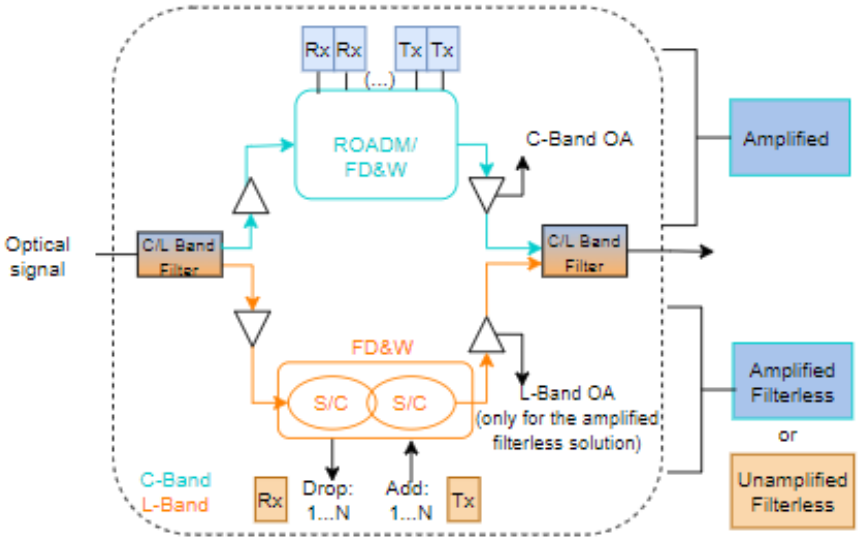

FIGURE 3.1. Tributary C+L-band node configuration.

3.3. Solutions for L-band node architectures

In this section we are going to describe two node architectures based on the FD&W architecture: the amplified and the unamplified solutions [**8**], [**9**] and [**10**]. We will also refer in this section some upgrading solutions for the L-band, namely the Single Region

(SR) and Dual Region (DR), disagregated FD&W exploiting configurable channels and a solution for low-latency edge computing [**9**].

The C+L band node amplified solution described in Fig. 3.1 rely on a single EDFA for each optical band and two C/L filters at the node input/output. As already referred a capacity penalty associated to this architecture is related to the bandwidth waste caused by the guard-band between C and L band imposed by the C/L filters before and after the EDFAs. To avoid this waste of bandwidth there are two other solutions for optical amplification in the C+L band nodes [**5**]. One of them rely on using single wide-band amplifiers based on semicondutor OA and the other one use a typical hybrid Raman-EDFA amplifier configuration [**5**].

In this dissertation we will not study these two solutions for amplified C+L band nodes, only the solution presented in Fig. 3.1 will be analyzed.

3.3.1. L-band amplified solution

In the amplified solution there are amplifiers inside the node before and after the FD&W block, whereas in the unamplified solution these amplifiers are not present, as depicted in Fig. 3.1 [**9**]. These amplifiers will introduce ASE noise that will contribute to degrade the system performance (see section 3.6).

Fig. 3.2 presents a possible wavelength planning for the amplified solution in the L-band in a horseshoe topology. This solution does not allow the reuse of frequencies inside the horseshoe network since each wavelength assigned in the network can only be extracted by the hub node. The tributary nodes have no such capacity since they are based on S/Cs (FD&W architecture). An example of this scenario can be seen in Fig. 3.2: the pink wavelength is assigned to the connection between the hub node and the tributary node *E*, but node *E* can not extract this wavelength, which is only extracted from the network at the other hub node (this path is represented by the dashed pink line in Fig. 3.2) [**8**], [**10**]. So, this solution, already discussed in chapter 2, wastes spectrum [**8**].

3.3.2. L-band unamplified solution

The main goal of the L-band unamplified solution is to reduce the nodes cost by not using OAs before and after the FD&W structure. Nevertheless, this solution limits the L-band signal transmission distance to adjacent nodes or near adjacent nodes [**10**]. Fig.

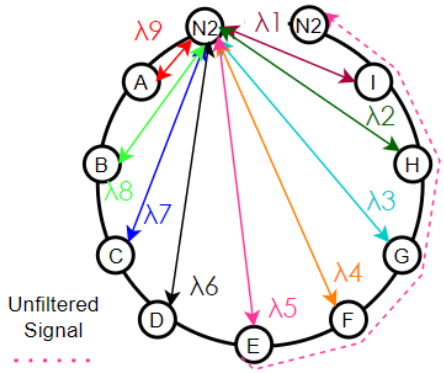

FIGURE 3.2. Amplified filterless solution with no frequency reuse for the horseshoe topology. Only the L-band wavelength assignment for the downlink transmission is depicted.

3.3 shows a possible wavelength planning for the unamplified solution, where there are no EDFAs inside the nodes.

As shown in Fig. 3.3, λ_2 is reused in the next-hop and λ_1 is reused after 1 hop. As in this unamplified solution the signal is not amplified it arrives to next node with very low power, and so a new signal with the same wavelength can be used. However, this weak signal contributes to impair the main signal and so this unamplified solution is impaired by in-band crosstalk [**8**]. So, with this solution it is possible to reuse the same wavelength, providing a simple and very low-cost capacity upgrade for MANs with dedicated capacity for short lightpaths between tributary nodes, albeit with a more challenging optical performance management.

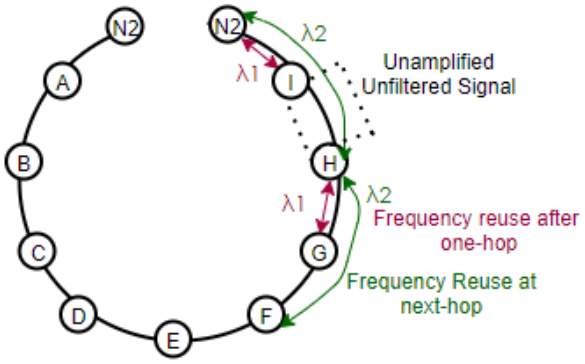

FIGURE 3.3. Unamplified filterless solution with frequency reuse for the horseshoe topology. Only the L-band wavelength assignment for the downlink transmission is depicted.

3.3.3. L-band upgrading solutions

Although filterless solutions have some problems, mainly due to the reduced optical range, they can lead to high savings in resources and maintenance expenses. For taking

advantage of these solutions at lower costs, 4 upgrading solutions emerged to be applied on the optical FD&W nodes, using the C+L-bands [**9**]: C+L-band capacity upgrade using SR and DR, disagregated FD&W exploiting configurable channels and a solution for low-latency edge computing.

The diagram of the SR solution is shown in Fig. 3.4 (a) and allows C+L transmission in the entire network [**51**]. All wavelengths can be received regardless of the band in each node, without restrictions on the wavelength. A L-band upgrade requires the total or partial upgrade of all the line spans and drop-stage amplifiers [**51**], which means that OAs are needed in the C+L-band.

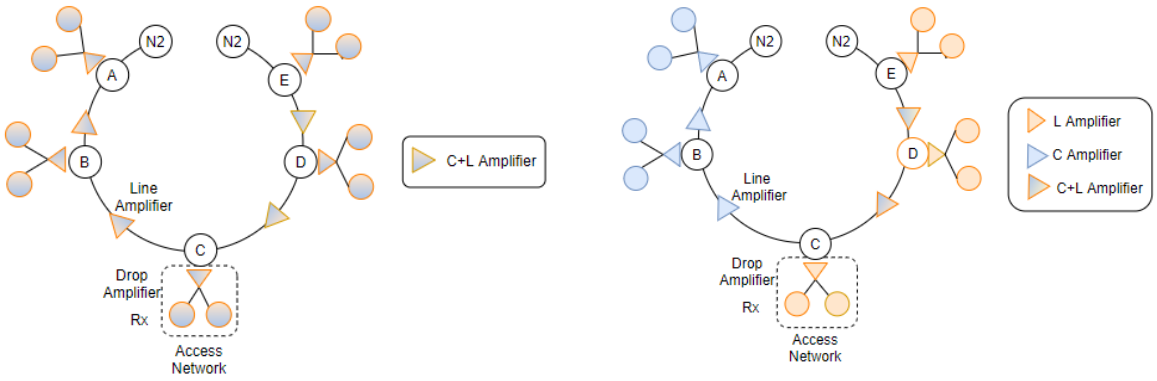

(a) (b)

FIGURE 3.4. C+L band upgrade of the horseshoe topology using (a) SR solution and (b) DR solution.

The DR solution upgrade is depicted in Fig. 3.4 (b). It divides the network into two different wavelengths domains, with the goal of reducing the total cost of the upgrade. In this solution, the L-band wavelengths must be received only in the first region of the FD&W-based networks because of the short distance (first three stages represented in orange in Fig. 3.4 (b)), while C-band channels are received in the second region (blue region). So, in the first half, the L-band requires amplification. This design has the goal of achieving a reduced EDFA placement using single C-band or single L-band EDFAs only where needed with a limited number of C+L band EDFAs, thus reducing the cost of upgrading.

The third solution for upgrading the L-band performance is the disaggregated FD&W that exploits configurable channels in order to improve the capacity by employing co-existing higher bit rate channels with an improved spectrum utilization. The transmission is made by a set of transponders that provide channels with different bit rates and

modulation formats, as depicted in Fig. 3.5, where the bit rates of 100 Gbps and 400 Gbps are considered. The signals coming from the different Txs are coupled together by a combiner and, then, are sent along the entire horseshoe network. The communication with the access network is performed with a line S/C, a drop amplifier and a drop S/C that divides the signals between the coherent Rxs [**9**]. The maximum distance the signal can reach the network is limited by the type of modulation format used, the signal bit rate and the FEC scheme used [**9**]. This means that this solution uses the signal characteristics to improve the network transmission efficiency. In Fig. 3.5, signals with bit rates of 400 Gbps reach shorter distances than signals with bit rates of 100 Gbps. Signals with bit rates of 400 Gbps require higher modulation formats such as 16-QAM or 64-QAM whereas in the case of signals with bit rates of 100 Gbps is used the QPSK modulation format [**9**].

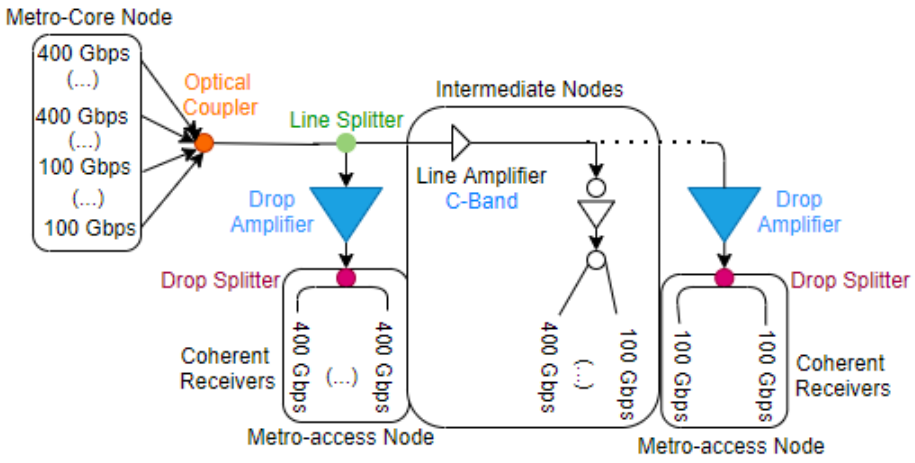

FIGURE 3.5. Diagram of a disaggregated FD&W network exploiting the coexisting bit rates of 100 Gbps and 400 Gbps.

The fourth and final solution for upgrading the L-band performance is the the low latency edge computing solution shown in Fig. 3.6. In this example, the hub nodes transmit the signal in the C-band to tributary nodes. The tributary nodes, which have micro data-center resources, provide a low latency connection to nearby tributary nodes using the L-band [**9**]. These micro data-centers are present in specific tributary nodes.

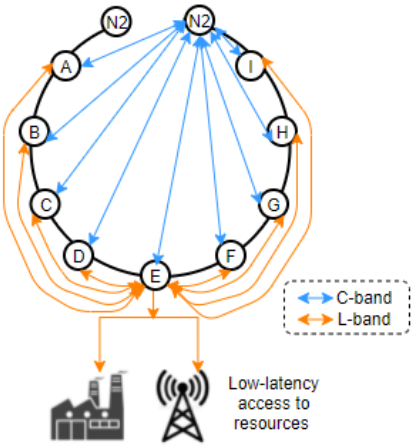

FIGURE 3.6. Dual C+L-band low latency edge computing solution.

3.4. Comparative analysis of hardware cost and power consumption

An analysis regarding the number of components involved in the metro horseshoe networks solutions using the L-band is performed in this section. The cost, power consumption and total offered capacity are also estimated. We will focus on the L-band amplified and unamplified FD&W solutions presented in subsections 3.3.1 and 3.3.2. As already pointed out the difference between the amplified and unamplified solutions is only concerning with the existence of amplifiers inside the L-band architecture node. The hardware count is performed following the steps considered in section 2.5. Thus, for L-band solutions, we consider two hub nodes with CD ROADM R&S architecture, similarly to the C-band, and 9 tributary dual-band nodes, as illustrated in Fig. 3.1, with FD&W ChD architecture in the L-band.

In Fig. 3.7, the tributary node architecture considering the FD&W ChD solution is presented, considering the transmission of 70 channels in the L-band per fiber, instead of 40 channels as in the C-band. Using Eq.(2.1), with $R = 2$ and $A/D = 20\%$, the number of required transponders in each L-band node is 28. Thus, beside considering two C/L filters to separate/aggregate the two bands and two amplifiers per node (in the case of the amplified solution, as depicted in Fig. 3.1), each tributary FD&W ChD node has four S/C 1:2, four S/C 1:16 (two per add and two per drop structure), each with 4 unused channels and 28 transponders, as shown in Fig. 3.7.

The hub node architecture for the L-band is based on a 5 degree CD ROADM R&S architecture as depicted in Fig. 3.8. Considering the metro network depicted in Fig. 2.3, where each hub node is connected to 3 different hub nodes and two tributary nodes, for an A/D ratio of 20%, a total of 112 wavelengths must be added/dropped per A/D

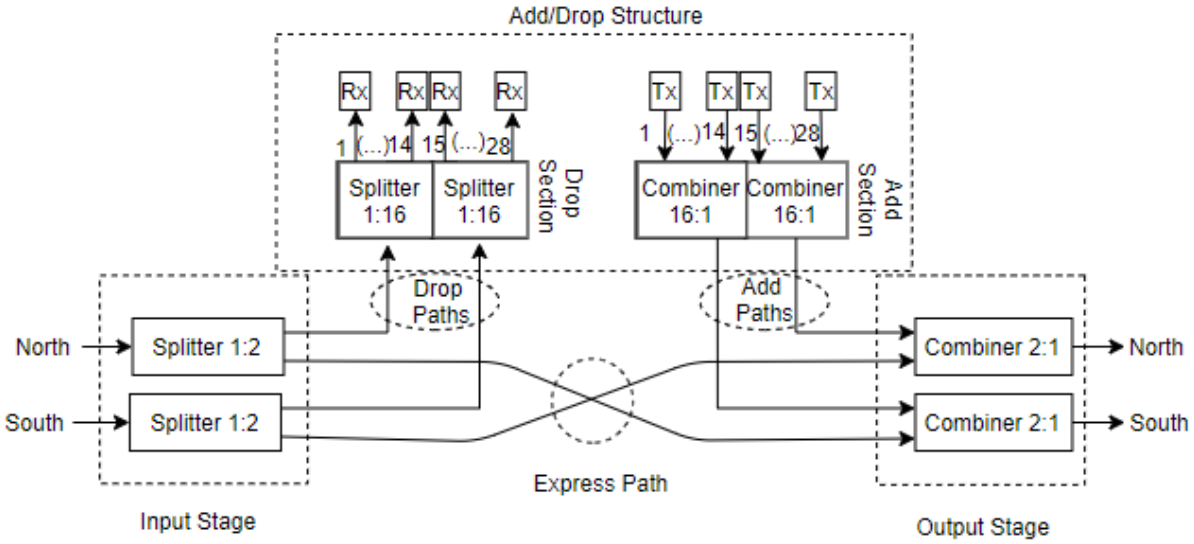

FIGURE 3.7. 2-Degree FD&W ChD tributary node.

structure in each hub node. As WSSs with maximum dimension of 1:20 are considered [**3**], it is necessary, in the A/D structure, to use 6 A/D cards to achieve this total of added/dropped wavelengths (which means we have a total of 12 WSSs 1:20 in the A/D structure). To connect each A/D card to the ROADM input/output directions, the size of the express WSSs must be at least 1:10. Fig. 3.8 shows input WSSs 1:20, as this is the only available size considered in Tab. 2.1. Hence, in Fig. 3.8, the hub node for the L-band has five WSSs 1:20 at the input and output stages, six WSSs 1:8 at the drop section, six S/Cs 1:8 at the add section and 112 transponders. Notice that, by comparing the add section in Fig. 3.8 and Fig. 2.18 (corresponding to the hub node for the C-band), we have chosen to use a WSS 20:1, instead of a S/C with very large size, 32:1, to reduce the losses in the add path in 12 dB, since the S/C 32:1 has losses of 19 dB [**27**].

In Tab. 3.1, considering components similar to the ones described in Tab. 2.1 for the hub and tributary nodes in the C-band, the total cost, power consumption and capacity per node in the L-band and the total cost and power consumption for the entire horseshoe network are shown. The total capacity per fiber reaching the tributary node and hub node in the L-band is, respectively, 7 Tbps and 28 Tbps, determined from the number of WDM channels and the transponder capacity, which is, respectively, 70 channels and 100 Gbps for the tributary node and, respectively, 140 channels and 200 Gbps between hub nodes. The total capacity per node, also shown in Tab. 3.1, is achieved by calculating the capacity per A/D structure (number of transponders $\times$ capacity of the transponder). So, the capacity per tributary node is 2.8 Tbps (28 transponders $\times$ 100 Gbps) and the average total capacity per hub node is calculated considering that 2/5 of the transponders of the

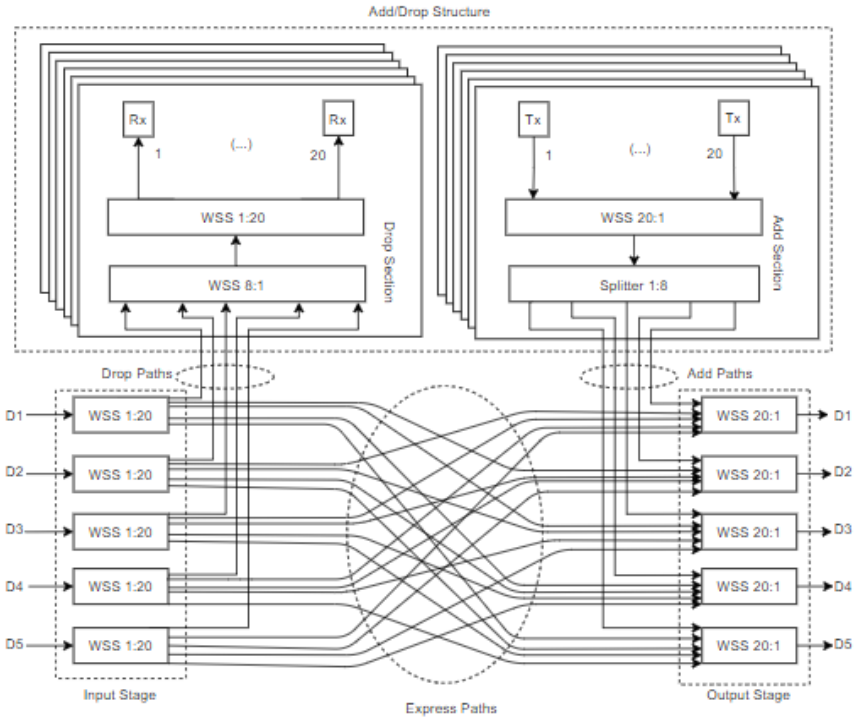

FIGURE 3.8. 5-Degree CD ROADM R&S hub node.

hub node are working at 100 Gbps (these transponders are used to communicate with the tributary nodes) and the other 3/5 are at 200 Gbps (these transponders are used to communicate with the other hub nodes). So, the average total capacity per hub node is 17.9 Tbps (2/5 × 112 transponders × 100 Gbps + 3/5 × 112 transponders × 200 Gbps).

It is known that the cost of the L-band components is higher than for C-band solutions [**5**]. So, for the study of the L-band hardware cost, we consider the normalized cost of each hardware component to be the double of the C-band components presented in Tab. 2.1. Note that, since the cost of the C/L band filter is around 110 €(considering it has similar cost as a red/blue filter in the C-band) [**52**], [**53**], we consider a normalized cost of 0.3 in relation to the 10 G transponder cost (330 €).

At the bottom of Tab. 3.1, the cost and power consumption per node and also the cost and power consumption for the all network, considering 9 tributary amplified or unamplified nodes combined with 2 hub nodes in the L-band are shown. The tributary node unamplified solution is cheaper (around 1.25 of normalized cost) and spends less power per node (around 20 W) than the tributary node amplified solution. Again, similarly to the C-band, the components that most contribute, around 99% (280/282.2 of normalized cost), to the final cost of the node are the transponders. The power consumption of the node tributary is about 3.4 kW, which is around 1.7 times higher than the consumption

TABLE 3.1. Hardware count, cost and power consumption of each optical component existing in the nodes tributary and hub in the L-band. The total cost of the hub and tributary nodes is shown at the bottom of the table.

Optical Components			**Number of components for each node architecture**		
Name	Normalized cost	Power consumption [W]	Tributary node based on FD&W ChD amplified	Tributary node based on FD&W ChD unamplified	Hub CD ROADM R&S
S/C 1×2	0.008	0	4	4	
S/C 1×8	0.04	0			6
S/C 1×16	0.08	0	4	4	
WSS 1×8	4.4	75			6
WSS 1×20	6	100			22
C/L band filter	0.3	0	2	2	2
Optical Amplifier	0.6	33	2		2
Flexible 200 Gbps BVT	16	145			112
100 Gbps coherent transponder	10	120	28	28	
Normalized cost per node			282.2	280.95	1952.44
Power consumption per node [kW]			3.43	3.36	18.96
Total capacity/node [Tbps]			2.8	2.8	17.9
Total cost/horseshoe [k]			6.45	6.43	
Total pow.cons./horseshoe [kW]			68.75	68.15	

of the FD&W ChD for the C-band. The normalized cost per tributary node is around 281, 3.5 times higher than in the C-band. This occurs because, in the L-band, the cost per component considered is the double and the number of transponders is almost the double too. The other components, such as the S/Cs have a small contribution to the final cost.

The hub node for the L-band is more expensive than the C-band. It has a normalized cost of around 3.5 times of the same node in the C-band, corresponding to almost twice higher the C-band node cost. The power consumption is also around 3.2 higher than the corresponding C-band node.

In Fig. 3.9, the total normalized cost of a horseshoe network as a function of the number of tributary nodes considering the FD&W ChD amplified and unamplified solutions is shown, considering that the L-band components cost is the double (blue line), three times more (cyan line), four times more (pink line) and five times more (green line) than the corresponding components of the C-band. Note that, for FD&W ChD nodes, since the cost of the amplified solution is very close to the cost of the unamplified solution, the two lines are practically superimposed in Fig. 3.9. The maximum and minimum costs

for 9 and 63 nodes are also presented in Fig. 3.9. Also in the L-band, the higher the number of tributary nodes, the greater the difference between the total network cost. For 9 tributary nodes, the cost difference between each line is around 5.3 k. For 63 tributary nodes, the cost difference between each line reaches around 21 k.

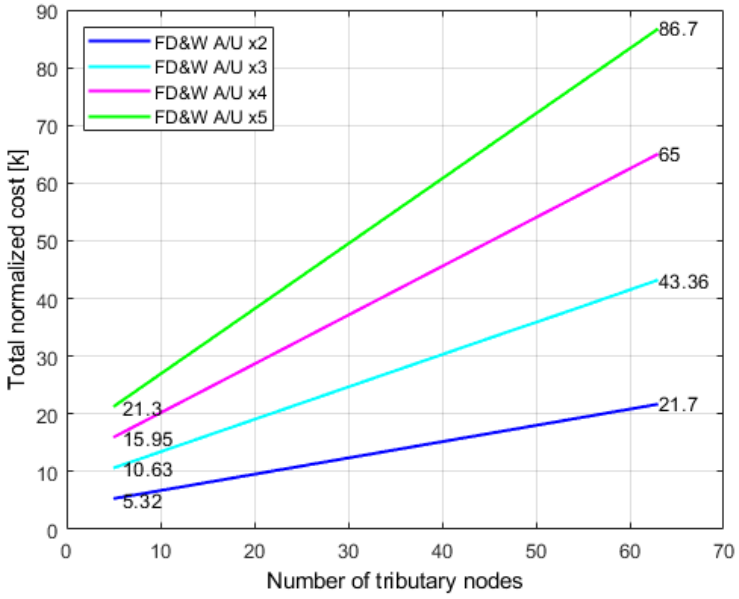

FIGURE 3.9. Total cost of a horseshoe network with two hub nodes as a function of the number of tributary FD&W ChD nodes with amplified and unamplified solutions, when the L-band components cost is twice, 3 times, 4 times and 5 times higher than the C-band components cost. Note that A/U means amplified/unamplified solutions.

As mentioned in section 2.5, the total normalized network costs presented are obtained in relation to 10 Gbps transponder cost, which is considered to be 330€. So, the total cost of the network using N1 FD&W ChD with amplified and unamplified is 2134 k€ and 2128.3 k€, respectively, when the components are twice expensive, which means that the unamplified solution is 3% less costly than the amplified one.

3.5. Physical layer impairments impact in L-band metro networks

In this section, the analysis of some PLIs, originated in the nodes as well as in the fiber, such as ILs, ASE noise, NLI noise and in-band crosstalk is performed, considering the signal transmission in the L-band using tributary nodes with the FD&W ChD solution.

For the L-band, we have to consider different system parameters from the C-band, as shown in Tab. 3.2. The noise figure (F_n) is at most 0.5 dB higher than in C-band, as considered in [**2**]. Hence, in this work, we consider a noise figure of 6.5 dB in the L-band. The fiber non-linearity coefficient in the L-band is slightly lower than in the C-band, with

γ= 1.2 W/km [**54**],[**55**], and the attenuation coefficient is α=0.25 dB/km, slightly higher than in the C-band.

TABLE 3.2. L-band system parameters [**2**],[**56**].

Parameters	**Values**
F_n [dB]	6.5
$\Delta_{fm} = R_s$ [GHz]	26.75
N_{ch}	40 (C-band) + 70 (L-band) + 3 (band gap)
Δ_{ch} [GHz]	100
α [dB/km]	0.25
γ [W/km]	1.2
ν_0 [THz]	188
D_λ [ps/nm/km]	17

Fig. 3.10 represents the spectral occupancy of the 70 channels belonging to the L-band and of the 40 channels belonging to the C-band, considering the ITU-T 100 GHz channel grid [**56**]. The L-band central frequency is 188 THz, while in the C-band is 193.7 THz. A band gap of 300 GHz between the C and L bands is considered, which contains 3 unused channels [**56**]. In order to have this gap, the WDM signal frequencies in the C-band are slightly shifted from the ones considered in Chapter 2.

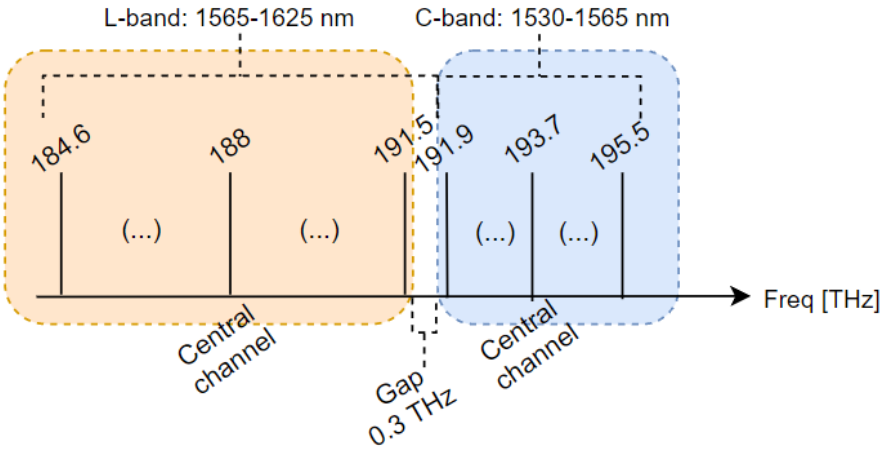

FIGURE 3.10. WDM signal frequencies for the C+L-band with 100 GHz channel spacing following the ITU-T grid [**56**], considering 40 channels for the C-band and 70 channels for the L-band.

Regarding the optical filtering effect in the L-band, only the WSSs in the hub nodes contribute to this effect. Hence, the effect of the optical filtering on the signal in the L-band FD&W solution should be very low, and is neglected in the following analysis.

The in-band crosstalk is also not considered in the amplified solution due to the absence of WSSs and frequency reuse in the FD&W ChD architecture, although 4 interfering terms

of second order are originated in the hub node, but they have a negligible influence on the performance, as shown in section 2.6.5. However, for the unamplified solution, the in-band crosstalk must be taken into account, since the wavelengths can be reused inside the horseshoe topology [**8**]. This case will be analyzed in section 3.5.4.

3.5.1. Insertion losses in amplified and unamplified solutions

In this section, we present the ILs of the two architectures applied to the L-band: amplified and unamplified. The hardware components are the same as used in FD&W-based nodes plus 2 C/L band filters. The losses of each hardware element are those considered in section 2.6.1. The losses of the C/L band WDM filters and hub node are around 0.6 dB. In this section, the losses of the connectors and splices are neglected.

In Tab. 3.3, the losses of the add, drop and express paths of the tributary and hub nodes are shown. The fiber losses after 10 km and 60 km spans are different from those found in the C-band, because the attenuation coefficient in the L-band is 0.25 dB/km. For this reason, the fiber losses after 10 km are 2.5 dB and after 60 km are 15 dB, shown at the bottom of the table, instead of 2.2 dB and 13.2 dB, respectively, observed in the C-band.

In the hub node architecture, and considering the Fig. 2.18, we should have a S/C 1:32 instead of a WSS 20:1 at the add section from the add path. However, since the S/C 1:32 has 19 dB of losses [**27**], the losses of the add path could achieved the 37 dB (IL_{sc}(32:1)+IL_{sc}(1:8)+IL_{wss}(20:1)=19+11+7=37 dB), which is very high to be compensating by the OA. Hence, the largest losses achieved by hub node considered to be 25 dB. In the case of the tributary node, the add and the drop paths have the same ILs of 19.6 dB, which is the value we will consider to calculate the amplifiers gain.

TABLE 3.3. ILs in the L-band, of the tributary node and the hub node.

	Tributary node	**Hub node**
Add_{path} [dB]	S/C 16:1+S/C 2:1+C+L filter 15+4+0.6=19.6	WSS 20:1+S/C 1:8+WSS 20:1 7+11+7=25
$Drop_{path}$ [dB]	S/C 1:2+S/C 1:16+ C+L filter 4+15+0.6=19.6	WSS 1:20 +WSS 1:8+WSS 1:20 7+7+7=21
$Express_{path}$ [dB]	S/C 1:2+ S/C 2:1+2 × C+L filter 4+4+2 × 0.6=9.2	WSS 1:20+WSS 20:1 7+7=14
10 km fiber [dB]	2.5	
60 km fiber [dB]	15	

In Tab. 3.4, the EDFA gains for the amplified solution in the L-band are presented. The gains of the pre and post-amplifiers along the network are set to compensate the corresponding ILs and are designed for the worst case of losses of the add, drop and express paths. When only pre-amplification is used, the amplifier gain is 22.1 dB because it compensates the overall losses of the 10 km and the tributary node. Any other case in Tab. 3.4 considers pre and post-amplification with perfect loss compensation. The hub node is the one that requires the highest amplifier gain to compensate 25 dB of loss. Amplifiers with higher gain will compensate higher losses, but originate higher ASE noise accumulation along the network.

TABLE 3.4. Pre and post EDFA gains considering 10 km and 60 km spans, for the tributary FD&W ChD node architecture and hub CD ROADM R&S node architecture and amplified solutions in the L-band.

Architecture Type	**N1 FD&W ChD amplified**		**N2 CD ROADM R&S**	
	10 km	60 km	10 km	60 km
$G_{pre,i}$ [dB]	22.1	15	2.5	15
$G_{pos,i}$ [dB]	-	19.6	25	25

3.5.2. Accumulated ASE noise in amplified solution

In this section, the accumulated ASE noise is calculated for the amplified solution in the L-band, which has OAs at the inputs/outputs of the tributary nodes. The accumulated ASE noise power in the L-band is calculated for 10 km and 60 km spans, considering the two worst paths represented in Fig. 2.23 (a) and (b), and depends on the gain and noise figure of the pre- and post-amplifiers presented in Tab. 3.4 and calculated from Eq. (2.4)-(2.6).

Tab. 3.5 shows the ASE noise power originated in the L-band at each pre- and post-amplifier for 10 and 60 km for the networks with hub FD&W ChD nodes. In the case of networks which use pre- and post-amplifiers, i.e., when the signal is inserted at the hub node, it contributes the most for the ASE noise power accumulation, producing the higher ASE noise power of -26.3 dBm to compensate the hub node in the beginning of the transmission. The lowest ASE noise power of -52.4 dBm is achieved for the span of 10 km and its contribution to the noise accumulation should be insignificant. The pre-amplifier used to compensate the losses of a 10 km span and a FD&W ChD tributary node leads to an ASE noise power of -29.2 dBm.

TABLE 3.5. ASE noise power originated at each pre- and post-amplifier for 10 km and 60 km spans, for the amplified solution using FD&W ChD node architecture in the L-band.

Architecture Type	**Tributary node**		**Hub node**	
	10 km	60 km	10 km	60 km
$P_{ase,pre,i}$ [dBm]	-29.2	-36.4	-52.4	-36.4
$P_{ase,pos,i}$ [dBm]		-31.7	-26.3	-26.3

Fig. 3.11 shows the OSNR evolution along the network for 10 km and 60 km, in the L-band, for the cases when the signal is inserted at tributary node or at node hub. When the signal insertion occurs at node tributary (blue and cyan lines), the OSNR is degraded significantly as the signal propagates along the nodes, decreasing 9.3 dB for 10 km spans and 9.6 dB for 60 km spans. In the case of signal insertion at the hub node (pink and green lines), the OSNR decreases 7.1 dB for the 10 km spans case and 5.8 dB for 60 km spans.

For the case of Fig. 2.23 (a), the OSNRs calculated in the L-band for the 10 km spans and 60 km spans cases are 5.3 dB and 4.2 dB lower, respectively, than the corresponding OSNRs obtained in the C-band. This occurs because the amplifiers in the L-band have higher ASE noise figure and gains.

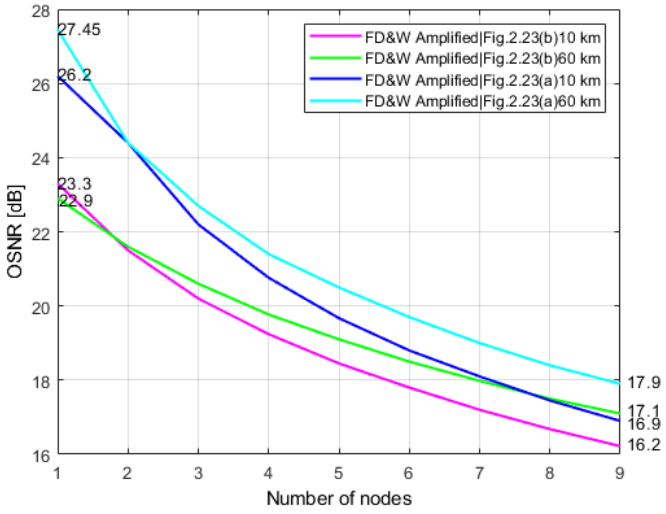

FIGURE 3.11. OSNR in the horseshoe topology, for the signal worst path with insertion at node tributary and the signal worst path with insertion at node hub, for tributary FD&W ChD amplified nodes in the L-band and 10 km spans and 60 km spans, for p_{Rx} equal to 0 dBm (assuming exact loss compensation).

For the case of Fig. 2.23 (b), the OSNRs achieved in the L-band are higher than in the C-band. This occurs because in the add section of the tributary node, a WSS is used, instead of a S/C, hence, reducing 8 dB the ILs in the L-band hub node compared to the C-band hub nodes ILs. However, as expected, compared to the case of Fig. 2.23 (a), the OSNRs are lower 6 and 5 dB, respectively, for 10 km and 60 km spans.

Since we are considering the same transponders in the C and L-bands, the minimum reference OSNR of the horseshoe network in the L-band is also 8.5 dB (@BER=4×10^{-3}). In Tab. 3.6, the OSNRs achieved at the optical Rx input, for the cases of Figs. 2.23 (a) and 2.23 (b) with 10 km and 60 km spans, considering the FD&W ChD amplified solution, are presented considering only the ASE noise accumulation. The OSNRs are higher for networks with 60 km spans, using pre- and post-amplification. The best OSNR achieved is 17.9 dB, for the case with signal insertion at tributary node for 60 km spans.

The OSNRs achieved at the Rx input are around 1 dB lower than the corresponding case in the C-band, for signal insertion at the tributary node.

TABLE 3.6. OSNR in the L-band for the cases of Fig. 2.23 (a) and (b) with 10 km and 60 km spans, for the tributary FD&W ChD amplified node architectures, at the end of the network after signal extraction.

	Span length	
	10 km	60 km
$OSNR_{R,min}$ [dB]	8.5	
$OSNR_{Fig.2.23(a)}$ [dB]	16.9	17.9
$OSNR_{Fig.2.23(b)}$ [dB]	16.2	17.1

3.5.3. Non-linear interference noise in amplified solution

In this section, the NLI noise power is studied, as well as the associated OSNRs for the amplified solution. To perform these studies, we do not use the Gaussian noise model described in section 2.6.3, because it does not take into account the presence of inter-channel Stimulated Raman Scattering (SRS). Inter-channel SRS induces power transfer among frequencies that are far apart, as happens with WDM channels inside the C+L band, since the C+L bandwidth has around 11 THz [**50**]. In this section, the Gaussian noise model presented in [**50**] is considered, where the effect of the SRS in the NLI noise is taken into account in simplified closed-form expressions used to evaluate the system performance with NLI considering inter-channel SRS.

The NLI parameter in the L-band, used in the calculation of the OSNR, given by [**50**]

$$\eta_n(f_i) \approx \sum_{j=1}^{n_{spans}} \left[\frac{P_{i,j}}{P_i}\right]^2 [\eta_{SPM,j}(f_i) n_{spans}^{\varepsilon} + \eta_{XPM,j}(f_i)] \tag{3.1}$$

where $\eta_{SPM,j}(f_i)$ is the Self-Phase Modulation (SPM) contribution generated in j-th span, $\eta_{XPM,j}(f_i)$ is the total Cross-Phase Modulation (XPM) contribution generated in j-th span and $P_{i,j}$ is the power of i-th channel at frequency f_i launched into the j-th span, and ε is the coherent factor of NLI accumulation along multiple fiber spans. If ε=0, the accumulation of NLI along the fiber spans is incoherent and if $\varepsilon \neq 0$, the NLI accumulates coherently [**50**]. Note that, in this work, we consider $P_{i,j}$=P_i. Thus, there is exact losses compensation.

The SPM contribution is given by [**50**]

$$\eta_{SPM}(f_i) \approx \frac{4}{9}\frac{\gamma^2}{B_i^2}\frac{\pi}{\Phi_i \overline{\alpha}(2\alpha+\overline{\alpha})}\left[\frac{T_i-\alpha^2}{\alpha}\operatorname{arcsinh}\left(\frac{\Phi_i B_i^2}{\pi\alpha}\right) + \frac{A^2-T_i}{A}\operatorname{arcsinh}\left(\frac{\Phi_i B_i^2}{\pi A}\right)\right] \tag{3.2}$$

where $\Phi_i = \frac{3}{2}\pi^2(\beta_2 + 2\pi\beta_3 f_i)$, $\beta_3 = \left(\frac{\lambda_0^2}{2\pi c}\right)^2 S_{\lambda_0} + \frac{\lambda_0^3 D_{\lambda_0}}{2\pi^2 c^2}$ is the higher order dispersion with $\lambda_0 = 1550$ nm, S is the dispersion slope, A= $\alpha + \overline{\alpha}$ and $T_i = (\alpha + \overline{\alpha} - P_{tot} C_r f_i)^2$, where P_{tot} is the WDM signal launch power, B_i is the bandwidth of the i-th WDM channel and C_r is the slope of the linear regression of the normalized Raman gain spectrum [**50**].

The total XPM contribution is given by [**50**]

$$\begin{aligned}\eta_{XPM}(f_i) \approx \frac{32}{27}\sum_{k=1,k\neq i}^{N_{ch}}\left(\frac{P_k}{P_i}\right)^2 \frac{\gamma^2}{B_k \Phi_{i,k}\overline{\alpha}(2\alpha+\overline{\alpha})} \\ \left[\frac{T_k-\alpha^2}{\alpha}\arctan\left(\frac{\Phi_{i,k}B_i}{\alpha}\right) + \frac{A^2-T_k}{A}\arctan\left(\frac{\Phi_{i,k}B_i}{A}\right)\right]\end{aligned} \tag{3.3}$$

where $\Phi_{i,k} = 2\pi^2(f_k - f_i)[\beta_2 + \pi\beta_3(f_i + f_k)]$. In this work, we consider the simplified case of $\alpha = \overline{\alpha}$ [**50**].

In order to confirm the correct implementation in Matlab of the expressions presented in [**50**] to compute the NLI parameter, we reproduced Fig. 5 (a) and 6 (b) of [**50**], in Fig. 3.12 (a) and (b), respectively, which shows the NLI parameter as a function of the WDM channels frequency, for input powers per channel of 0 and 2 dBm. In Fig. 3.12 (a), the NLI parameter is shown for only one 100 km span and in Fig. 3.12 (b), the NLI parameter is determined after six 100 km spans with coherent and incoherent accumulation. The Matlab implementation of Eqs.(3.1)-(3.3) is an adaptation of the code, available in [**57**]. To obtain the results shown in Fig. 3.12, we consider α=0.2 dB/km,

D=17.0 ps/nm/km, dispersion slope at the reference wavelength S=0.067 ps/nm^2/km, γ=1.2 1/W/km, C_r=0.028 1/W/km/THz, B_i=40.004 GHz, P_i=0 dBm and P_{tot}=24 dBm for 251 channels [**50**]. A very good agreement between Fig. 3.12 and Fig. 5 (b) and 6 (b) of [**50**] has been achieved, hence, ensuring the correct implementation of Eqs. (3.1)-(3.3).

As seen in Fig. 3.12, and except for the outer channels, the NLI parameter decreases from lower to higher channel frequencies due to SRS. The slope of this decrease is enhanced for higher channel powers. From Fig. 3.12 (a), the NLI parameter has a maximum value of 30.9 dB/W^2 for the $\nu_0 - 3.64$ THz (ν_0 is the central frequency of the C+L band) considering a 0 dBm channel power, whereas for a 2 dBm power, the maximum value of 31.75 dB/W^2 occurs for $\nu_0 - 4.2$ THz. The optical frequencies corresponding to the maximum of the NLI parameter for 0 and 2 dBm are in the L-band, respectively, 186.4 and 185.8 THz since ν_0=190 THz.

Regarding Fig. 3.12 (b), the coherent accumulation of NLI along the fiber spans (ϵ=0) leads to a higher NLI parameter in comparison with incoherent scenario, for the same launch power (0 dBm), because the SPM contribution (Eq. (3.2)) has more impact in the coherent scenario than in the incoherent one, whereas the XPM contribution (Eq. (3.3)) originate the same impact for both coherent and incoherent scenarios. Note that, the coherent accumulation scenario is more realistic [**50**], and, so, in subsequent studies, we will always consider coherent accumulation by setting ϵ=1;

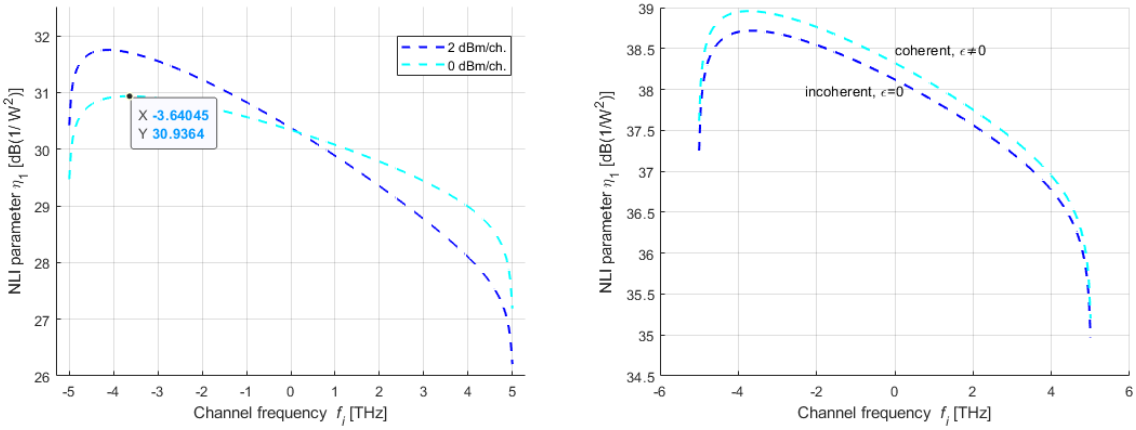

(a) (b)

FIGURE 3.12. NLI parameter after (a) one span with 100 km and (b) six spans with a total of 600 km as a function of the channel frequency for input powers per channel of (a) 0 dBm and 2 dBm and (b) 0 dBm considering NLI coherent and incoherent accumulation, for the example shown in [**58**].

In Figs. 3.13 (a) and (b), the NLI parameter as a function of WDM channels frequency is shown, respectively, for 10 and 60 km spans, after 9 spans as considered in the horseshoe network studied in this work, for the input powers per channel of -2, 0, 2 and 4 dBm. We have considered a WDM channel bandwidth of 26.75 GHz, with a total of 113 channels (40 for the C-band, 70 for the L-band and 3 for the guard-band) with a 100 GHz channel spacing and $\epsilon = 1$, i.e. coherent accumulation.

The NLI parameter obtained in Fig. 3.13 is higher ∼3 dB for 10 km spans than for 60 km spans, for all cases of input power per channel, because the coherent accumulation in shorter spans leads to an higher impact of NLI [**50**]. Another observation from Fig. 3.13 (a) and (b) is a dip in the NLI parameter variation due to the band gap between the C and L bands. This dip becomes more pronounced for the 60 km span scenario. A last observation from Fig. 3.13 reveals that for both span lengths, for higher channel input power, the higher the NLI parameter η_{NLI}, and the steepest its tilt, due to the stronger power transfer from higher to lower frequencies.

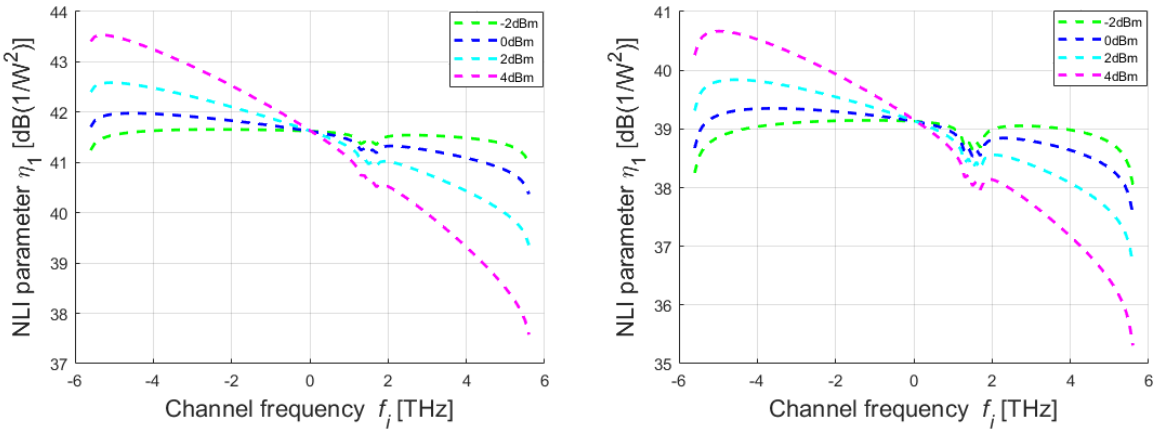

FIGURE 3.13. NLI parameter as a function of the channels frequency for (a) 10 km spans and (b) 60 km spans after 9 spans as in the horseshoe network considering coherent NLI accumulation, for the input powers per channel of -2 dBm, 0 dBm, 2 dBm and 4 dBm.

In Figs. 3.14 (a) and (b), the NLI power as a function of the WDM channels frequency is shown, for several input powers per channel and two span distances, 10 and 60 km, considering the horseshoe topology analyzed in this work, which has 9 spans. The NLI power is calculated using Eq. (2.17) with the NLI parameter taken from Fig. 3.13. As can be observed, the NLI power increases almost 5 dB, for a 4 dBm power channel, as the channel frequency decreases from the highest to the lowest channels for both span

distances. Also, it can be observed that, as the input power decreases, the NLI power increase is smoother from the highest to the lowest frequency channel for both span distances. So, the higher the input power, the higher the NLI power variation between lower and higher channel frequencies due to the stronger SRS. For the -2 dBm channel power the NLI power remains practically constant for all frequency channels due to the reduced SRS. Notice that the results presented for the NLI power are independent on where the signal is inserted in the horseshoe network. They only depend on the total path length and the number of nodes in the lightpath, which is 10 km for Fig. 3.14 (a) and 60 km for Fig. 3.14 (b).

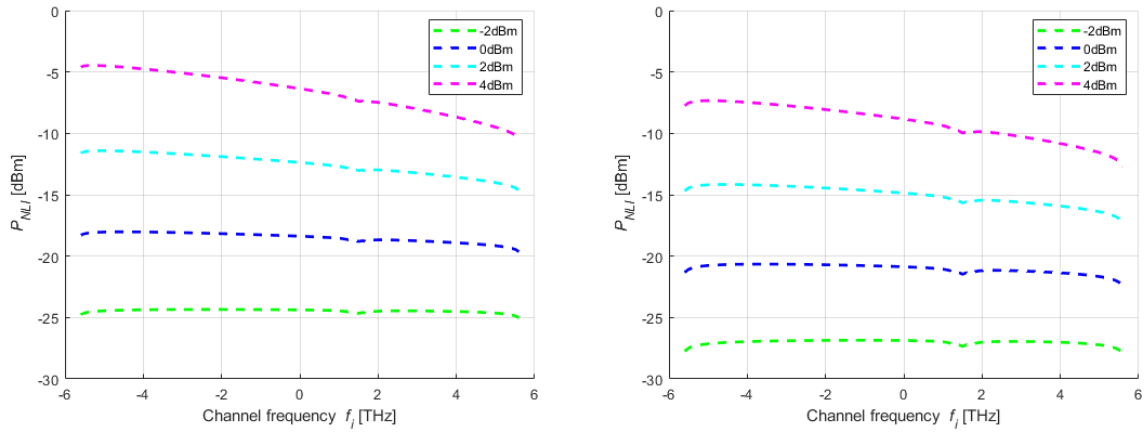

FIGURE 3.14. NLI power as a function of the channels frequency, for (a) 10 km spans and (b) 60 km spans after 9 spans as in the horseshoe network with coherent accumulation, for the input powers per channel of -2 dBm, 0 dBm, 2 dBm and 4 dBm.

In Fig. 3.15, the ASE noise power as a function of channel frequency after 9 spans of the horseshoe network for the cases of Figs. 2.23 (a) and 2.23 (b) and 10 km and 60 km spans is represented. We are going to study the ASE noise power variation in order to be able to compute the OSNR. As observed in Fig. 3.15 the ASE noise power increases with frequency, as predicted with Eqs. (2.5) and (2.6). The accumulated ASE noise power is higher for networks with 10 km spans than for networks with 60 km spans. The difference between the ASE noise power obtained considering the worst path shown in Fig. 2.23 (a) with 60 km spans and the ASE noise power corresponding to Fig. 2.23 (b) with 10 km spans is around 1.7 dB. The ASE noise power difference between the first and the last channel frequencies is about 0.26 dB. When considering 10 and 60 km spans, the

ASE noise power is respectively, 0.7 and 0.9 dB higher for the case of Fig. 2.23 (b) in comparison with Fig. 2.23 (a).

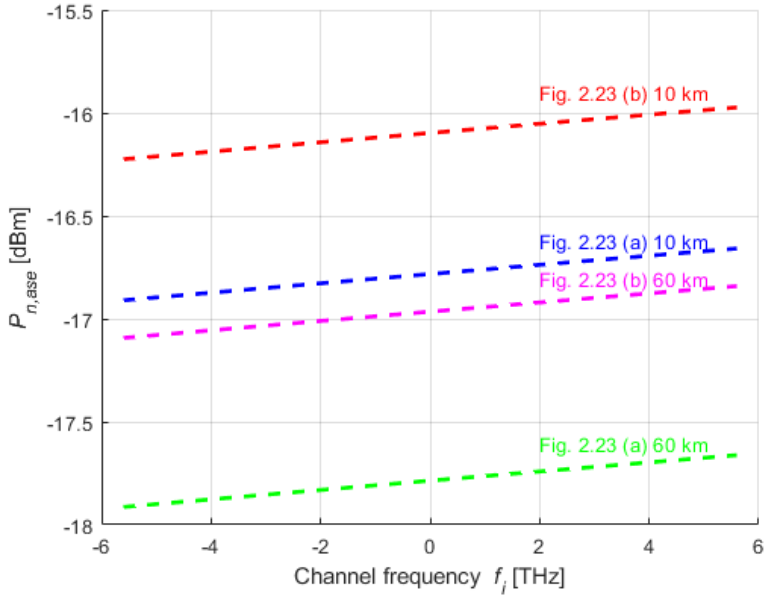

FIGURE 3.15. Accumulated ASE noise power as a function of channel frequency after 9 spans of the horseshoe network for cases of Fig. 2.23 (a) and Fig. 2.23 (b) for 10 and 60 km spans.

The OSNR as a function of channel frequency after 9 spans considering the ASE noise power and NLI (including inter-channel SRS) is shown in Fig. 3.16, for several scenarios. Fig. 3.16 (a), (b), (c) and (d) correspond to the OSNRs in the case of Fig. 2.23 (a) with (a) 10 km and (b) 60 km spans and Fig. 2.23 (b) with (c) 10 km and (d) 60 km spans, respectively, for various input channel powers (-2, 0, 2 and 4 dBm), including the optimal power per channel (red line), which leads to the best OSNR, and the maximum power per channel (dashed line) to comply the minimum OSNR in each case, for the worst channel. The minimum OSNR to comply the target BER of 4×10^{-3} is 8.5 dB, as calculated in Chapter 2.

The behaviour of the OSNR as a function of the channel frequency in Fig. 3.16 depends on the ASE and NLI noise powers. The ASE noise power increases with the channel frequency, but the NLI power decreases along the WDM signal bandwidth and as can be seen in Fig. 3.16, for higher input powers, the OSNR increases with the channel frequency due to the higher NLI power contribution to the OSNR slope variation.

It can be observed in Fig. 3.16 (a) to (d) that for the cases where the input power per channel is -2 and 0 dBm, the NLI power tilt has almost no influence, so an almost constant OSNR along all channels is observed. For input powers higher than 0 dBm we observe

that the OSNR increases as the channel frequency increases. From this behavior, we can state that there is an input power that gives an optimum OSNR (i.e. the maximum OSNR value) for each frequency channel. This optimum OSNR case is evaluated by varying the channel input power between -2 and 0 dBm with steps of 0.1 dB, and by analyzing the best possible OSNR, with the highest flatness along the WDM signal bandwidth (slope as close to zero as possible). Hence, for Fig. 3.16 (a), (b), (c) and (d), it has been found that the optimal input power that leads to the best OSNRs is -1, -0.5, -0.8 and -0.2 dBm, respectively. So, networks with 10 km spans require, slightly lower input powers to achieve the best OSNRs than for 60 km spans. The best OSNRs achieved in Fig. 3.16 (a), (b), (c) and (d) are around 14.5, 16, 14 and 15.4 dB, respectively. It can be observed that the optimal OSNR is practically constant along all the frequency channels ensuring the same received quality for all WDM channels.

Regarding the OSNR differences due to span distances, we can observe that for 60 km spans, the OSNRs achieved for the optimum launch power are 1.5 dB higher than for 10 km spans, due to the lower NLI and ASE noise powers. When the signal is inserted in the hub node as in the case of Fig. 2.23 (b), the optimum OSNRs are around 0.5 dB lower than in the case of Fig. 2.23 (a) due to the higher ASE noise power added by the hub node.

Finally, it can be observed that all cases shown in Fig. 3.16 comply with the minimum OSNR required of 8.5 dB, except for the cases with 10 km spans and input power of 4 dBm, where this value is not achieved in the lowest channel frequencies. The maximum input power that ensures the minimum OSNR for all WDM channels is represented in Fig. 3.16 and varies between 3.8 dBm and 5 dBm for networks with 10 and 60 km spans, respectively. Therefore, the difference between the optimal OSNR and the minimum OSNR is at least 5.5 dB higher for all cases of Fig. 3.16, which ensures enough margin to include other PLIs. For example, if we consider a minimum system margin of 3 dB and an extra power penalty due to other transmission effects of 1.5 dB, like components aging the minimum required OSNR is still accomplished.

3.5.4. In-band crosstalk in unamplified solution

In this subsection, the analysis of PLIs, considering the signal transmission in the L-band in a horseshoe topology based on tributary nodes with the FD&W ChD unamplified solution is performed. In this scenario, the main PLIs is the in-band crosstalk that arises due to the wavelength reuse in these networks. This impairment has been deeply studied

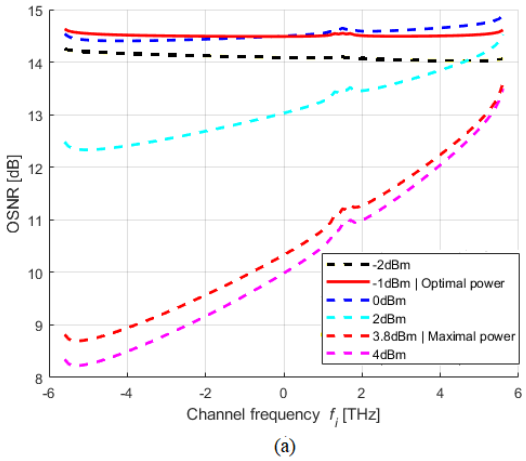

(a) Fig. 2.23 (a) with 10 km spans.

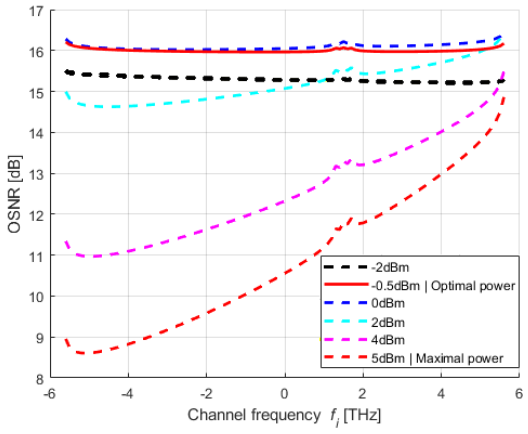

(b) Fig. 2.23 (a) with 60 km spans.

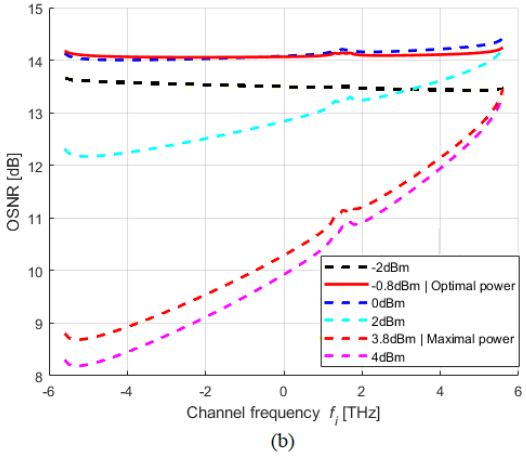

(c) Fig. 2.23 (b) with 10 km spans.

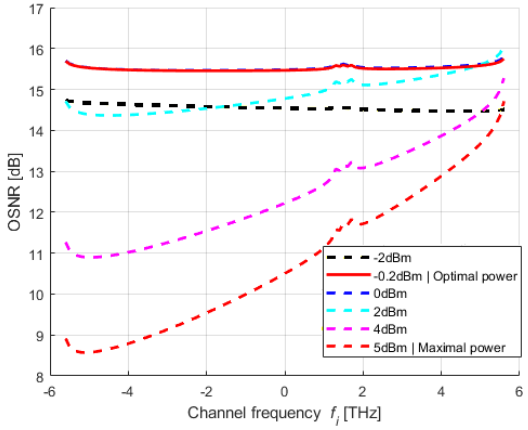

(d) Fig. 2.23 (b) with 60 km spans.

FIGURE 3.16. OSNR as a function of the channel frequency after 9 spans considering the ASE noise power and NLI (including inter-channel SRS), for several input channel powers.

in optical networks with both direct and coherent detection schemes [**12**]. Nevertheless, its influence in metro networks with unamplified coherent solutions has been less analyzed. In [**8**], the impact of this impairment is obtained by simulation in a horseshoe topology. In this subsection, we present an analytical formalism to assess the impact of this phenomena, based on the SNR ratio at the Rx output. We start our analysis by presenting the SNR at the Rx output without in-band crosstalk, and in this scenario, we assess the maximum number of spans in a lightpath. After that we introduce the in-band crosstalk in our model and assess the respective degradation in terms of the number of spans.

The Rx performance, without in-band crosstalk, is measured through the SNR and is given by [**58**]

$$snr = \frac{p_{R_x}}{\frac{\sigma_{th}^2}{P_L^{CW}} + P_L^{CW} \cdot \sigma_{nLO}^2 \cdot CMRR + \sigma_{shot}^2 + \frac{p_{R_x}}{SNR_q}} \tag{3.4}$$

where P_L^{CW} is the Continuous Wave (CW) optical power of the Local Oscillator (LO), $CMRR$ is the Common Mode Rejection Ratio of the balanced photodetector, SNR_q is an additional term to include several implementation penalties occurring in a coherent system (phase noise, quantization noise and imperfect constellation generation), σ_{th}^2 is the variance of the Transimpedance Amplifier (TIA) thermal noise, σ_{nLO}^2 is the variance of the LO Relative Intensity Noise (RIN) and σ_{shot}^2 is the variance of the shot noise generated in the photodetection process. The variances σ_{th}^2, σ_{nLO}^2 and σ_{shot}^2 are given, respectively, by

$$\sigma_{th}^2 = \frac{i_{TIA}^2 \cdot B_{eq}^{RX}}{8 \cdot R_\lambda^2} \tag{3.5}$$

$$\sigma_{shot}^2 = \frac{q \cdot B_{eq}^{RX}}{2 \cdot R_\lambda} \tag{3.6}$$

$$\sigma_{nLO}^2 = RIN \cdot \frac{B_{eq}^{RX}}{2} \tag{3.7}$$

where R_λ is the overall responsivity (in [A/W]) of the coherent Rx (considering also the passives losses before the photodiodes), i_{TIA} is the input-referred noise current density (in $p\text{A}/\sqrt{Hz}$) of a TIA, B_{eq}^{RX} is the effective noise bandwidth of the Rx, $q = 1.602176634 \times 10^{-19}$ C is the electron charge and RIN is the LO RIN parameter.

In Tab. 3.7, the parameters used to calculate the SNR are given and are based on the fitting to experimental results performed in [**58**]. Note that, typically the responsivity is between 0.6 and 1.0 A/W [**31**],[**59**]. However, in the model presented in [**58**], the responsivity definition takes into account the losses introduced by the Rx optical passive elements, such as polarizing beam splitter and optical hybrid.

In Fig. 3.17, the BER as a function of the received signal power for different LO powers of 6, 10, 14 and 18 dBm is shown. Considering QPSK modulation (M=4), the BER is obtained from Eq. (2.8) using the SNR obtained from Eq. (3.4) with the parameters presented in Tab. 3.7. The required target BER assumed for the system is 4×10^{-3} (HD-FEC) or 2×10^{-2} (Soft-Decision (SD)-FEC) [**58**].

As observed in Fig. 3.17, for each LO powers of 6, 10, 14 and 18 dBm, the minimum received power required to achieve the target BER is, respectively, -36.1, -35.7, -35.6 and -33.8 dBm, for HD-FEC. For SD-FEC, for each LO power, the minimum received powers

TABLE 3.7. L-band system parameters for the unamplified solution [**58**].

Parameters	**Values**
R_λ [A/W]	0.07
$CMRR$ [dB]	-20
i_{TIA} [pA/$\sqrt{Hz}$]	19
SNR_q [dB]	18.4
B_{eq}^{RX}	0.6 × R_s, where R_s=26.75 Gbaud
RIN [dB/Hz]	-145

required are, respectively, -38.9, -38, -37.9 and -36 dBm, which leads to at least 2.2 dB of power budget improvement for SD-FEC in relation to HD-FEC.

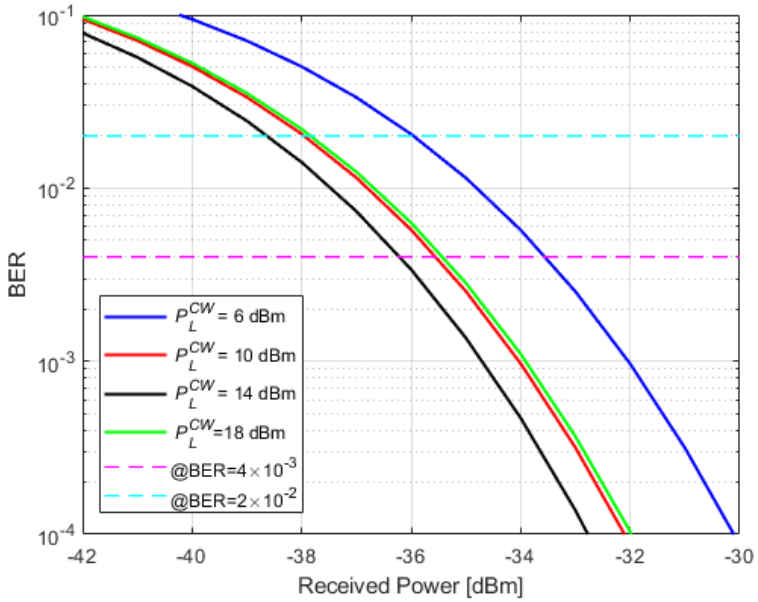

FIGURE 3.17. BER as a function of the received signal power for different LO powers P_L^{CW}, for QPSK signals.

From Fig. 3.17 can also be observed that the LO power of 14 dBm leads to the minimum received power that ensures the target BER, while $P_L^{CW} = 6$ dBm leads to the highest and most demanding received power to reach the same target BER. LO powers above the optimum require a higher received power to reach the target BER, as shown in Fig. 3.17, where for $P_L^{CW} = 18$ dBm, the required received power is similar to the one obtained for $P_L^{CW} = 10$ dBm. Hence, in the following results, we consider $P_L^{CW} = 14$ dBm, as the optimum LO power that leads to the minimum BER and, consequently, to a higher power budget.

So, knowing the minimum received power for a specific target BER, the main goal is to compute the maximum power budget and the maximum reach of the horseshoe network with an unamplified solution, considering 10 and 60 km spans, for a reference input power of 0 dBm, taken from the maximum input power considered in [**58**]. Hence, the maximum power budget is 36.1 dB and 38.9 dB, respectively for the HD-FEC and SD-FEC.

The next step in this analysis is to compute the insertion losses per span for the various scenarios considered in this work, hub-span-tributary, tributary-span-hub and tributary-span-tributary, as shown in Fig. 3.18. In Fig. 3.18 (a), the losses for 10 or 60 km spans, are, respectively, 47.1 dB (25 dB for the add in the hub node, plus 2.5 dB for the span losses, plus 19.6 dB, for the drop at the tributary node, as considered in Tab. 3.3) and 59.6 dB (25 dB for the add in the hub node, plus 15 dB for the span losses, plus 19.6 dB, for the drop at the tributary node, as considered in Tab. 3.3). In Fig. 3.18 (b), the losses include the tributary node losses in an add operation (also 19.6 dB) and the hub losses, when performing a drop (21 dB), which leads to 43.1 and 55.6 dB of total losses, respectively, for 10 and 60 km spans. In Fig. 3.18 (c), the losses are 41.7 and 54.2 dB, respectively, for 10 and 60 km spans.

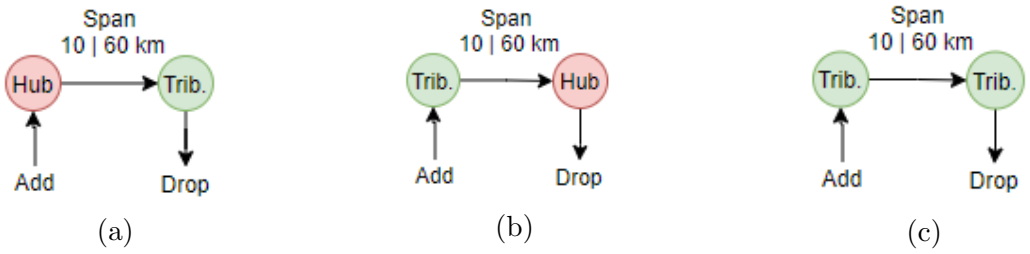

FIGURE 3.18. Possible span configurations considered to evaluate the performance of the unamplified solution.

As can be seen by comparing the power budgets and the ILs of just one span for the various scenarios, it can be concluded that the power budgets are not sufficient to accommodate the ILs.

A possible solution to decrease the ILs per span is to reduce the S/C dimension in the add/drop structures. Instead of using S/C 1:16, we are going to consider S/C 1:8, 1:4 and 1:2 solutions only for the add/drop structure of tributary nodes. So, in the tributary nodes shown in Fig. 3.7, the S/C 1:16 in the A/D structure is replaced by S/Cs with smaller size, as considered already in other works [**8**], [**10**], for the unamplified solution. In this unamplified scenario, the A/D structure of the hub node remains the same as in the amplified scenario.

In Tab. 3.8, the total ILs for the three configurations presented in Fig. 3.18, for 10 and 60 km spans considering different S/C dimensions are shown.

TABLE 3.8. ILs considering the configurations of Fig. 3.18 for different S/C dimensions for the add/drop structure of the tributary node.

Total insertion losses [dB]	S/C 1:2		S/C 1:4		S/C 1:8		S/C 1:16	
	10 km	60 km	10 km	60 km	10 km	60 km	10 km	60 km
Hub-span-tributary	36.1	48.6	39.1	51.6	43.1	55.6	47.1	59.6
Tributary-span-hub	32.1	44.6	35.1	47.6	39.1	51.6	43.1	55.6
Tributary-span-Tributary	19.7	32.2	25.7	38.2	33.7	46.2	41.7	54.2

As can be observed in Tab. 3.8, for 60 km span, the ILs are always higher than the power budget (38.9 dB @$BER = 2 \times 10^{-2}$), except for tributary-span-tributary configuration with S/C 1:2 and 1:4, so this span distance does not work in most cases of the unamplified solution. Regarding 10 km spans, it can be concluded that one span is possible with S/C 1:2 for all the configurations of Fig. 3.18, whereas only the tributary-span-hub and tributary-span-tributary configurations are possible for S/C 1:4 dimension, and it can be also concluded that for the S/C 1:8 dimension only the tributary-span-tributary configuration is possible. Two spans are not possible with any of the configurations of Fig. 3.18.

In the following, we are going to consider the impact of in-band crosstalk in the performance of the unamplified solution considering spans with 10 km only. In order to take into account the impact of in-and crosstalk, the SNR given by Eq. (3.4) is rewritten as (see Appendix A),

$$snr = \frac{p_{R_x}}{\frac{\sigma_{th}^2}{P_L^{CW}} + P_L^{CW} \times \sigma_{nLO}^2 \times CMRR + \sigma_{shot}^2 + \frac{p_{Rx}}{SNR_q} + p_{X_c}} \tag{3.8}$$

where the crosstalk power p_{X_c} (defined in section 2.6.5) is added in the denominator.

In Fig. 3.19, the BER as a function of the received signal power with different crosstalk levels of -35, -30, -25 and -20 dB, is shown considering P_L^{CW}=14 dBm. The BER curve without crosstalk is also represented for comparison purposes and in this case, the minimum received signal power is -36.1 and -38.9 dBm corresponding, respectively, to the target BERs of 4×10^{-3} and 2×10^{-2}.

As can be concluded from Fig. 3.19, for an input signal power of 0 dBm, and considering the ILs shown in Tab. 3.8, for S/Cs 1:2, 1:4 and 1:8, when the crosstalk level ranges between -35 and -25 dB, the optical power budget is still accomplished for all cases. For

a crosstalk power of -20 dB, the minimum received power is about -37.4 dBm, for a SD-FEC, leading to 1.5 dB degradation in relation to the case without crosstalk. In this case, although the optical power budget is reduced, the unamplified solution is still feasible. For a two spans transmission, the most feasible configuration is tributary-span-tributary due to its lower ILs, which are very close to the highest power budget (19.7+19.7 dB = 39.4 dB compared to 38.9 dB).

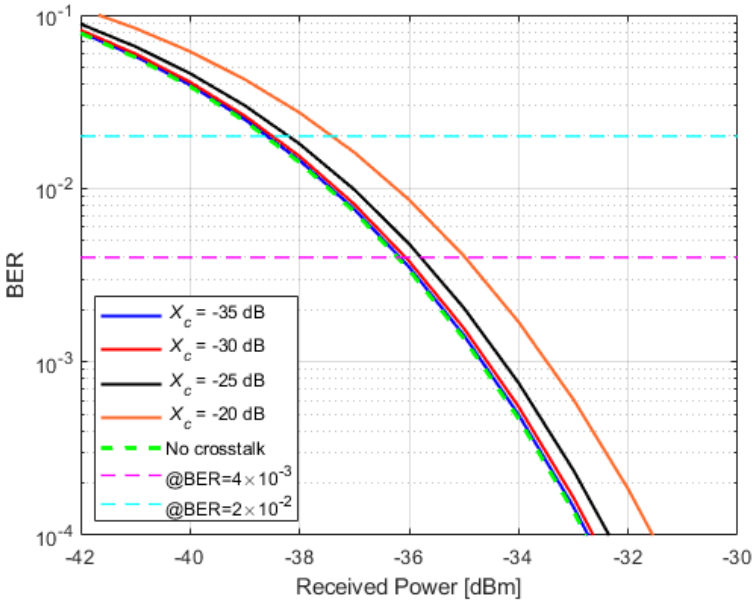

FIGURE 3.19. BER as a function the received signal power with the crosstalk level as a parameter. The case without crosstalk is also represented.

3.6. Conclusions

In this chapter, FD&W ChD amplified and unamplified solutions have been studied for L-band tributary nodes. The hardware components, cost, power consumption, total node capacity, and the main PLIs that impair the L-band transmission performance have been assessed for the horseshoe network with 2 hub nodes and 9 tributary nodes, considering 10 km and 60 km spans either with signal insertion at a tributary or hub nodes. Some L-band upgrading solutions have been also briefly discussed.

We concluded that the total cost of the horseshoe network considering amplified and unamplified solution is 2134 k€, and 2128.3 k€, respectively (40% higher than in the C-band). The total power consumption per horseshoe network is around 68.75 kW, higher than in the C-band.

For the amplified solution, considering only the ASE noise effect and signal insertion in the hub node, the OSNR ranges between 16.2 dB and 17.1 dB for, respectively, 10 km and 60 km spans, which is at least 1.4 dB higher than in the C-band, because the hub node in the L-band uses a WSS at the add section instead of a S/C, reducing the ILs. For signal insertion in the tributary node, in the L-band, the OSNR ranges between 16.9 dB and 17.9 dB for, respectively, 10 km and 60 km spans, which is at least 4.2 dB lower than the OSNRs obtained in the C-band, because the influence of the tributary node is higher than the hub node and has less ILs. Considering the ASE noise, NLI and signal insertion in the hub node, the OSNRs ranges between 14 and 15.4 dB for, respectively, 10 and 60 km spans, which is at least 1.8 dB higher than in the C-band. For signal insertion in the tributary node, the OSNR ranges between 14.5 and 16 dB, which is at least 1 dB lower than in the C-band. For 60 km spans and for the optimum launch power, the OSNRs achieved are around 1.5 dB higher than for 10 km spans because they have lower NLI and ASE noise.

In FD&W unamplified solutions, the BER is evaluated considering the SNR at the receiver input with and without crosstalk. The study was performed for P_L^{CW}=14 dBm and 0 dBm of transmitted signal power and the maximum power budget achieved without crosstalk was 38.9 dB. To accomplish this power budget, for a single fiber span of 10 km, smaller S/Cs (1:2 and 1:4) must be used in the A/D structure of the tributary nodes, reducing the A/D ratio capacity of these nodes in comparison with the amplified solution. When considering the in-band crosstalk due to frequency reuse in the horseshoe network, a crosstalk level of -20 dB causes a degradation on the optical power budget of 1.5 dB in comparison to the situation without a crosstalk, but a single span transmission is still feasible.

CHAPTER 4

Conclusions and future work

In this chapter, the main conclusions of this dissertation are presented. Furthermore, some suggestions for future work are also proposed.

4.1. Final conclusions

In this dissertation, we studied several nodes architectures for implementation in C+L band horseshoe network, namely CD ROADM B&S and FD&W ChD solutions for the C-band and FD&W ChD amplified and unamplified solutions for the L-band. The impact of several PLIs on the horseshoe network topology with the different architectures solutions has been also assessed.

In Chapter 2, the C-band node architectures for the horseshoe topology and the corresponding hardware components have been presented and the corresponding cost, assuming an end of life scenario, and power consumption analyzed. For the C-band, the network is composed by 2 hub nodes based on CD ROADM R&S and 9 tributary nodes based on CD ROADM B&S or FD&W ChD. Tributary CD ROADMs provides the same capacity (2.8 Tbps) and flexibility as the FD&W architecture, however, the FD&W ChD architecture is less expensive and consumes less power. We have also concluded that the transponders are the components that contributes the most to the cost and power consumption of each node. The PLIs impact on the horseshoe network performance has been also assessed for both tributary nodes solutions by estimating the OSNR. Considering the ASE noise only, the ROADM tributary nodes solution provides a 9 dB lower OSNR than the one obtained in FD&W-based nodes. The NLI contributes to at least 0.1 dB lower OSNR for the ROADM-based networks. In any case, considering NLI, the OSNRs are lower when signal insertion occurs at the hub node, with a higher OSNR decrease for the FD&W solution than for the ROADM node architectures.

In Chapter 3, the C+L-band node architectures solutions and their hardware components have been described. The L-band nodes are based on FD&W amplified and unamplified solutions. The amplified solution cost is around 40% higher than the C-band network, considering components that are twice expensive in the L-band. We also

concluded that the FD&W amplified solution provides more capacity than the unamplified solution, but the cost and power consumption of the two solutions are similar. The transponders contribute around 99% to the node final cost.

For the amplified solution, considering an horseshoe network with 2 hub nodes, tributary nodes, and 10 km spans, and two worst path cases of signal transmission, the optimum OSNR achieved at the optical receiver input is above 14 dB, when ASE noise and NLI are considered. This leaves enough margin to guarantee the minimum OSNR in the amplified solution.

In unamplified solutions, to accomplish the power budget, smaller S/Cs 1:2 and 1:4 must be used in the A/D structure of the tributary nodes, and transmission should not exceed one fiber span. Due to frequency reuse in the unamplified solution, in-band crosstalk arises. For a crosstalk level of -20 dB, a 1.5 dB degradation on the optical power budget is observed.

4.2. Future work

The following topics are proposed for future investigation:

- Study the PLIs of the L-band upgrading network solutions, such as the ones described in section 3.3.3;
- Study the L-band network performance of the L-band solutions considering other modulations formats, such as 16-QAM and 64-QAM and also other channel spacings, different from the 100 GHz considered in this work;
- Develop a Monte-Carlo simulator to study the performance of the horseshoe network to assess the accuracy of the analytical results presented in this work;
- Develop a rigorous analytical model to study the in-band crosstalk in networks for the L-band unamplified solution.

References

[1] P. J. Winzer, D. T. Neilson, and A. R. Chraplyvy, "Fiber-optic transmission and networking: the previous 20 and the next 20 years [invited]," *Optics Express*, vol. 26, no. 18, pp. 24 190–24 239, Sep. 2018.

[2] B. Correia, R. Sadeghi, E. Virgillito, A. Napoli, N. Costa, J. Pedro, and V. Curri, "Power control strategies and network performance assessment for C+L+S multiband optical transport," *Journal of Optical Communications and Networking*, vol. 13, no. 7, pp. 147–157, Jul. 2021.

[3] J. A. Hernandez, M. Quagliotti, L. Serra, L. Luque, R. L. D. Silva, A. Rafel, O. G. D. Dios, V. Lopez, A. Eira, R. Casellas, A. Lord, J. Pedro, and D. Larrabeiti, "Comprehensive model for technoeconomic studies of next-generation central offices for metro networks," *Journal of Optical Communications and Networking*, vol. 12, no. 12, pp. 414–427, Dec. 2020.

[4] A. Ferrari, A. Napoli, J. K. Fischer, N. Costa, A. D'Amico, J. Pedro, W. Forysiak, E. Pincemin, A. Lord, A. Stavdas, J. P. F. Gimenez, G. Roelkens, N. Calabretta, S. Abrate, B. Sommerkorn-Krombholz, and V. Curri, "Assessment on the achievable throughput of multi-band ITU-T G.652.D fiber transmission systems," *Journal of Lightwave Technology*, vol. 38, no. 16, pp. 4279–4291, 2020.

[5] M. Cantono, R. Schmogrow, M. Newland, V. Vusirikala, and T. Hofmeister, "Opportunities and challenges of C+L transmission systems," *Journal of Lightwave Technology*, vol. 38, no. 5, pp. 1050–1060, Mar. 2020.

[6] I. T. Union, "Handbook – optical fibres, cables and systems," 2009. [Online]. Available: www.itu.int

[7] A. Napoli and J. Pedro, "Getting the most from currently deployed optical fiber infrastructure," Coriant, Fiber Systems, Jun. 2017. [Online]. Available: https://www.fibre-systems.com/viewpoint/getting-most-currently-deployed-optical-fiber-infrastructure

[8] R. Emmerich, A. Eira, N. Costa, P. W. Berenguer, R. Elschner, C. Schubert, J. K. Fischer, J. Pedro, and R. Freund, "Dual-band node architectures for C+L-band capacity upgrades in optical metro transport networks," *Photonic Networks, VDE, 21th ITG-Fachtagung*, Dec. 2020.

[9] F. Paolucci, A. Sgambelluri, F. Cugini, R. Emmerich, A. Eira, N. Costa, J. Pedro, P. W. Berenguer, C. Schubert, J. K. Fischer, and F. Fresi, "Disaggregated edge-enabled C+L-band filterless metro networks," *Journal of Optical Communications and Networking*, vol. 12, no. 3, pp. 2–12, Mar. 2020.

[10] R. Emmerich, A. Eira, N. Costa, P. W. Berenguer, C. Schubert, J. K. Fischer, and J. Pedro, "Capacity limits of C+L metro transport networks exploiting dual-band node architectures," *Optical Fiber Communication Conference (OFC), OSA Technical Digest (Optical Society of America)*, San Diego, CA, USA, paper M2G.5, Mar. 2020.

[11] A. Eira, N. Costa, and J. Pedro, "On the capacity and scalability of metro transport architectures for ubiquitous service delivery," *International Conference on Transparent Optical Networks*, 2018.

[12] D. Sequeira, L. Cancela, and J. Rebola, "CDC ROADM design tradeoffs due to physical layer impairments in optical networks," *Optical Fiber Technology*, vol. 62, Article 102461, Mar. 2021.

[13] P. Pavon-Marino, F. J. Moreno-Muro, M. Garrich, M. Quagliotti, E. Riccardi, A. Rafel, and A. Lord, "Techno-economic impact of filterless data plane and agile control plane in the 5G optical metro," *Journal of Lightwave Technology*, vol. 38, no. 15, pp. 3801–3814, Aug. 2020.

[14] N. Sambo, A. D'Errico, C. Porzi, V. Vercesi, M. Imran, F. Cugini, A. Bogoni, L. Potì, and P. Castoldi, "Sliceable transponder architecture including multiwavelength source," *Journal of Optical Communications and Networking*, vol. 6, no. 7, pp. 590–600, Jul. 2014.

[15] A. Eira and J. Pedro, "The role of metro transport node architectures in optimized edge datacenter dimensioning," *International Conference on Optical Network Design and Modeling (ONDM)*, Barcelona, Spain, Jul. 2020.

[16] S. Woodward, M. Feuer, and P. Palacharla, "ROADM-node architectures for reconfigurable photonic networks," *Optical Fiber Telecommunications VIB*, pp. 683–707, Kaminov, T. Li, and A. Willner, eds.6, Academic Press, Dec. 2013.

[17] J. M. Simmons, *Optical network design and planning*, 2nd ed. Springer International Publishing, 2014.

[18] Lumentum, "Optical communications products," 2020. [Online]. Available: https://www.lumentum.com/en/optical-communications/all-products

[19] B. C. Collings, "Advanced ROADM technologies and architectures," *Optical Fiber Communication Conference*, Los Angeles, California United States, paper Tu3D.3, Mar. 2015.

[20] S. Gringeri, B. Basch, V. Shukla, R. Egorov, and T. J. Xia, "Flexible architectures for optical transport nodes and networks," *IEEE Communications Magazine*, vol. 48, no. 7, pp. 40–50, 2010.

[21] M. Feuer, S. Woodward, P. Palacharla, X. Wang, I. Kim, and D. Bihon, "Intra-node contention in dynamic photonic networks," *Journal of Lightwave Technology*, vol. 29, no. 4, pp. 529–535, Feb. 2011.

[22] T. Zami, "High degree optical cross-connect based on multicast switch," *Optical Fiber Communication Conference and Exhibition (OFC)*, San Francisco, CA, USA, paper W2A.36, Mar. 2014.

[23] T. Zami and B. Lavigne, "Advantages at network level of contentionless N×M adWSS," *Optical Fiber Communication Conf. (OFC)*, San Diego, CA, USA, paper MIA.2, Mar. 2019.

[24] P. Colbourne, S. McLaughlin, C. Murley, S. Gaudet, and D. Burke, "Contentionless twin 8x24 WSS with low insertion loss," *Optical Fiber Communication Conf. (OFC)*, San Diego, California United States, paper Th4A.1, Mar. 2018.

[25] "Ekinops 360 Series PM1001RR 10G Metro, Regional E Longas-haul Transponder xs-v4," https://www.ebay.com/itm/143902584149, accessed: 2020-05-03.

[26] ThorLabs, "1 x 2 and 2 x 2 mems optical switch kits." [Online]. Available: https://www.thorlabs.com/catalogpages/V21/1135.pdf

[27] T. F. O. A. Inc., "Testing fiber optic couplers, splitters or other passive devices," *Available: www.thefoa.org/tech/ref/testing/test/couplers.html*, 2019.

[28] ThorLabs, "0.22 NA Solarization-Resistant step index multimode optical fibers." [Online]. Available: https://www.thorlabs.com/newgrouppage9.cfm?objectgroup_id=6840

[29] Cisco, "Calculating the maximum attenuation for optical fiber links." [Online]. Available: http://www.cisco.com/warp/customer/127/max_att_27042.html

[30] R. Ramaswami, K. Sivarajan, and G. Sasaki, "Optical networks: A practical perspective," *San Francisco, CA: Morgan Kaufmann, 3rd ed.*, 2009.

[31] G. Agrawal, "Fiber-optic communication systems," *New York: Wiley, 14th ed.*, 2010.

[32] I. FiberLabs, "Erbium-doped fiber amplifier (EDFA)." [Online]. Available: https://www.fiberlabs.com/glossary/erbium-doped-fiber-amplifier/

[33] I.-T. R. G. Telecommunication Standardization Sector of ITU, "ITU-T forward error correction for high bit-rate DWDM submarine systems," p. 19, Feb. 2004.

[34] N. Sambo, A. Ferrari, A. Napoli, N. Costa, J. Pedro, B. Sommerkorn-Krombholz, P. Castoldi, and V. Curri, "Provisioning in multi-band optical networks," *Journal of Lightwave Technology*, vol. 38, no. 9, pp. 2598–2605, May. 2020.

[35] E. Ip, A. P. T. Lau, A. P. T. L. Ezra Ip, and J. M. Kahn, "Coherent detection in optical fiber systems," *Optics Express*, Express, vol. 16, no. 2, pp. 753–791, Jan. 2008.

[36] P. Poggiolini, G. Bosco, A. Carena, V. Curri, Y. Jiang, and F. Forghieri, "The GN-model of fiber non-linear propagation and its applications," *Journal of Lightwave Technology*, vol. 32, no. 4, pp. 694–721, 2014.

[37] P. Johannisson and E. Agrell, "Modeling of nonlinear signal distortion in fiber-optic networks," *Journal of Lightwave Technology*, vol. 32, no. 23, pp. 4544–4552, Dec 2014.

[38] E. Grellier and A. Bononi, "Quality parameter for coherent transmissions with gaussian-distributed nonlinear noise references and links," *Optics express*, vol. 19, no. 13, pp. 12 781–8, Jun 2011.

[39] R. Pastorelli, G. Bosco, A. Nespola, S. Piciaccia, and F. Forghieri, "Network planning strategies for next-generation flexible optical networks [invited]," *Journal of Optical Communications and Networking*, vol. 7, no. 3, pp. A511–A525, San Francisco, California United States, Mar. 2014.

[40] C. Pulikkaseril, L. A. Stewart, M. A. F. Roelens, G. W. Baxter, S. Poole, and S. Frisken, "Spectral modeling of channel band shapes in wavelength selective switches," *Optics Express*, vol. 19, no. 9, p. 4–11, Apr. 2011.

[41] J. Pedro, "Designing transparent flexible-grid optical networks for maximum spectral efficiency [invited]," *Journal of Optical Communications and Networking*, vol. 9, no. 4, pp. C35–C44, Apr. 2017.

[42] S. Tibuleac and M. Filer, "Transmission impairments in DWDM networks with reconfigurable optical add-drop multiplexers," *J. Lightwave Technol.*, vol. 28, no. 4, pp. 557–568, Feb. 2010.

[43] D. G. Sequeira, L. G. Cancela, and J. L. Rebola, "Impact of physical layer impairments on multi-degree CDC ROADM-based optical networks," *2018 International Conference on Optical Network Design and Modeling (ONDM)*, pp. 94–99, 2018.

[44] Z. Pan, J. Wang, and Y. Weng, "Digital signal processing techniques in Nyquist-WDM transmission systems," *Photonic Network Communications*, vol. 32, pp. 236–245, Aug. 2015.

[45] T. A. Strasser and J. L. Wagener, "Wavelength-selective switches for ROADM," *IEEE Journal on Selected Topics in Quantum Electronics*, vol. 16, no. 5, pp. 1150–1157, Sep. 2010.

[46] Y. Hsueh, "Passband narrowing and crosstalk impairments in ROADM-enabled 100 G DWDM networks," *J. Lightwave Technol*, vol. 30, no. 24, p. 3980–3986, Dec. 2012.

[47] I. Monroy and E. Tangdiongga, *Crosstalk in WDM Communication Networks.* Springer, Norwell, MA:Springer, 2002.

[48] M. Filer and S. Tibuleac, "Generalized weighted crosstalk for DWDM systems with cascaded wavelength-selective switches," *Optics Express*, vol. 20, no. 16, pp. 17 620–17 631, Jul. 2012.

[49] F. Labs, "C and C/L band WDM filters." [Online]. Available: https://www.fiberdyne.com/

[50] D. Semrau, R. Killey, and P. Bayvel, "A closed-form approximation of the Gaussian noise model in the presence of inter-channel stimulated raman scattering," *Journal of Lightwave Technology*, vol. 37, no. 9, pp. 1924–1936, May 2019.

[51] F. Paolucci, R. Emmerich, F. Fresi, I. Sackey, L. Potì, C. Schubert, J. K. Fischer, and F. Cugini, "Filterless optical WDM metro networks exploiting C+L band," 2018. [Online]. Available: https://ieeexplore.ieee.org/abstract/document/8535529

[52] Fibermart, "1x2 DWDM red/blue C band filter with 1RU 19' rack mount package." [Online]. Available: https://www.fiber-mart.com/1x2-dwdm-redblue-c-band-filter-with-1ru-19-rack-mount-package-p-1890.html

[53] F. Europe, "Customized 1x2 single fiber DWDM splitter red/blue C band filter." [Online]. Available: https://www.fs.com/products/65981.html

[54] K. Song and M. Premaratne, "Effects of SPM, XPM, and four-wave-mixing in L-band EDFAs on fiber-optic signal transmission," *IEEE Photonics Technology Letters*, vol. 12, no. 12, pp. 1630–1632, Dec. 2000.

[55] D. Semrau, R. I. Killey, and P. Bayvel, "The Gaussian noise model in the presence of inter-channel stimulated raman scattering," *Journal of Lightwave Technology*, vol. 36, no. 14, pp. 3046–3055, Jul 2018.

[56] I.-T. R. G. Telecommunication Standardization Sector of ITU, "Spectral grids for WDM applications: DWDM frequency grid," Oct. 2020.

[57] D. Semrau, "ISRSGmodel." [Online]. Available: https://github.com/dsemrau/ISRSGNmodel/blob/master/Functions/Matlab/ISRSGNmodel.m?fbclid=IwAR2GuaggO_446iN069oBfaYuLZkRBefTREHhb-nnO5U9_BrAFTqBaCc7QtM

[58] G. R. Martella, A. Nespola, S. Straullu, F. Forghieri, and R. Gaudino, "Scaling laws for unamplified coherent transmission in next-generation short-reach and access networks," *Journal of Lightwave Technology*, vol. 39, no. 18, pp. 5805–5814, Sep. 2021.

[59] ThorLabs, "Mounted photodiodes." [Online]. Available: https://www.thorlabs.com/newgrouppage9.cfm?objectgroup_id=1285

[60] R.-J. Essiambre, G. Kramer, P. J. Winzer, G. J. Foschini, and B. Goebel, "Capacity limits of optical fiber networks," *Journal of Lightwave Technology*, vol. 28, no. 4, pp. 662–701, Feb. 2010.

[61] M. Seimetz, *High-Order Modulations for Optical Fiber Transmission.*, T. Rhodes, Atlanta. ed. Springer, 2009.

Appendices

APPENDIX A

Deduction of Eq. (3.8)

In this appendix, the main steps in the deduction of Eq. (3.8) are shown. The model of a typical optical coherent receiver [**60**], which consists of a 2x4 90° hybrid, two balanced photodetectors, two RRC filters and two decision circuits, is depicted in Fig. A1.

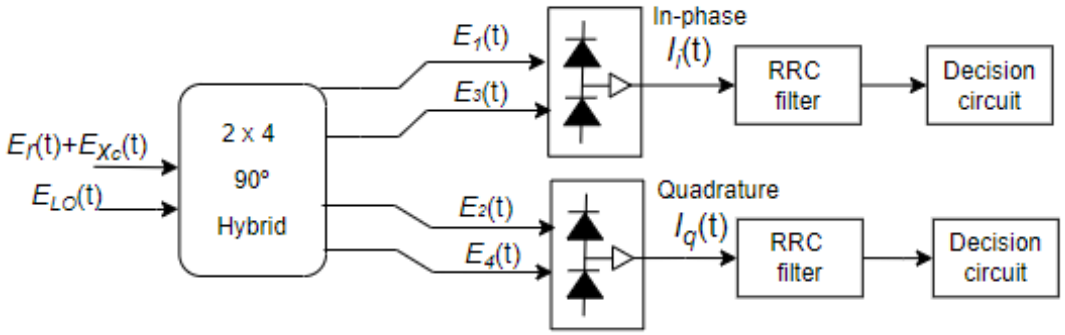

FIGURE A1. Block diagram of an optical coherent receiver for a single polarization of the incoming optical signal.

In Fig. A1, $E_r(t)$, $E_{X_c}(t)$ and $E_{LO}(t)$ are, respectively, the received signal, in-band crosstalk and LO electrical fields. The eletrical fields at the four photodetectors inputs can be given by [**61**]:

$$E_1(t) = \frac{1}{2}[E_r(t) + E_{X_c}(t) + E_{LO}(t)] \tag{A.1}$$

$$E_2(t) = \frac{1}{2}[E_r(t) + E_{X_c}(t) + jE_{LO}(t)] \tag{A.2}$$

$$E_3(t) = \frac{1}{2}[E_r(t) + E_{X_c}(t) - E_{LO}(t)] \tag{A.3}$$

$$E_4(t) = \frac{1}{2}[E_r(t) + E_{X_c}(t) - jE_{LO}(t)] \tag{A.4}$$

The two balanced photodetectors, depicted in Fig. A1, are used to convert the optical signal to an eletrical signal and the corresponding photocurrents, assuming R_λ=1 A/W, can be given by

$$I_1(t) = \frac{1}{4}|E_r(t) + E_{X_c}(t) + E_{LO}(t)|^2 \tag{A.5}$$

$$I_2(t) = \frac{1}{4}|E_r(t) + E_{X_c}(t) + jE_{LO}(t)|^2 \tag{A.6}$$

$$I_3(t) = \frac{1}{4}|E_r(t) + E_{X_c}(t) - E_{LO}(t)|^2 \tag{A.7}$$

$$I_4(t) = \frac{1}{4}|E_r(t) + E_{X_c}(t) - jE_{LO}(t)|^2 \tag{A.8}$$

The in-phase and quadrature photocurents, respectively, I_i(t) and I_q(t), can be given by [**60**]

$$I_I(t) = I_1(t) - I_3(t) = 2\Re[E_r(t)E^*_{LO}(t) + E_{X_c}(t)E^*_{LO}(t)] \tag{A.9}$$

$$I_Q(t) = I_2(t) - I_4(t) = 2\Im[E_r(t)E^*_{LO}(t) + E_{X_c}(t)E^*_{LO}(t)] \tag{A.10}$$

where $\Re$(Z) and $\Im$(Z) are, respectively, the real part and the imaginary part of a complex number Z, with the complex conjugate represented by Z^*. At the right-hand side, the first sum term represents the signal detected and the second sum term represents the detected crosstalk. Assuming that the detected signal power is also impaired by thermal noise, RIN of the LO, shot noise and an additional noise as in [**58**], the SNR can be given by:

$$\begin{aligned} snr &= \frac{p_{R_x}P_L^{CW}}{\sigma_{th}^2 + P_L^{CW^2}\sigma_{nLO}^2 CMRR + \frac{q \cdot B_{eq}^{RX} P_L^{CW}}{2} + \frac{p_{Rx}P_L^{CW}}{SNR_q} + p_{X_c}P_L^{CW}} \\ &= \frac{p_{R_x}}{\frac{\sigma_{th}^2}{P_L^{CW}} + P_L^{CW}\sigma_{nLO}^2 CMRR + \sigma_{shot}^2 + \frac{p_{Rx}}{SNR_q} + p_{X_c}} \end{aligned} \tag{A.11}$$

APPENDIX B

Scientific contributions

Impact of physical layer impairments on C+L-band metro networks

Filipa F. Gomes[1],Luís G. Cancela[1,2]and João L. Rebola[1,2]
[1]*Optical Communications and Photonics Group, Instituto de Telecomunicações, Lisbon, Portugal*
[2]*Department of Information Science and Technology, Instituto Universitário de Lisboa (ISCTE-IUL), Portugal*
{*ffgsa, luis.cancela, joao.rebola*}*@iscte-iul.pt*

Keywords: ASE noise, In-band crosstalk, Metro networks, Multi-band transmission, Nonlinear interference noise

Abstract: To ensure future data traffic capacities, multi-band transmission in optical networks is being proposed, by adding wavelength division multiplexing channels in the L-band to the existing C-band channels. In this work, we study the filterless drop and waste amplified and unamplified solutions used in metro networks with L-band tributary nodes. The cost and power consumption of these nodes is evaluated, as well as the impact of several physical layer impairments on the network performance. In amplified solutions, we show that L-band networks with 9 tributary nodes are feasible, being the optical signal-to-noise ratio achieved when considering amplifiers noise and fiber non-linear interference above 14 dB. In unamplified solutions, to fullfil the power budget, frequency reuse should be used between spans. We show that the in-band crosstalk caused by this frequency reuse leads to 1.5 dB power budget degradation, for a crosstalk level of -20 dB.

1 INTRODUCTION

To offer the best Internet experience, nowadays, it is necessary to resort to cloud services which, in the future, will probably saturate the transport capacity of existing metro networks. Several solutions based on multi-band transmission are being investigated to overcome this possible capacity crunch (Ferrari et al., 2020), but the introduction of the L-band (by adding wavelength division multiplexing (WDM) channels) opens the opportunity for cheaper solutions than placing several fibres in parallel.

Filterless solutions, both amplified and unamplified, are being proposed to reduce even more the cost of upgrading the optical networks to the L-band (Emmerich et al., 2020b), (Paolucci et al., 2020). In particular, the filterless solution is usually applied to networks with horseshoe topology (Emmerich et al., 2020b). In (Paolucci et al., 2020), the L-band filterless unamplified solution is proposed, but due to frequency reuse, in-band crosstalk becomes a relevant impairment that degrades the network performance. As this solution is only suitable for short-reach spans, noise from the amplifiers and fiber non-linearities can be neglected. Due to the impossibility of reusing frequencies in the amplified solution, amplified spontaneous emission (ASE) noise and fiber non-linear interference (NLI) become the main impairments that degrade the network performance.

In all these works, regarding filterless L-band transmission, we have seen that they resort on experimental results and simulations to study the upgrade of the metro area networks. However, an analytical study of the filterless solutions has not been performed in these works.

In this work, we analyse the node components and architectures for the C+L-band, and their cost and power consumption are estimated. A simple analytical formalism of the various physical layer impairments (PLIs) that affect the performance of the filterless solution, either amplified or unamplified, in the horseshoe topology is provided. The impact of ASE noise and NLI on the optical signal-to-noise ratio (OSNR) of the horsehoe topology is studied for filterless L-band amplified solutions and the influence of in-band crosstalk on the electrical signal-to-noise ratio (SNR) is assessed for unamplified solutions.

This work is organized as follows. In section 2, we review the L-band node architectures amplified and unamplified solutions for the C+L transmission. In section 3, we perform an analysis regarding the L-band hardware cost and power consumption. In section 4, the several PLIs that impair the L-band nodes network performance are studied for the amplified and unamplified solutions. In section 5, the final conclusions are drawn.

2 NODE ARCHITECTURE FOR C+L-BAND

Several solutions regarding metro networks with C+L band transmission rely on the horseshoe network topology to manage the access/metro network data traffic (Paolucci et al., 2020). The horseshoe topology is usually composed of two hub nodes (which are nodes that communicate in a meshed topology with other hub nodes) and several tributary nodes (which are nodes that connect with the hub nodes or other tributary nodes, and perform the interface with access metro networks) (Paolucci et al., 2020), (Emmerich et al., 2020a). As shown in Fig. 1, a C+L tributary node architecture has two independent structures, one for C-band signals and other for L-band signals (Emmerich et al., 2020a). These two bands are separated/aggregated by a C/L band filter at the input/output of the node, which typically provides high bands isolation and low insertion losses, introducing a 300 to 500 GHz gap between the C and L bands. The separated L-band solution causes a minimum disruption with pre-existing metro networks working only in the C-band (Emmerich et al., 2020a).

The node configuration used for the C-band, which is shown at the top of Fig. 1 (blue color), can be implemented with various nodes architectures such as filterless drop and waste (FD&W), fixed optical add/drop multiplexers (FOADM) and reconfigurable optical add/drop multiplexer (ROADM) solutions (Emmerich et al., 2020a).

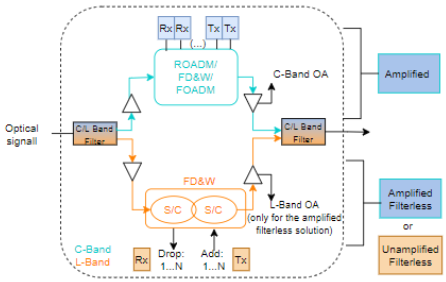

Figure 1: Tributary C+L-band node configuration.

The node configuration for the L-band is shown at the bottom of Fig. 1 (orange color). It is based only on the FD&W solution, whose architecture relies only on splitter/couplers (S/Cs), and can be either amplified or unamplified (Emmerich et al., 2020a). This solution has no filtering in the tributary nodes, which means that when a wavelength is added to the network, it remains in the network until the hub node removes it (amplified solution) or until it is reused once again in the network (unamplified solution) (Emmerich et al., 2020b), (Paolucci et al., 2020). The hub node L-band structure typically uses ROADMs as in the C-band structure counterpart (Hernandez et al., 2020).

2.1 L-band amplified solution

In the amplified solution, there are optical amplifiers (OAs) inside the node before and after the FD&W block, see Fig. 1 (Paolucci et al., 2020).

Fig. 2 presents a possible wavelength planning for the amplified solution in the L-band in a horseshoe topology, where each tributary node has a specific wavelength to communicate with the hub node. This solution does not allow the reuse of frequencies inside the network since each wavelength can only be extracted by the hub node (represented in pink in Fig. 2). The tributary nodes (represented in green in Fig. 2) do not have such capacity since they are based on S/Cs. In Fig. 2, the pink wavelength λ_5 is assigned to the connection between the hub node 1 and the tributary node *E*, but node *E* can not remove this wavelength, which is only removed from the network at the hub node 2. This path is represented by the dashed pink line, and represents a wasted wavelength for nodes F to I (Emmerich et al., 2020a).

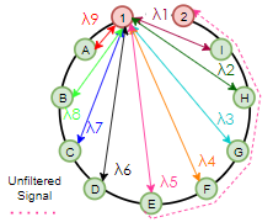

Figure 2: Amplified filterless solution with no frequency reuse for the horseshoe topology. Only the L-band wavelength assignment for the downlink transmission is depicted.

2.2 L-band unamplified solution

The main goal of the L-band unamplified solution is to reduce the nodes cost by not using OAs. This solution limits the L-band transmission distance to adjacent nodes or near adjacent nodes (Emmerich et al., 2020a).

Fig. 3 shows an example of a wavelengh assignment for the unamplified solution, to illustrate a wavelength reuse possibility. As shown in Fig. 3, the wavelength λ_2 is reused in the next-hop and λ_1 is reused

after one hop. As the WDM channel is not amplified, it arrives to the next node with very low power, meaning that a new channel with the same wavelength can be used. However, the (even weak) power leakage on node H can impair the new channel leading to in-band crosstalk. (Emmerich et al., 2020b).

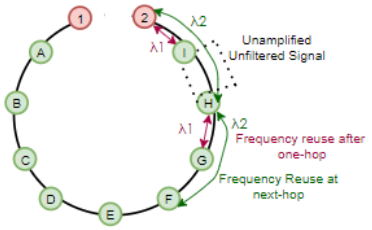

Figure 3: Unamplified filterless solution with frequency reuse for the horseshoe topology. Only the L-band wavelength assignment for the downlink transmission is depicted.

2.3 L-band nodes architectures

In the L-band, the tributary nodes use a FD&W architecture, while the hub nodes have usually a colorless and directionless (CD) ROADM route and select (R&S) architecture, as shown, respectively, in Figs. 4 and 5.

In Fig. 4, the tributary node architecture considers the transmission of 70 WDM channels with a 100 GHz channel spacing in each fiber direction. For two directions and a add/drop (A/D) ratio of 20%, the number of required coherent detection transponders in each L-band node is 28. Thus, beside considering two C/L filters to separate/aggregate the two bands and two amplifiers per node (in the case of the amplified solution), each tributary FD&W node has four S/Cs 1:2, four S/C 1:16, each with 4 unused channels and 28 transponders, as shown in Fig. 4.

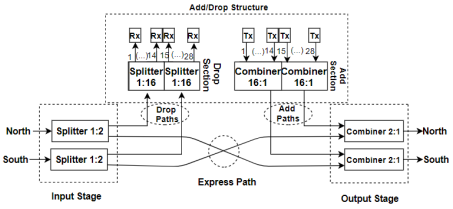

Figure 4: 2-Degree FD&W tributary node.

In Fig. 5, we consider that each 5-degree hub node is connected to 3 different hub nodes and two tributary nodes. So, for an A/D ratio of 20%, a total of 112 wavelengths must be added/dropped in each hub node. As wavelength selective switches (WSSs) with maximum dimension of 1:20 are considered (Hernandez et al., 2020), it is necessary to use 6 cards in the A/D structure to achieve this number of wavelengths. To connect each A/D card to the ROADM input/output directions, express WSSs 1:20 are considered. So, in Fig. 5, the hub node has five WSSs 1:20 at the input and output stages, twelve WSSs 1:20 in the A/D structure, six WSSs 1:8 at the drop section, six S/Cs 1:8 at the add section and 112 transponders.

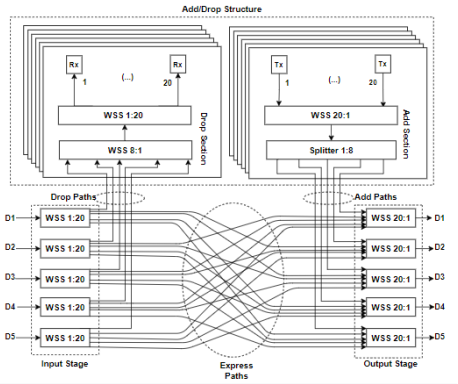

Figure 5: 5-Degree CD ROADM R&S hub node.

3 HARDWARE COST AND POWER CONSUMPTION

In this section, an analysis regarding the cost, power consumption and total offered capacity of an horseshoe topology with 2 hub nodes and 9 tributary nodes (as shown in Fig. 2) is performed and presented in Tab. 1. The analysis is performed considering that the cost and power consumption of the hardware components in the L-band is twice the C-band components cost, which is taken from (Hernandez et al., 2020). The cost is normalized to the cost of a 10 Gbps transponder, whose price is around 330 € (Hernandez et al., 2020).

For comparison purposes, the cost and power consumption of the same horseshoe network have been calculated for the C-band FD&W solution considering the components presented in (Hernandez et al., 2020), and the same A/D ratio of 20%.

The total capacity per fiber reaching the tributary

and hub nodes in the L-band is, respectively, 7 Tbps and 28 Tbps, determined from the number of WDM channels and the transponder capacity, which is, respectively, 70 channels and 100 Gbps for the tributary node and, respectively, 140 channels and 200 Gbps between hub nodes. The total capacity per node presented corresponds to the capacity per A/D structure. So, the capacity per tributary node is 2.8 Tbps and the average total capacity per hub node is calculated considering that 2/5 of the transponders are working at 100 Gbps (to communicate with tributary nodes) and the other 3/5 are at 200 Gbps (to communicate with other hub nodes). Hence, the average total capacity per hub node is 17.9 Tbps.

Table 1: Total cost, power consumption and capacity of the hub and tributary nodes and per horseshoe network.

Cost/Consumption	**Node architecture**
	Hub
Normalized cost/node	1952.44
Power consumption/node [kW]	18.96
Total capacity/node [Tbps]	17.9
	Trib. Amplified
Normalized cost/node	282.2
Power consumption/node [kW]	3.43
Total capacity/node [Tbps]	2.8
Total cost/horseshoe [k]	6.45
Total pow.cons./horseshoe [kW]	68.75
	Trib. Unamplified
Normalized cost/node	280.95
Power consumption/node [kW]	3.36
Total capacity/node [Tbps]	2.8
Total cost/horseshoe [k]	6.43
Total pow.cons./horseshoe [kW]	68.15

The tributary node unamplified solution is cheaper (less 1.25 of normalized cost) and spends less power per node (around 20 W) than the tributary node amplified solution. The difference between these solutions is only due to the existence or not of OAs. The components that most contribute, around 99%, to the final cost of the node are the transponders. The normalized cost per tributary node is around 3.5 times higher than in the C-band. This occurs because, in the L-band, the number of transponders is almost the double. The power consumption of the tributary node is 3.4 kW, which is around 1.7 times higher than the consumption of the FD&W for the C-band. Other components, such as the S/Cs have a small contribution to the final cost.

The hub node has a normalized cost around 3.5 times higher than the C-band node cost. The power consumption is also around 3.2 times higher than the corresponding C-band node power consumption.

So, the estimated total network cost using FD&W with amplified and unamplified soutions is 2134 k€ and 2128.3 k€, respectively, when the components are twice expensive, which means that the unamplified solution is 3% cheaper than the amplified one.

4 PHYSICAL LAYER IMPAIRMENTS IN THE L-BAND

In this section, the analysis of several PLIs, originated inside the nodes as well as in fiber transmission, such as insertion losses, ASE noise, NLI noise and in-band crosstalk is performed, considering quadrature phase-shift keying (QPSK) signal transmission in the L-band. The PLIs impact is quantified by the optical signal-to-noise-ratio (OSNR) given by (Semrau et al., 2019):

$$osnr = \frac{p_{Rx}}{p_{n,ASE} + p_{NLI}} \quad (1)$$

where p_{Rx} is the average signal power at the optical receiver input, $p_{n,ASE}$ is the accumulated ASE noise power and p_{NLI} is the NLI power at the receiver input. The following parameters are considered: the amplifiers noise figure (F_n) is 6.5 dB, at most 0.5 dB higher than in C-band (Correia et al., 2021). The fiber non-linear coefficient in the L-band, $\gamma = 1.2$ W/km, is slightly lower than in the C-band (Semrau et al., 2018), and the attenuation coefficient is α=0.25 dB/km, slightly higher than in the C-band. The channel bandwidth of 26.75 GHz is equal to the symbol rate, R_s, and the WDM channel spacing is 100 GHz.

Fig. 6 represents the spectral occupancy of the 70 channels belonging to the L-band and of the 40 C-band channels, considering the International Telecommunication Union (ITU)-T 100 GHz channel grid (Telecommunication Standardization Sector of ITU, 2020). The L-band central frequency is 188 THz, while, in the C-band, is 193.7 THz. A band gap of 300 GHz between the C and L bands is considered, which contains 3 unused channels.

Regarding the optical filtering effect in the L-band, only the WSSs in the hub nodes contribute to this effect. Hence, the effect of the optical filtering is neglected in the following analysis.

4.1 Insertion losses in amplified and unamplified solutions

In this section, we present the insertion losses of the amplified and unamplified solutions. The losses of each hardware element are those considered in (Hernandez et al., 2020). The WSS losses, which are in-

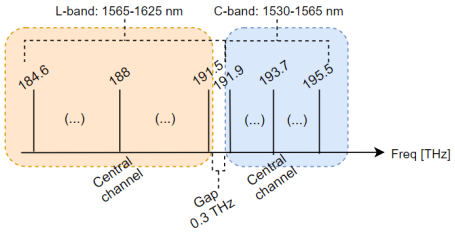

Figure 6: WDM signal frequencies for the C+L-band with 100 GHz channel spacing following the ITU-T grid, considering 40 channels for C-band and 70 channels for L-band.

dependent of the WSS size are 7 dB (Sequeira et al., 2021). The insertion losses considered for the S/Cs 1:2, 1:4, 1:8 and 1:16, are respectively, 4, 7, 11 and 15 dB (Inc., 2019). The losses of the C/L band filters are around 0.6 dB (Fiberdyne labs, 2021). The connectors and splices losses are neglected.

In Tab. 2, the insertion losses inside the add, drop and express paths of the tributary and hub nodes are shown. The fiber losses after 10 km are 2.5 dB. The hub node leads to the highest losses, 25 dB. For the tributary node, the add and drop paths losses are the same, 19.6 dB.

Table 2: Insertion losses in the L-band, of the tributary node the hub node.

	Tributary node
Add_{path}	S/C 16:1+S/C 2:1+C/L filter=19.6 dB
$Drop_{path}$	S/C 1:2+S/C 1:16+C/L filter=19.6 dB
$Express_{path}$	S/C 1:2 +S/C 2:1 + 2 ×C/L filter=9.2 dB
	Hub node
Add_{path}	WSS 20:1+S/C 1:8+WSS 20:1=25 dB
$Drop_{path}$	WSS 1:20 +WSS 1:8+WSS 1:20=21 dB
$Express_{path}$	WSS 1:20 +WSS 20:1=14 dB
10 km fiber	2.5 dB

The amplifier gains are designed to perfectly compensate the insertion losses of the worst path inside the node, the add path. For tributary nodes, only pre-amplification is used and the amplifier gain is 22.1 dB to compensate the losses of the 10 km span and node losses.

4.2 ASE noise in the amplified solution

In this section, the accumulated ASE noise power is calculated for the amplified solution in the L-band, considering two worst paths in the horseshoe network, 1) channel insertion at the hub node 1 and drop at node I in Fig. 2, and 2) channel insertion at node A and drop at hub node 2. The accumulation of ASE noise is quantified by the OSNR using (1), firstly, considering the absence of NLI.

The accumulated ASE noise power is given by:

$$p_{n,ASE} = 2 \times \sum_{i=1}^{n_{spans}} [p_{ASE,pre,i} + p_{ASE,pos,i}] \quad (2)$$

where n_{spans} is the number of spans, $p_{ASE,pre,i}$ is the ASE noise power per polarization generated at each i-th pre-amplifier output and $p_{ASE,pos,i}$ is the ASE noise power per polarization generated at each i-th post-amplifier output. The ASE noise power of each amplifier is given by

$$p_{ASE,m,i} = \frac{f_{n,m,i}}{2} \times (g_{m,i} - 1) \times h \times \nu_0 \times R_s \quad (3)$$

where m=*pre* or *pos*, h is the Planck's constant and ν_0 is the optical frequency. The ASE noise power as a function of the channel frequency (in lowpass equivalent definition) after nine spans of the horseshoe network for the cases of channel insertion at tributary node A and hub node 1 is shown in Fig. 7. The ASE noise power increases slightly with frequency and the difference between first and last channel frequencies is less than 0.3 dB. The ASE noise power is about 0.7 dB higher, when the channel insertion is in the tributary node in comparison with insertion in the hub node.

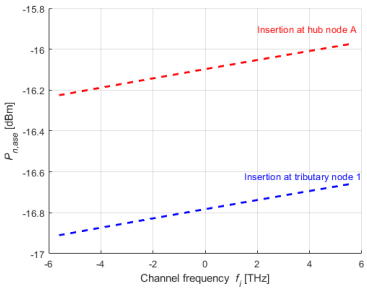

Figure 7: Accumulated ASE noise power as a function of the channel frequency after 9 spans of the horseshoe network for channel insertion in hub 1 and tributary A nodes.

Fig. 8 shows the OSNR evolution along the network, for both cases of signal insertion, for the channel frequency of 188 THz. When signal insertion occurs at node 1, the OSNR is significantly degraded as the signal crosses the nodes, decreasing 9.3 dB. For signal insertion at node A, the OSNR decreases 7.1 dB. The minimum reference OSNR is 8.5 dB to achieve a target BER 4×10^{-3} (Sambo et al., 2020). Fig. 8 shows that, for both cases of signal insertion,

the OSNR achieved at the optical receiver input provides a good safety margin in relation to the minimum OSNR.

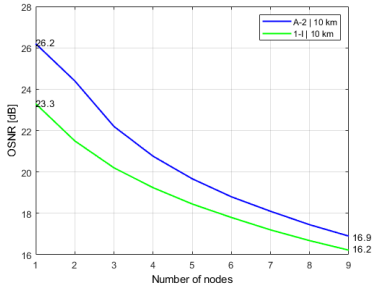

Figure 8: OSNR in the horseshoe topology, for signal insertion at the tributary node A and signal insertion at the hub node 1 for p_{Rx}=0 dBm.

4.3 NLI in the amplified solution

In this section, the NLI noise power and the associated OSNRs are studied for the amplified solution. To perform these studies, the NLI calculation and the OSNR formulation must take into account the presence of inter-channel Stimulated Raman Scattering (SRS). In this section, the Gaussian noise model presented in (Semrau et al., 2019) is considered, where the effect of the SRS in the NLI noise is taken into account in simplified closed-form expressions.

The NLI parameter in the L-band, used in the calculation of the OSNR, is given by (Semrau et al., 2019)

$$\eta(f_i) \approx \sum_{j=1}^{n_{spans}} \left[\frac{P_{i,j}}{P_i}\right]^2 \left[\eta_{SPM,j}(f_i) n_{spans}^{\varepsilon} + \eta_{XPM,j}(f_i)\right] \tag{4}$$

where $\eta_{SPM,j}(f_i)$ is the SPM contribution generated in j-th span at frequency f_i, $\eta_{XPM,j}$ (f_i) is the total XPM contribution generated in j-th span, and $P_{i,j}$ is the power of i-th channel launched into the j-th span, and ε is the coherent factor of NLI accumulation along multiple fiber spans. In this work, as we consider exact loss compensation, $P_{i,j}$=P_i, and NLI coherent accumulation is assumed. The SPM contribution is given by (Semrau et al., 2019)

$$\eta_{SPM}(f_i) \approx \frac{4}{9}\frac{\gamma^2}{B_i^2}\frac{\pi}{\Phi_i \overline{\alpha}(2\alpha+\overline{\alpha})} \cdot \left[\frac{T_i-\alpha^2}{\alpha}\operatorname{arcsinh}\left(\frac{\Phi_i B_i^2}{\pi\alpha}\right) + \frac{A^2-T_i}{A}\operatorname{arcsinh}\left(\frac{\Phi_i B_i^2}{\pi A}\right)\right] \tag{5}$$

where Φ_i=$\frac{3}{2}$ π^2 (β_2+ 2π β_3 f_i), β_2 is the group-velocity dispersion and β_3 is the higher order dispersion parameter (Agrawal, 2010), A= $\alpha+\overline{\alpha}$ and $T_i=(\alpha+\overline{\alpha}-P_{tot}C_r f_i)^2$, where P_{tot} is the WDM signal launch power, B_i is the bandwidth of the i-th channel and C_r is the slope of the linear regression of the normalized Raman gain spectrum (Semrau et al., 2019). The total XPM contribution is given by (Semrau et al., 2019)

$$\eta_{XPM}(f_i) \approx \frac{32}{27}\sum_{k=1,k\neq i}^{N_{ch}}\left(\frac{P_k}{P_i}\right)^2 \frac{\gamma^2}{B_k \Phi_{i,k}\overline{\alpha}(2\alpha+\overline{\alpha})} \cdot \left[\frac{T_k-\alpha^2}{\alpha}\arctan\left(\frac{\Phi_{i,k}B_i}{\alpha}\right) + \frac{A^2-T_k}{A}\arctan\left(\frac{\Phi_{i,k}B_i}{A}\right)\right] \tag{6}$$

where $\Phi_{i,k} = 2\pi^2(f_k - f_i)[\beta_2 + \pi\beta_3(f_i+f_k)]$. In this work, we consider the simplified case of $\alpha=\overline{\alpha}$.

For the NLI study, C_r=0.028 1/W/km/THz, the dispersion parameter is 17 ps/nm/km and the dispersion slope is ps/nm^2/km. In Fig. 9 (a), the NLI parameter as a function of the WDM channels frequency is shown, for several input powers per channel, considering the horseshoe topology with 9 tributary nodes and 10 km spans. Fig. 9 (a) reveals that, for higher channel input power, the higher the NLI parameter and the steepest its tilt, due to the stronger power transfer from higher to lower frequencies caused by SRS.

In Fig. 9 (b), the corresponding NLI power as a function of the WDM channels frequency is shown. The NLI power is determined by $p_{NLI} = \frac{P_{ex}^3}{\eta}$ (Semrau et al., 2019), As can be observed in Fig. 9 (b), the NLI power increases almost 5 dB, for a 4 dBm power channel, as the channel frequency decreases from the highest to the lowest channels. Also, it can be observed that, as the input power decreases, the NLI power increase is smoother from the highest to the lowest frequency channel. For the -2 dBm channel power, the NLI power remains practically constant for all frequency channels due to the reduced SRS. Notice that the results presented for the NLI power are independent on where the signal is inserted in the network.

The OSNR as a function of the channel frequency after 9 spans considering the ASE noise power and NLI is shown in Fig. 10, for several input channel powers, including the optimal power per channel, which leads to the best OSNR, and the maximum power per channel to comply the minimum OSNR, for the worst channel. Fig. 10 corresponds to the case of: (a) channel insertion at the tributary node A and (b) channel insertion at the hub node 1. The OSNR is calculated using Eq. (1).

As can be seen in Fig. 10, for the input power

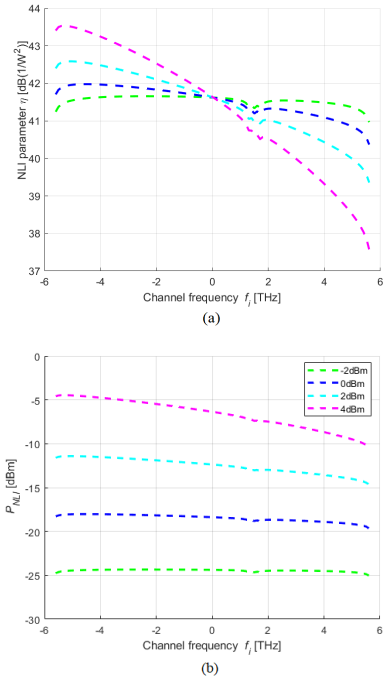

Figure 9: NLI parameter and p_{NLI} as a function of the channels frequency after nine 10 km spans considering coherent NLI accumulation, for several input powers per channel.

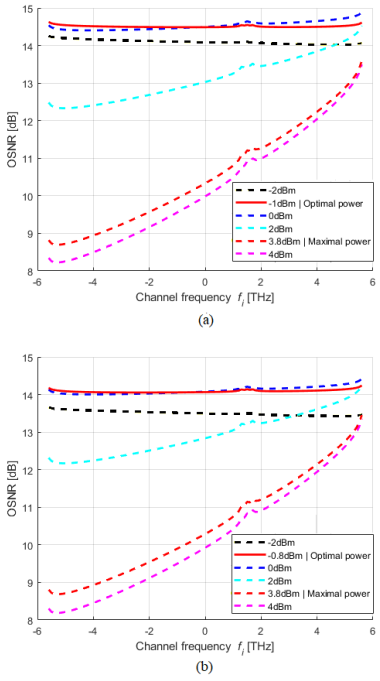

Figure 10: OSNR as a function of the channel frequency after 9 spans considering the ASE noise power and NLI, for several input channel powers and insertion channel in the (a) tributary node A and (b) hub node 1.

per channel of -2 and 0 dBm, the NLI power tilt has practically no influence, so an almost constant OSNR along all channels is observed. For input powers higher than 0 dBm, we observe that the OSNR increases as the channel frequency increases due to the higher NLI power contribution to the OSNR slope variation. So, we can state that there is an input channel power that gives an optimum OSNR. This optimum OSNR is obtained by evaluating the best possible OSNR, with the highest flatness along the WDM signal bandwidth (slope as close to zero as possible). Hence, the optimal input power that leads to the best OSNR is -1 and -0.8 dBm, respectively, in Fig. 10 (a) and (b), corresponding to the optimal OSNRs of 14.5 and 14 dB. It can be observed that the optimal OSNR is practically constant along frequency ensuring the same received quality for all WDM channels. When the signal is inserted in the hub node, the optimum OSNRs are around 0.5 dB lower than in the case of channel insertion in the tributary node due to the higher ASE noise power added by the hub node.

Finally, it can be observed that all channel powers considered in Fig. 10 comply with the 8.5 dB minimum OSNR required, except for the input power of 4 dBm, where this value is not achieved in the lowest channel frequencies. The maximum input power that ensures the minimum OSNR for all WDM channels is also represented in Fig. 10 and corresponds to 3.8 dBm, for both cases of channel insertion. Therefore, the difference between the optimal OSNR and the minimum OSNR is at least 5.5 dB higher, which ensures enough margin to include other PLIs. For example, if we consider a minimum system margin of 3 dB and an extra power penalty due to other transmission effects of 1.5 dB, like components aging, the minimum OSNR is still accomplished.

4.4 In-band crosstalk in the unamplified solution

In this subsection, the analysis of PLIs, considering the signal transmission in the L-band in a horseshoe topology based on tributary nodes with the FD&W unamplified solution is performed. In this scenario, the main PLI is the in-band crosstalk that arises due to the wavelength reuse in these networks. First, we present the analytical formalism used to assess the impact of this phenomenon, based on the electrical SNR at the receiver output. We start our analysis by presenting the SNR at the receiver output without in-band crosstalk (Rizzelli et al., 2021), and assess the maximum number of spans a signal can cross in a lightpath of the horseshoe topology. After, we introduce the in-band crosstalk in our formalism and assess the respective degradation in terms of the number of spans.

The SNR without in-band crosstalk is given by (Rizzelli et al., 2021)

$$snr = \frac{p_{Rx}}{\frac{\sigma^2_{th}}{P_L^{CW}} + P_L^{CW}\sigma^2_{nLO}CMRR + \sigma^2_{shot} + \frac{p_{Rx}}{SNR_q}} \quad (7)$$

where P_L^{CW} is the continuous wave optical power of the local oscillator (LO), $CMRR$ is the Common Mode Rejection Ratio of the balanced photodetector, SNR_q is an additional term to include several implementation penalties occurring in a coherent system, σ^2_{th} is the variance of the transimpedance amplifier thermal noise (TIA), σ^2_{nLO} is the variance of the LO transmitter relative intensity noise (RIN) and σ^2_{shot} is the variance of the shot noise. The variances σ^2_{th}, σ^2_{nLO} and σ^2_{shot} are given, respectively, by (Rizzelli et al., 2021) $\sigma^2_{th} = \frac{i^2_{TIA}\cdot B^{RX}_{eq}}{8\cdot R^2_\lambda}$; $\sigma^2_{shot} = \frac{q\cdot B^{RX}_{eq}}{2\cdot R_\lambda}$; $\sigma^2_{nLO} = RIN\cdot\frac{B^{RX}_{eq}}{2}$, where R_λ is the overall responsivity of the coherent receiver (considering also the passives losses before the photodiodes), i_{TIA} is the input-referred noise current density of a TIA, B^{RX}_{eq} is the the receiver effective noise bandwidth, q is the electron charge and RIN is the LO RIN parameter. The parameters used to calculate the SNR are based on the fitting to experimental results and are given in (Rizzelli et al., 2021). Only a different symbol rate of 26.75 Gbaud is considered.

In Fig. 11, the BER as a function of the received signal power for different local oscillator powers is presented, considering QPSK modulation, and obtained from the SNR calculated from Eq. 7. The required target BER assumed for the system is 4×10^{-3} (HD-FEC) or 2×10^{-2} (SD-FEC) (Rizzelli et al., 2021). As observed in Fig. 11, for each LO powers of 6, 10, 14 and 18 dBm, the minimum received power required to achieve the target BER is -36.1, -35.7, -35.6 and -33.8 dBm, respectively, for HD-FEC and -38.9, -38, -37.9 and -36 dBm for SD-FEC, which leads to at least 2.2 dB of power budget improvement for SD-FEC in relation to HD-FEC.

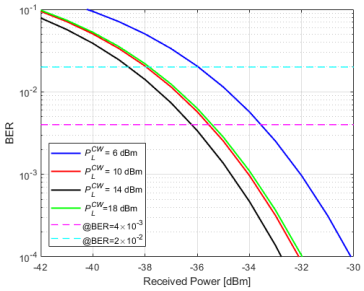

Figure 11: BER as a function of the received signal power for different local oscillator powers P_L^{CW}, for QPSK signals.

From Fig. 11, it can also be observed that the LO power of 14 dBm leads to the minimum received power that ensures the target BER, while $P_L^{CW} = 6$ dBm leads to the higher and most demanding received power to reach the same target BER. Hence, in the following results, we consider $P_L^{CW} = 14$ dBm, as the optimum LO power that leads to the target BER. So, knowing the minimum received power, the main goal is to compute the maximum power budget and the maximum reach of the horseshoe network with an unamplified solution, considering 10 km spans and a reference input power of 0 dBm, taken from the maximum input power considered in (Rizzelli et al., 2021). The maximum power budget is, therefore, 36.1 dB and 38.9 dB, respectively for the HD-FEC and SD-FEC.

Then, the insertion losses per span for hub-span-tributary, tributary-span-hub and tributary-span-tributary transmission, as shown in Fig. 12, are computed.

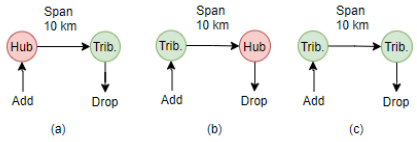

Figure 12: Possible span configurations considered to evaluate the performance of the unamplified solution.

In Tab. 3 are shown, the insertion losses considering the configurations of Fig. 12 for different S/C

dimensions are shown. Note that, the green values are the ones that are feasible for each configuration. As can be seen in Tab. 3, by comparing the power budgets and the insertion losses of just one span with S/Cs 1:16, it can be concluded that the power budgets are not sufficient to accommodate these insertion losses. A possible solution to decrease the insertion losses per span is to reduce the S/C dimension in the A/D structures. So, in the tributary nodes shown in Fig. 4, the S/Cs 1:16 are replaced by S/Cs with smaller size, as considered already in some works (Emmerich et al., 2020b), (Emmerich et al., 2020a), for the unamplified solution. The associated insertion losses are shown in Tab. 3. The A/D structure of the hub node remains the same as in the amplified scenario.

Table 3: Insertion losses considering the configurations of Fig. 12 for different S/C dimensions in the A/D structure of the tributary node.

Total ILs [dB]	S/C 1:2	S/C 1:4	S/C 1:8	S/C 1:16
Hub-span-trib.	36.1	39.1	43.1	47.1
Trib.-span-hub	32.1	35.1	39.1	43.1
Trib.-span-trib.	19.7	25.7	33.7	41.7

It can be concluded that one span is possible with S/Cs 1:2 for the configurations of Fig. 12, whereas only the tributary-span-hub and tributary-span-tributary configurations are possible for S/Cs 1:4, and, for the S/C 1:8, only the tributary-span-tributary configuration is possible. Two spans transmission is not possible.

In order to take into account the impact of in-band crosstalk, the SNR given by Eq. (7) is rewritten as,

$$snr = \frac{p_{Rx}}{\frac{\sigma^2_{th}}{P^{CW}_L} + P^{CW}_L \sigma^2_{nLO} CMRR + \sigma^2_{shot} + \frac{p_{Rx}}{SNR_q} + p_{xc}} \tag{8}$$

where p_{xc} is the crosstalk power defined as $p_{xc} = X_c \times p_{rx}$, with X_c the crosstalk level.

In Fig. 13, the BER as a function of the received signal power with different crosstalk levels is shown. The BER without crosstalk is also represented for comparison purposes. We have considered P^{CW}_L=14 dBm since it leads to the lowest received optical signal power. So, for an input signal power of 0 dBm, and considering the insertion losses shown in Tab. 3, for S/Cs 1:2, 1:4 and 1:8, when the crosstalk level ranges between -35 and -25 dB, the optical power budget is still feasible for all cases assuming a BER=2×10^2 (SD-FEC). For X_c=-20 dB, the minimum received power is about -37.4 dBm, considering SD-FEC, leading to 1.5 dB degradation in relation to the case without crosstalk. Although the optical power budget is reduced, the unamplified solution is still feasible for all the configurations in Fig. 12 for one span. For a 2 spans transmission, the most feasible configuration is tributary-span-tributary due to its lower insertion losses, which are very close to the highest power budget.

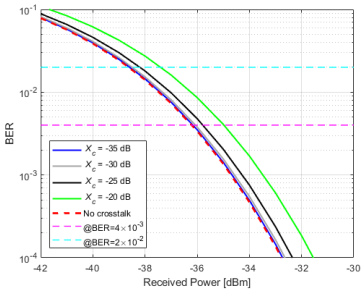

Figure 13: BER as a function of the received signal power with the crosstalk level as a parameter.

5 CONCLUSIONS

In this work, the L-band tributary node architectures known as FD&W with amplified and unamplified solutions have been studied analytically. The hardware components, cost, power consumption, offered capacity and the main PLIs that impair the transmission performance in such nodes have been studied,

When the L-band components cost is twice the C-band cost, the L-band hub and tributary nodes cost is 3.5 times higher than the corresponding C-band node cost. The transponders contribute around 99% to the node final cost.

For the amplified solution, considering an horseshoe network with 2 hub nodes, tributary nodes, and 10 km spans, and two worst path cases of signal transmission, the optimum OSNR achieved at the optical receiver input is above 14 dB, when ASE noise and NLI are considered. This leaves enough margin to guarantee the minimum OSNR in the amplified solution.

In unamplified solutions, to accomplish the power budget, smaller S/Cs 1:2 and 1:4 must be used in the A/D structure of the tributary nodes, and transmission should not exceed one fiber span. This allows frequency reuse in the horseshoe network, leading to in-band crosstalk. For the crosstalk level of -20 dB, a 1.5 degradation on the optical power budget is observed.

ACKNOWLEDGEMENTS

This work was supported under the project of Instituto de Telecomunicações UIDB/50008/2020.

REFERENCES

Agrawal, G. (2010). Fiber-optic communication systems. *New York: Wiley, 14th ed.*

Correia, B. et al. (2021). Power control strategies and network performance assessment for C+L+S multiband optical transport. *Journal of Optical Communications and Networking*, 13:147–157.

Emmerich, R. et al. (2020a). Capacity limits of C+L metro transport networks exploiting dual-band node architectures. *Optical Fiber Communication Conference (OFC) 2020, OSA Technical Digest (Optical Society of America, 2020).*

Emmerich, R. et al. (2020b). Dual-band node architectures for C+L-band capacity upgrades in optical metro transport networks. *21th ITG-Fachtagung*.

Ferrari, A. et al. (2020). Assessment on the achievable throughput of multi-band itu-t g.652.d fiber transmission systems. *Journal of Lightwave Technology*, 38:4279–4291.

Fiberdyne labs, i. (2021). C and C/L band WDM filters.

Hernandez, J. A. et al. (2020). Comprehensive model for technoeconomic studies of next-generation central offices for metro networks. *Journal of Optical Communications and Networking*, 12:414–427.

Inc., T. F. O. A. (2019). Testing fiber optic couplers, splitters or other passive devices. *Available: www.thefoa.org/tech/ref/testing/test/couplers.html*.

Paolucci, F. et al. (2020). Disaggregated edge-enabled C+L-band filterless metro networks. *Journal of Optical Communications and Networking*, 12:2–12.

Rizzelli, G., Nespola, A., Straullu, S., Forghieri, F., and Gaudino, R. (2021). Scaling laws for unamplified coherent transmission in next-generation short-reach and access networks. *Journal of Lightwave Technology*.

Sambo, N., Ferrari, A., Napoli, A., Costa, N., Pedro, J., Sommerkorn-Krombholz, B., Castoldi, P., and Curri, V. (2020). Provisioning in multi-band optical networks. *Journal of Lightwave Technology*, 38:2598–2605.

Semrau, D. et al. (2018). The Gaussian noise model in the presence of inter-channel stimulated raman scattering. *Journal of Lightwave Technology*, 36:3046–3055.

Semrau, D., Killey, R., and Bayvel, P. (2019). A closed-form approximation of the Gaussian noise model in the presence of inter-channel stimulated raman scattering. *Journal of Lightwave Technology*, 37:1924–1936.

Sequeira, D., Cancela, L., and Rebola, J. (2021). CDC ROADM design tradeoffs due to physical layer impairments in optical networks. *Optical Fiber Technology*, 62:102461.

Telecommunication Standardization Sector of ITU, I.-T. R. G. (Oct. 2020). Spectral grids for WDM applications: DWDM frequency grid.